AN ABSTRACT OF THE THESIS OF

KIRK POWELL GALBRAITH (Name) for the DOCTOR OF PHILOSOPHY (Degree)

in CHEMICAL ENGINEERING (Major) presented on August 10, 1970 (Date)

Title: SINGLE PHASE TURBULENT MIXING BETWEEN ADJACENT CHANNELS IN ROD BUNDLES

Abstract approved: Redacted for Privacy

James G. Knudsen

The turbulent interchange of matter between parallel adjacent subchannels in a simulated rod bundle for single phase flow was investigated to determine the effects of mass flow rate and rod spacing.

The simulated rod bundle was made by placing six 1-inch diameter rods in a square-square array. The overall test section was 42.5 inches in length with a 16-inch entrance section, a 16-inch mixing section and a 10.5-inch exit section. The test section was built so that several rod spacings could be investigated.

Water was used as the fluid for the system and it flowed in the axial direction of the rods. The turbulent mixing was the lateral transport in the test section and was measured by using a dye tracer technique. The technique involved initially tracing one side of the test section and measuring the exit dye concentration for the initially untraced system. This result plus the subchannel mass flow rate was

then used in an analytical model to calculate numerically the turbulent mixing rate.

The experimental program considered five rod spacings 0.011, 0.028, 0.063, 0.127 and 0.228 inches and a range of mass flow rates that resulted in a Reynolds number range of 8×10^3 to 3×10^4.

The results of this study are as follows:

1. The turbulent mixing between adjacent subchannels can be correlated with turbulent eddy diffusivities for duct flow.
2. The turbulent mixing is a function of the rod spacing and subchannel Reynolds number and increases with increasing rod spacing and Reynolds number.
3. Although the results may be correlated with the subchannel Reynolds number, the flow conditions in the immediate vicinity of the rod spacing are important especially for the smallest rod spacing.
4. Small pressure gradients between adjacent subchannels have a significant effect upon the mixing results.

Single Phase Turbulent Mixing Between Adjacent Channels in Rod Bundles

by

Kirk Powell Galbraith

A THESIS

submitted to

Oregon State University

in partial fulfillment of
the requirements for the
degree of

Doctor of Philosophy

June 1971

APPROVED:

Redacted for Privacy

Professor of Chemical Engineering

in charge of major

Redacted for Privacy

Head of Department of Chemical Engineering

Redacted for Privacy

Dean of Graduate School

Date thesis is presented August 12, 1949

Typed by Clover Redfern for Kirk Powell Galbraith

ACKNOWLEDGMENTS

I wish to extend my grateful appreciation to:

Dr. James G. Knudsen for his guidance and professional assistance throughout the duration of this investigation.

Department of Health, Education and Welfare for financial assistance in the form of a three-year NDEA Fellowship.

Oregon State University Engineering Experimental Station for financial assistance in the form of a one-year Research Assistantship.

Department of Chemical Engineering and Dr. C. E. Wicks, Head, for the excellent instruction received during my graduate studies and for the use of its facilities.

My parents for their support and encouragement during my entire university career.

And to my wife, Pat, whose understanding and patience has given this experience unmeasured meaning.

TABLE OF CONTENTS

LIST OF FIGURES

LIST OF TABLES

SINGLE PHASE TURBULENT MIXING BETWEEN ADJACENT CHANNELS IN ROD BUNDLES

INTRODUCTION

An important factor in a nuclear fuel rod design is the ability to predict subchannel flow conditions such as bulk velocity and bulk temperature of the coolant fluid. It has been shown by Knudsen (26) that mixing between various subchannels could be used to obtain a better estimate of coolant enthalpies or temperature in the case of single phase systems. In a fuel rod bundle matrix, such as that shown in Figure 1, the coolant flow rates vary in the different types of subchannels because of the variation in the flow areas and equivalent diameter. Thermal variations between subchannels also exist since there are significant differences in the wetted and heated surface areas between subchannels. The dashed lines on Figure 1 outline the various subchannel geometries that can be obtained in most fuel rod bundle designs. Because of the variations between subchannels mentioned, different subchannel thermal (temperature) conditions would exist if subchannel mixing did not occur. It should be noted that the ultimate fuel bundle condition would be a uniform temperature profile for the coolant at any cross-section. This could be accomplished by very high mixing rates between channels. Since this situation is not likely nor feasible, it is important that the subchannel conditions can

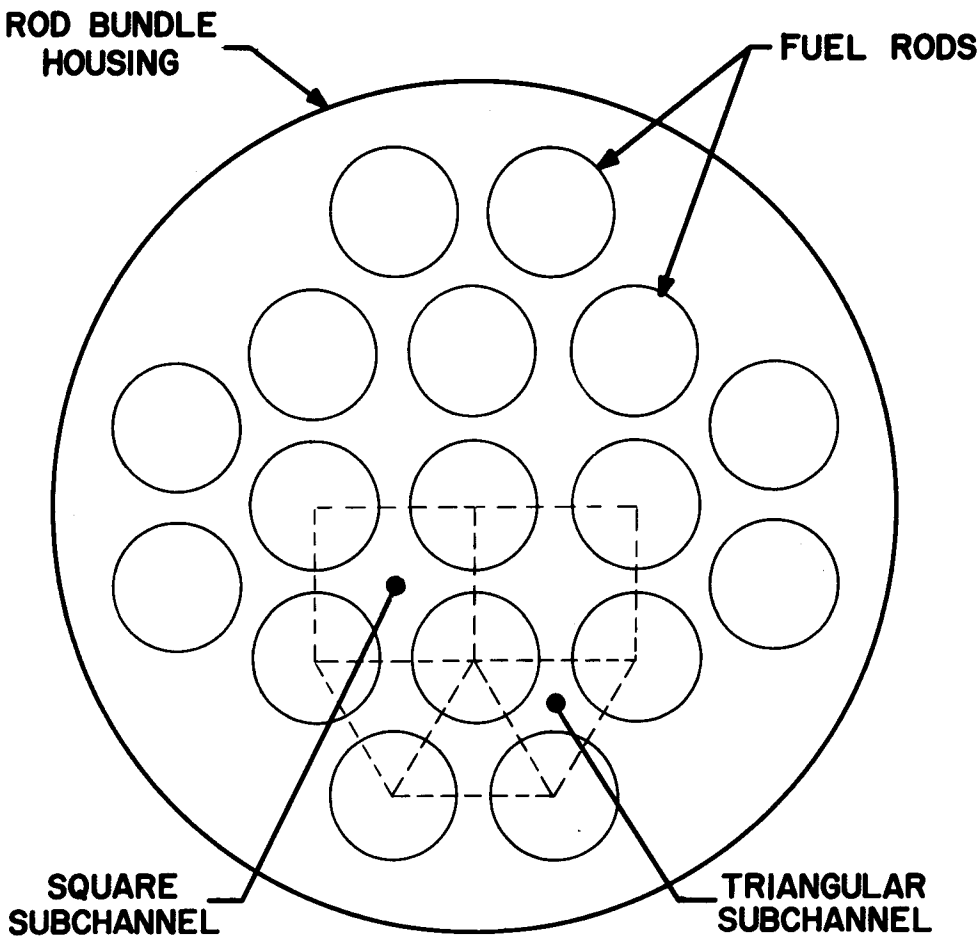

Figure 1. Rod bundle matrix.

be predicted.

In the past a designer was dependent upon experimental results for rod bundle mock-ups of the actual geometry of concern. These results although helpful were generally limited to the geometry of the particular study and as such offered very little generalization for other designs.

This work considers what could be called a two-channel flow system with water used as the coolant. Figure 2 shows the cross-section for the flow system with pertinent geometrical data. The test section was constructed of plexiglass (acrylic plastic). This was used to study the effects of mass flow and rod separation on natural or turbulent mixing between the two main subchannels. The test section design was such that rod spacings (separations of 0.011, 0.028, 0.063, 0.137, and 0.228 inches) could be obtained while the subchannel mass fluxes ranged from 0.3×10^6 to 2×10^6 $\frac{lb_m}{ft^2\text{-}hr}$. This gave a Reynolds number range of 8×10^3 to 3.2×10^4 depending on the rod spacing.

Figure 3 shows a simple cut-away of the two-channel test section and depicts the mixing that will be considered in this work. As mentioned earlier, this study will consider only the turbulent mixing.

The turbulent or natural mixing was measured by using a dye tracer technique employing rhodamine B. The dye analysis procedure used offered some unique advantages over previous experimental techniques reported in the literature.

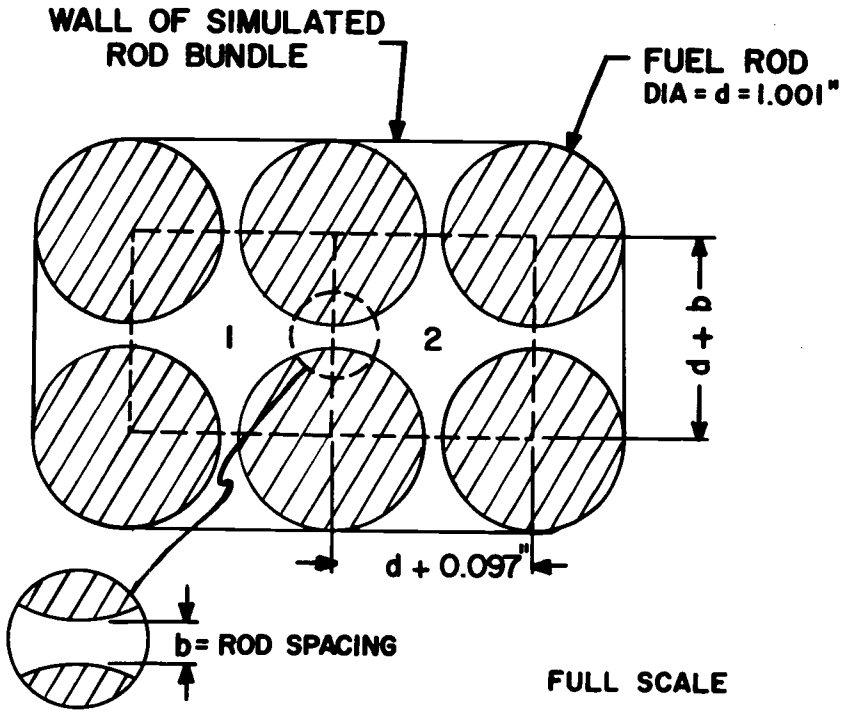

Figure 2. Test section cross-section.

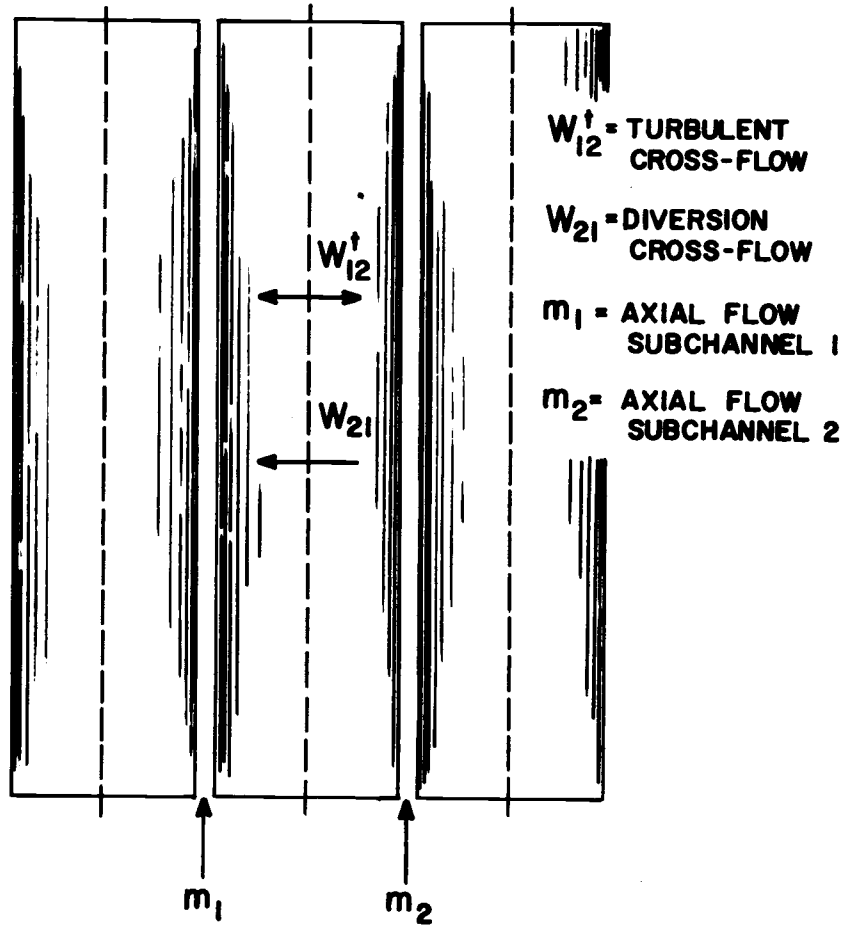

Figure 3. Cut-away of the test section.

THEORETICAL ASPECTS AND LITERATURE SURVEY

Turbulent Mixing

Although the literature contains several references on turbulent mixing between adjacent channels and in rod bundles, the results have not lent themselves to a common correlation. It is important to note that there is at present a consensus of opinion with respect to the general nature of the mixing or transport process. Rogers and Tarasuk (36) give a complete discussion of the various modes of mixing. They have categorized the mixing process as natural or forced and directional and nondirectional.

The forced mechanism is that mixing which is a direct result of some mechanical device. Such devices are generally warts or spacers that are attached to the surface of the otherwise smooth fuel rod. This type of mixing may be directional or nondirectional depending on the design of the device.

Natural mixing is that mechanism by which the coolant is transported between subchannels in the absence of any forced mixing devices. The directional mixing or diversion cross-flow between subchannels is caused by pressures tending to equalize and results in a flow redistribution between adjacent subchannels. The pressure gradients might be a result of large temperature variations between

subchannels or cross-sectional area variations.

The nondirectional natural mixing mechanism is the process of interest in this work. This mode of transport between adjacent subchannels has been called turbulent mixing, turbulent cross-flow or lateral transport by many of the earlier investigators of coolant mixing phenomena (23; 31; 32, p. 4; 36; 39; 53). This type of subchannel transport causes no flow redistribution between subchannels when averaged over short periods of time. The similarity between the turbulent cross-flow mechanism and the eddy diffusivity transport process for fluids in turbulent motion is the basis for the theoretical and experimental development of this work.

For turbulent fluid motion in a duct, the eddy diffusivity (lateral eddy diffusivity) has been shown to be a function of space and time (3, p. 320; 27, p. 115; 42, p. 433). The lateral eddy diffusivity can be written for the turbulent transfer process of interest such as E_M for momentum transport, E_h for thermal transport and E_m for mass transport. If the classical development of the turbulent eddy diffusivities is considered, it is reasonable to assume that all modes of turbulent transport can be described by a single eddy diffusivity, E. This result is the exception rather than the rule, but it has been used successfully by several investigators (2; 9; 36; 49). This fact suggests that subchannel mixing experiments using mass transport as a means of investigation will be applicable to the actual mechanism of

concern, thermal subchannel mixing.

Although most fluid mechanics texts consider turbulent flow and turbulent eddy transport in some detail, it will be considered here since it will play an important role in later arguments.

Osborne Reynolds (34) in 1883 investigated the flow of fluids in ducts and demonstrated the qualitative differences between laminar and turbulent flow. The conclusions that can be drawn from the investigation are:

1. Above a certain mean velocity for a given system rather large eddies form that flow cross-stream in some random behavior.
2. The eddies are larger and more abundant at the duct center than in the vicinity of the walls.
3. As the mean velocity is increased the eddy activity expands to fill a larger portion of the duct cross-section.

All of this implies the transient nature of turbulent motion and suggests why description of this motion has been largely empirical.

Closer investigation of the eddies indicate that they may be considered as macroscopic fluid lumps of varying sizes (43, p. 525). These fluid lumps or eddies are continually growing and decaying as dictated by their immediate flow conditions. When this eddy activity is considered in light of the desired subchannel mixing there is a clear similarity. The eddies developed in one subchannel pass to the

adjacent subchannel and in doing so transport thermal energy (momentum or mass). If the eddy is considered to have the average properties of the subchannel in which it was initially developed, the adjacent subchannel transport between hot and cold subchannels would reduce this non-uniform thermal state between the subchannels.

J. Boussinesq, who was one of the initial investigators of turbulent motion, introduced a mixing coefficient, A_τ, for turbulent momentum transfer. This turbulent mixing coefficient is analogous to the coefficient of viscosity, μ, for laminar flow.

If a momentum balance is considered for a section of a duct the following relationship is obtained:

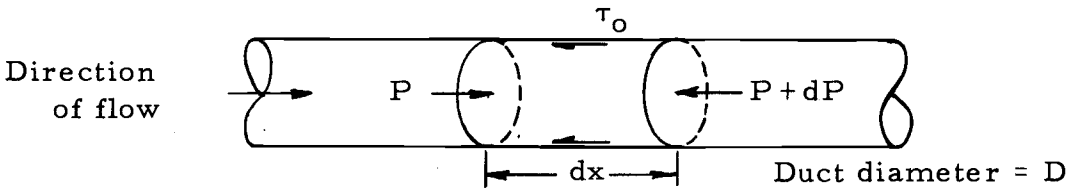

$$-\frac{dP}{dx}(Ac) = \tau_o(Pw) \qquad (1)$$

where

$$\tau_o = \text{total wall shear stress} = (\mu + A_\tau)\frac{du}{dy}\Big|_{y=0}$$

Ac is the cross-sectional area of the duct, $\frac{\pi D^2}{4}$, and Pw is the solid surface, πD. The shear stress, τ_o, at the wall of the duct represents the force of resistance to the flow and $\frac{dP}{dx}$ is the pressure

loss per unit length due to friction. The expression for the shear stress shows that resistance to the flow is a function of the fluid property, μ, and flow regime or turbulent motion. The eddy diffusivity of momentum, E_M, is thus A_τ/ρ. The primary disadvantage with this relationship is the fact that A_τ is dependent upon the flow conditions.

Although there have been many hypotheses and theories presented to describe A_τ, Prandtl's (33) mixing length theory is still the focal point for most developments. Prandtl's phenomenological theory maintains that the eddy (fluid lump) retains its identity while traversing a distance, ℓ, the mixing length. When this idea is applied with the transient nature of turbulent motion, the following result may be obtained:

$$E_M = \ell^2 \left|\frac{du}{dy}\right| \qquad (2)$$

where $\left|\frac{du}{dy}\right|$ is the absolute value of the mean velocity gradient. Note that the direction of y is normal to the wall of the duct and as such E_M is considered a lateral eddy diffusivity. If Equation 2 is used in Equation 1 for A_τ/ρ and if the resulting equation were used as a means of developing the duct velocity profile, the result would be a fair representation of the actual velocity profile (42, p. 566). Very similar developments for E_m and E_h may be found in other

references (25, p. 155; 27, p. 415; 28; 45).

Before Equation 2 can be used, the mixing length, ℓ, must be evaluated and this ultimately relys upon experimental data. There have been numerous attempts to develop mathematical models of Equation 2 such that turbulent flow phenomena might be better represented with a minimum of complexity (9). Each mathematical representation has its advantages and shortcomings. With this in mind Deissler's (9) eddy diffusivity in the region close to the wall of a duct will be used to lay the ground work for later considerations.

Deissler's equation, which is based largely on intuition, has been successfully applied both for turbulent momentum and thermal transport. It is shown below and is written in terms of a general eddy diffusivity, E.

$$E = n^2 uy \tag{3}$$

where

n = empirical constant

u = point velocity

y = distance from the wall

If a Reynolds number is defined as

$$Re_y = \frac{uy}{\nu} \tag{4}$$

and applying the definition of Equation 4 to Equation 3 results in the

following:

$$E = n^2 Re_y \nu \tag{5}$$

Equation 5 is a space or position oriented result that is of limited use in its present form since point velocities must be known. For flow in a circular duct of diameter, D, and average velocity, U, Equation 5 might be written as follows:

$$E = n^2 (\frac{y}{D}) Re_D \nu \tag{6}$$

Assuming u is proportional to U (this is true close to the wall), the proportionality factor is included in n. The same definition of the Reynolds number has been used with UD replacing uy in Equation 4 and thus the need for point velocity data has been eliminated. Equation 6 suggests that in the vicinity of the wall the dimensionless parameters, y/D and Reynolds number, and the fluid property kinematic viscosity, ν, are sufficient to describe the eddy diffusivity.

In checking the various reported experimental expressions for the lateral eddy diffusivity in a duct, it is generally reported as

$$E = 0.04\, Re_D \sqrt{f}\, \nu \tag{7}$$

where f = Fanning friction factor (24, p. 341; 28). Equation 7

offers some latitude since there are a number of expressions that can be used for the friction factor. For many heat transfer processes (27, p. 173) the following equation has been suggested:

$$f = 0.046\ Re_D^{-0.2} \tag{8}$$

while Blasius's equation for turbulent flow in ducts is also a widely used expression, i.e.,

$$f = 0.079\ Re_D^{-0.25} \tag{9}$$

When either of Equations 8 or 9 is used in Equation 7 the result fits the data within the experimental accuracy (14, 17, 44, 45).

Although Equations 6 and 7 are very different in form, this is not surprising as the region close to the wall comprises a very small portion of the entire cross-sectional flow area. The importance of the two equations is that they suggest possible limits on the lateral eddy diffusivity for the experimental system.

Deissler (9) has defined the region close to the wall for his eddy diffusivity model as that region for which $y^+ \leq 26$. The region beyond $y^+ = 26$ is the turbulent core. y^+ is a dimensionless length defined as

$$y^+ = \frac{\left(\sqrt{\frac{\tau_o}{\rho}}\, y\right)}{\nu}$$

For this work $y^+ = 26$ would correspond to about 0.020 inches from the subchannel walls. It is important to recognize that both flow regions will be important in the discussion of the results in this work.

Experimental measurements of eddy diffusivities for the turbulent core in ducts generally employ some graphical techniques for the determination of velocity, temperature or concentration gradients from the measured profiles (17, 28, 45). For open channel or wetted wall studies vaporization rates have been used to calculate the turbulent core eddy diffusivity (46). These methods of lateral diffusivity measurement are not readily applicable to the fuel rod bundle geometries.

A method similar in practice to the wetted wall eddy diffusivities studies is used and is based on the following single phase mixing model proposed by Rogers and Tarasuk (36). For the case of thermal transport between adjacent subchannels, i and j, it is postulated that lateral mixing is equal between the subchannels which is consistant with the eddy transport phenomena. An energy balance between the postulated lateral mixing and the eddy transport gives

$$w'_{ij} Cp(\bar{T}_i - \bar{T}_j) = b\rho CpE\left(\frac{d\bar{T}}{dz}\right)_{ij} \qquad (10)$$

where E is the average lateral eddy diffusivity and w'_{ij} is the subchannel natural mixing rate per unit length. If the average

temperature gradient between subchannels is approximated by a divided difference, the following is obtained:

$$\left(\frac{d\overline{T}}{dz}\right)_{ij} \simeq \frac{\overline{T}_i - \overline{T}_j}{z_{ij}}$$

Using this result Equation 10 becomes

$$w'^{t}_{ij} = \frac{\rho b E}{z_{ij}} \tag{11}$$

Equation 11 is thus the basic equation for turbulent subchannel mixing where z_{ij} is some sort of mixing distance between subchannels. The mixing distance was postulated by Rogers and Tarasuk to be a function of the rod spacing, b, and subchannel geometry with the functional relationship dependent upon experimental results. Note that Equation 11 could also be obtained for turbulent mass transport between subchannels and as such is a general expression for turbulent mixing between adjacent subchannels.

Using Equations 6 and 7 on the basic mixing equation, Equation 11 results in the following:

$$w'^{t}_{ij} = \frac{\rho b}{z_{ij}} n^2 \left(\frac{y}{D}\right) Re_D \nu \tag{12}$$

for the region in the vicinity of the wall and

$$w_{ij}^{t} = \frac{\rho b}{z_{ij}} (0.04\ Re_{D}\sqrt{f})\nu \qquad (13)$$

in the turbulent core. These results thus indicate the parameters that should be considered when studying subchannel mixing. Specifically the following parameters appear to be important:

1. b = rod spacing (note that it is conceivable that y in Equation 12 might be proportional to b and as such will not be considered independently)
2. D = subchannel diameter or in general subchannel geometry
3. U = subchannel average velocity.

The above leads to the question of what geometry must be used to adequately investigate subchannel mixing in rod bundles. Earlier investigators have considered multi-channel or entire rod bundle systems and two-channel and two-channel rod bundle simulated systems.

Moyer (30) and Rogers and Tarasuk (36) have analyzed most of the multi-channel experimental studies in an attempt to obtain a general subchannel mixing model. Both references note that the multi-channel experiments gave erratic results and were subject to subchannel transport from spacers, warts and lateral pressure imbalances because of poor system design. Rogers and Tarsuk (35) have since modified their original result by including results of some of the published two-channel experimental results. The results of both of these works may be found in Table 1.

Table 1. Turbulent subchannel mixing correlations.

Investigator	Geometrical System	Correlation**
Hetsroni (23)	simulated B (Figure 4b)	$\frac{w_{ij}^t}{\mu} = 0.0061\ Re^{0.98}$
Moyer (30)	multi-channel	$\frac{w_{ij}^t}{\mu} = \frac{\sqrt{2}}{40}\sqrt{f}Re(\frac{de}{d+b})$
Petrunik (32)	two-channel (Figure 4a)	$\frac{w_{ij}^t}{\mu} = 0.041\ Re^{0.783}(\frac{b}{de})$
Rogers and Tarasuk (36)	combined multi- and two-channel	$\frac{w_{ij}^t}{\mu} = 0.05(\frac{d}{b})^{0.57}Re^{0.68}$
Rowe and Angle (40, 41)	simulated rod bundle (Figure 4c)	$\frac{w_{ij}^t}{\mu} = 0.0036\ Re^{0.90}$
	simulated rod bundle (Figure 4d)	$\frac{w_{ij}^t}{\mu} = 0.0062\ Re^{0.90}$
Walton (52)	simulated rod bundle (Figure 4e)	same as Petrunik

** Mixing correlations are not necessarily in the original form, but are in terms consistent with this work.

The two-channel experiments are considered in two categories because of the significant geometric differences in the two systems. Figures 4a, 4b, 4c, 4d and 4e are the cross-sectional views of the various two-channel flow systems. Since the system used in this

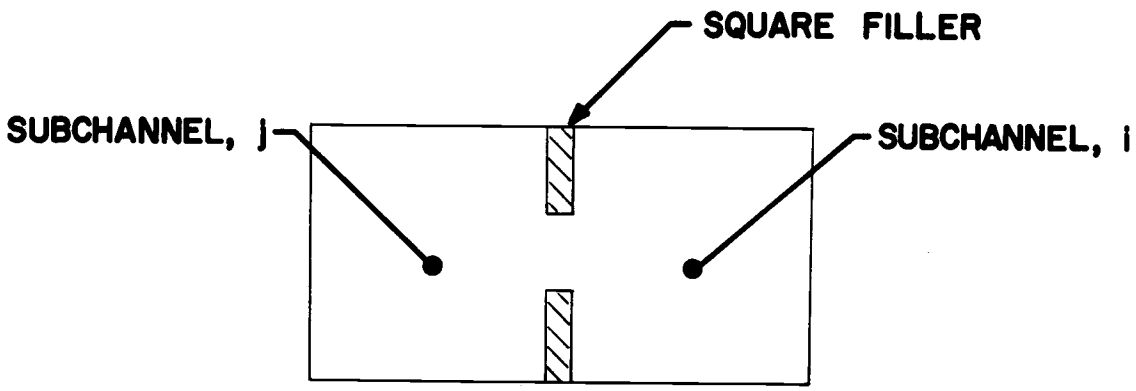

Figure 4a. Two square-square geometry.

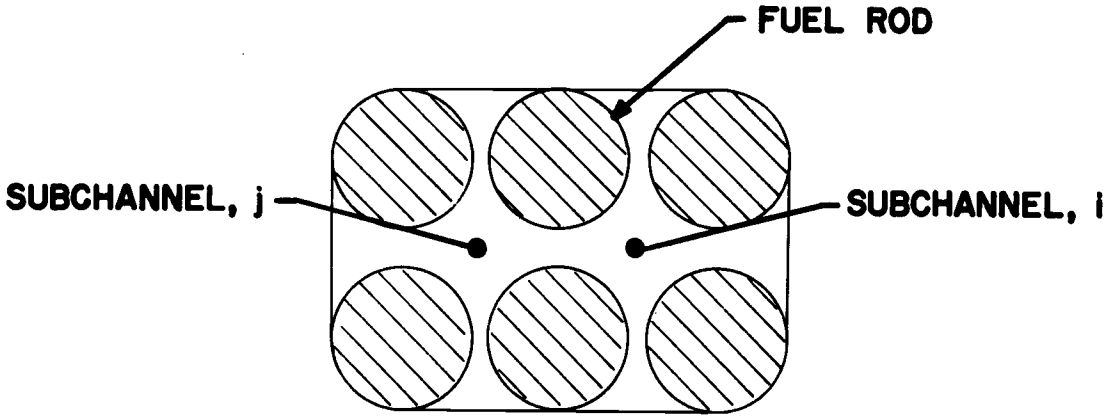

Figure 4b. Simulated rod bundle.

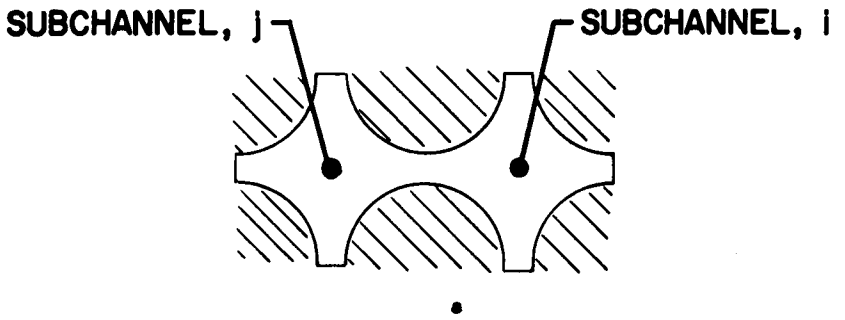

Figure 4c. Square-square simulated rod bundle.

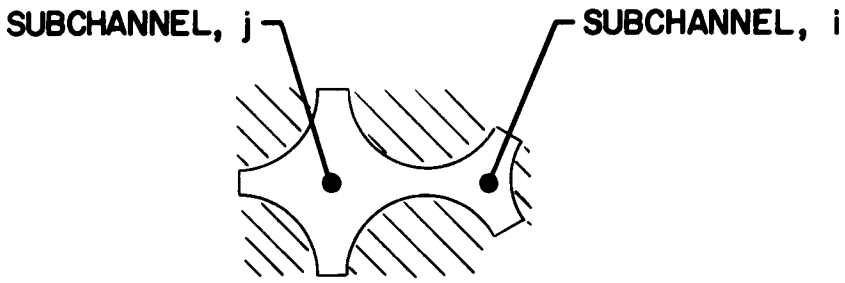

Figure 4d. Square-triangle simulated rod bundle.

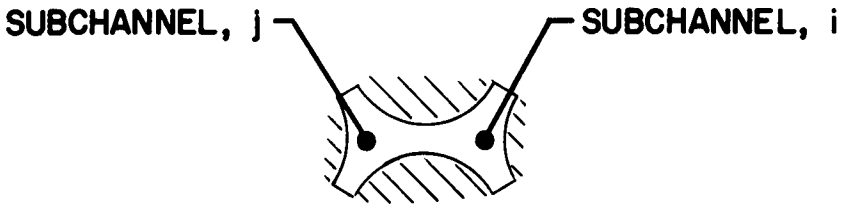

Figure 4e. Triangle-triangle simulated rod bundle.

study was a two-channel simulated geometry, particular attention will be given to each two-channel experiment.

Singleton (47, p. 60) used a two-channel system to make his exploratory investigation of the turbulent subchannel mixing process. His results indicated that the mixing rate between subchannels was approximately proportional to rod spacing. Petrunik (32, p. 48) also studied mixing in a two-channel system and found that his results could be correlated with St. Pierre's (49) equation, which recognizes the effect of subchannel spacing.

Rowe and Angle (40, 41), Hetsroni, Leon and Hakim (23) and Walton (52, p. 1) conducted various experimental studies on simulated two-channel systems. Their results indicated the geometry, whether it be square-square, square-triangle, or triangle-triangle, plays a significant role in the turbulent subchannel mixing rate. The experimental results of Rowe and Angle (40) suggest that rod spacing is not an important factor affecting the mixing. This contradicts the work of Walton, Singleton and Petrunik.

Both Walton and Petrunik found their work could be correlated by St. Pierre's correlation. This correlation was based on values of duct diffusivities and the general turbulent mixing expressed by Equation 11.

Table 2 lists the above mentioned experimental studies and the pertinent details of each work so that the scope of each is properly

Table 2. Description of previous two-channel investigations.

Investigator	Geometrical System	b/b	Coolant Fluid	Mass Flux $lb_m/hr\text{-}ft^2$	Mixing Techniques
Hetsroni (23)	square-square	0.25	water	$1.5\text{-}2.2 \times 10^6$	enthalpy balance
Petrunik (32)	rectangular	0.320	water	$0.2\text{-}2.0 \times 10^6$	KNO_3 tracer
	fillers	0.800	air	$0.1\text{-}1.0 \times 10^5$	CH_4 tracer
Rowe and Angle (40, 41)	square-triangle	0.036	water	$1\text{-}3 \times 10^6$	enthalpy balance and LiOH, D_2O and T_2O tracers
	square-square	0.152			
Singleton (47)	square-fillers	0.453	water	$0.3\text{-}2 \times 10^6$	dye injection
		0.840			
	semi-circle fillers	0.207			
		0.400			
Walton (52)	triangle-triangle	0.052	water	$0.37\text{-}1.07 \times 10^6$	KNO_3 tracer
			air	$0.16\text{-}3.06 \times 10^5$	CH_4 tracer

compared.

Subchannel Mean Velocity

The subchannel mean velocities for the two-channel systems, Figures 4a, 4c and 4e, are easily defined and as such are of limited concern to the experimentalist. This is not the case for the other systems, Figures 4b and 4d. The importance of knowing the subchannel average velocity for the system shown in Figure 4b will become apparent when the theoretical considerations for that system are presented later in this section. The ability of predicting and controlling the subchannel velocities for the system shown in Figure 4d is necessary if the experimental result is to have significance. If the velocities are not correct, diversion crossflow will result and the experimental work will have measured turbulent mixing plus or minus the diversion crossflow, depending on the experimental technique. Recalling Equation 1

$$-\left(\frac{dP}{dx}\right)Ac = \tau_o Pw$$

If this equation is considered for any multi-channel geometry, the following can be written for each subchannel within the system:

$$-\left(\frac{dP}{dx}\right)_i Ac_i = \tau_{o_i} Pw_i \qquad (14)$$

where

i designates the particular subchannel

i = 1, 2, . . . , N subchannels

Ac_i = subchannel cross-sectional area for i

Pw_i = subchannel solid surface in contact with the fluid for i.

The results of numerous studies on turbulent flow have shown that the friction losses from fluid motion are proportional to the kinetic energy of the fluid per unit volume. Shown mathematically it is

$$\text{Friction loss} = F \propto \frac{\rho U^2 Ac}{2g_c}$$

This equation is the basis of the definition of the Fanning friction factor, f.

$$F = \frac{f\rho U^2 Ac}{2g_c} \tag{15}$$

Noting that F/Ac is equal to the shear force at the wall, the following useful expression results:

$$\tau_o = \frac{f\rho U^2}{2g_c} \tag{16}$$

For non-circular flow areas it is useful to have a characteristic dimension for the desired geometry such as the diameter for the

circular geometry. The hydraulic diameter has proven to be a most adequate dimension. It can be defined as follows:

$$de = \frac{4(\text{flow area})}{\text{solid wetted surface}} \tag{17}$$

Note that $de = D$ in the case of a circular duct.

Applying Equations 16 and 17 to Equation 14 gives

$$-\left(\frac{dP}{dx}\right)_i = \left(\frac{2f\rho U^2}{g_c de}\right)_i \tag{18}$$

Assuming that the flow within each subchannel is fully developed (not varying with axial position) the following expression holds:

$$\left(\frac{dP}{dx}\right)_1 = \left(\frac{dP}{dx}\right)_2 = \ldots = \left(\frac{dP}{dx}\right)_N$$

or

$$\left(\frac{f\rho U^2}{de}\right)_1 = \left(\frac{f\rho U^2}{de}\right)_2 = \ldots = \left(\frac{f\rho U^2}{de}\right)_N \tag{19}$$

The friction factor can be expressed as a function of the subchannel Reynolds number of the following form:

$$f_i = aRe_{de_i}^{c} \tag{20}$$

where a and c are constants (51). Note for a constant temperature (isothermal) system the density, ρ, will be a constant and thus

may be canceled from Equation 19. Now applying Equation 20 to Equation 19, and considering a square-triangle two-channel geometry the following result is obtained:

$$\frac{U_1}{U_2} = \left(\frac{de_1}{de_2}\right)^{\frac{1+c}{2-c}} \qquad (21)$$

The constant, c, may generally be assumed to be -0.25 for the range of conditions investigated in this and the other studies cited (51). This procedure has been successfully used by several experimenters (2, 30, 31, 40) and has been shown by Tarasuk and Kempe, as cited by Rogers and Tarasuk (36) to be within ±5 percent of the actual subchannel mean velocity.

Theoretical Aspects

Derivation of the Subchannel Mixing Equations

Consider the turbulent flow of fluid in subchannels 1 through 8 of Figure 5. Subchannels 7 and 8 are connected through a rod spacing or gap, b, for a length, L, through which the turbulent transfer takes place. Although subchannels 7 and 8 are the subchannels of prime interest, the peripheral subchannels 1 through 6 must be considered. Hetsroni, Leon and Hakim (23) considered the geometry of Figure 5 as a strict two-channel system and made a two-channel

theoretical analysis rather than an eight-channel analysis that will also be considered here.

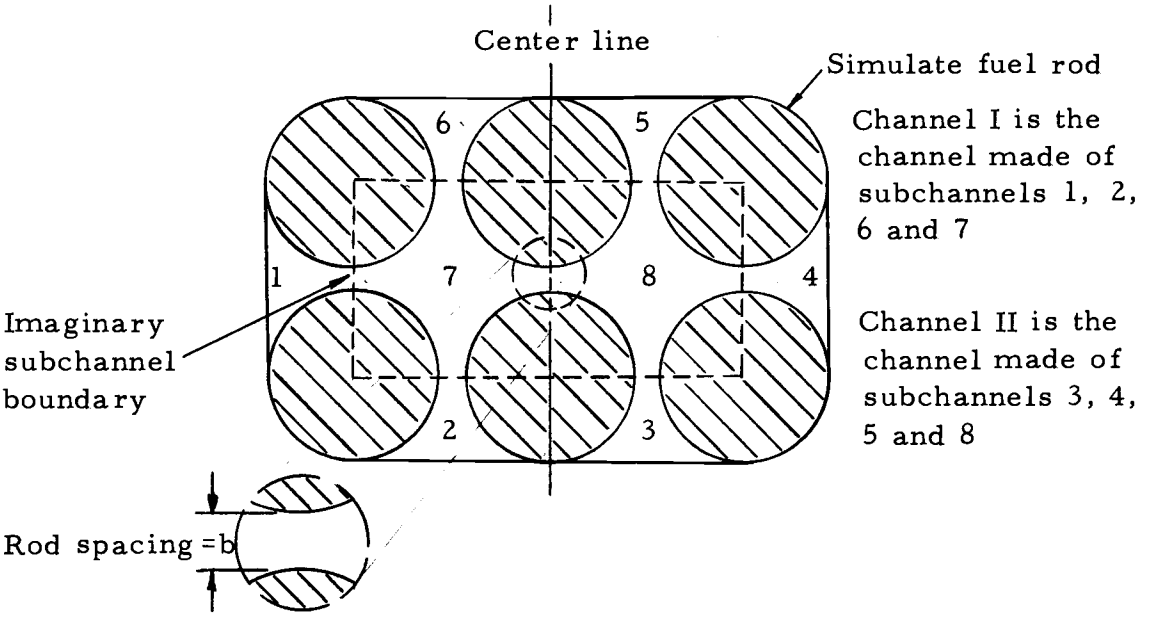

Figure 5. Test section cross-section and subchannel designation.

The experimental technique involves the addition of tracer to one-half of the geometry while the other half is maintained free of tracer initially. This sets the boundary conditions for the mathematical model used to describe the turbulent mixing. The mathematical model attempts to describe the dye (tracer) concentration change as a function of the axial position. A mass balance for the dye is written for each subchannel over a differential length of the axial position, L. The following basic assumptions were used in the analytical development:

1. There is no flow redistribution (diversion flow not considered).

2. The injection of tracer does not effect subchannel fluid properties or flow rates.
3. The molecular diffusion of the dye is negligible.
4. The dye is instantaneously mixed upon entering a subchannel.
5. The subchannel velocity profiles are fully developed.
6. The fluid transported between subchannels has the average dye concentration of the subchannel at the axial position where the eddy was initiated.
7. The total mass flow rate is the same for each half of the system.

Two-Channel Model

The two-channel analysis for subchannels 7 and 8 offers a simple and explicit result for the turbulent cross-flow mixing, w'_{78}. Recalling Figure 3 and making dye concentration mass balance over a differential length of each subchannel gives

$$-m_7 \frac{dC_7}{dL} + w'_{78}(C_8 - C_7) = 0 \qquad (22)$$

and

$$-m_8 \frac{dC_8}{dL} + w'_{87}(C_7 - C_8) = 0 \qquad (23)$$

where

$m_7 = m_8$ = mass flow rate in the subchannel.

When the continuity equation over the same differential length, dL, is considered in light of assumption 1

$$w_{78}^{t} = w_{87}^{t} \tag{24}$$

the boundary conditions for Equation 22 and 23 are

$$L = 0; \quad C_7 = 0; \quad C_8 = C_o \tag{25}$$

where

C_o = initial dye concentration.

An analytical solution for Equations 22, 23, and 24 with boundary conditions (initial conditions) of Equation 25 can be found by using Laplace Transforms (5, p. 19) and the result may be written explicitly for w_{78}^{t} as follows:

$$w_{78}^{t} = -\frac{m_7}{2L} \log_e\left(1-2\left(\frac{C_7^f}{C_o}\right)\right) \tag{26}$$

where C_7^f is the final dye concentrate for subchannel 7.

Eight-Channel Model

The dye concentration mass balance over a differential length gives the following set of equations when subchannel 2 = subchannel 6 and subchannel 3 = subchannel 5:

$$-m_1 \frac{dC_1}{dL} + \gamma w'_{78}(C_7 - C_1) = 0 \tag{27}$$

$$-m_2 \frac{dC_2}{dL} + \alpha w'_{78}(C_7 - C_2) = 0 \tag{28}$$

$$-m_3 \frac{dC_3}{dL} + \alpha w'_{78}(C_8 - C_3) = 0 \tag{29}$$

$$-m_4 \frac{dC_4}{dL} + \gamma w'_{78}(C_8 - C_4) = 0 \tag{30}$$

$$-m_7 \frac{dC_7}{dL} + w'_{78}(C_8 - C_7) + 2\alpha w'_{78}(C_2 - C_7) + \gamma w'_{78}(C_1 - C_7) = 0 \tag{31}$$

$$-m_8 \frac{dC_8}{dL} + w'_{78}(C_7 - C_8) + 2\alpha w'_{78}(C_3 - C_8) + \gamma w'_{78}(C_4 - C_8) = 0 \tag{32}$$

where α and γ are correction factors to account for rod spacing and geometrical considerations that might effect the turbulent mixing rate for these subchannels. The initial conditions for this system of equations are

$$C_1 = C_2 = C_7 = 0; \quad L = 0 \tag{33}$$

$$C_3 = C_4 = C_8 = C_o; \quad L = 0 \tag{34}$$

It is impractical to present an analytical solution for the above system of equations. In view of this, the Runge-Kutta-Merson (RKM) numerical algorithm (15) was used and solutions were obtained on the Oregon State University CDC 3300 computer. This algorithm was

used because of its capability of making stepsize adjustments during a calculation so as to maintain a set solution accuracy. This accuracy was set at 0.00001 for all the calculations considered in this study.

Since w_{78}^{t} is not an explicit variable in the system of equations, an iterative scheme was necessary to obtain its value. This technique used the exit dye mass balance of the initial untraced channel as the solution check point.

EXPERIMENTAL EQUIPMENT

The experimental system and associated equipment used for this investigation were located in the basement of the Chemical Engineering Building at Oregon State University. Figure 6 shows a schematic of the experimental test loop. The major components of the test loop included: the test section; dye injection system; gear pump and motor; and various measuring devices. All the components with the exception of the gear pump and motor were assembled or designed specifically for this investigation.

Water from the city water main was used for all experimental runs and was brought to the desired operational temperature through the addition of live steam to a constant head tank. The test loop was an open system and the used water passed to the drain or to the fluorometer and then to the drain upon leaving the system.

Test Section

The test section can be subdivided into the two following regions: (a) inlet and exit headers and (b) simulated rod bundle section. Figure 7 is a line schematic of the entire test section.

Inlet and Exit Headers

For this system (test section) the inlet header had two primary

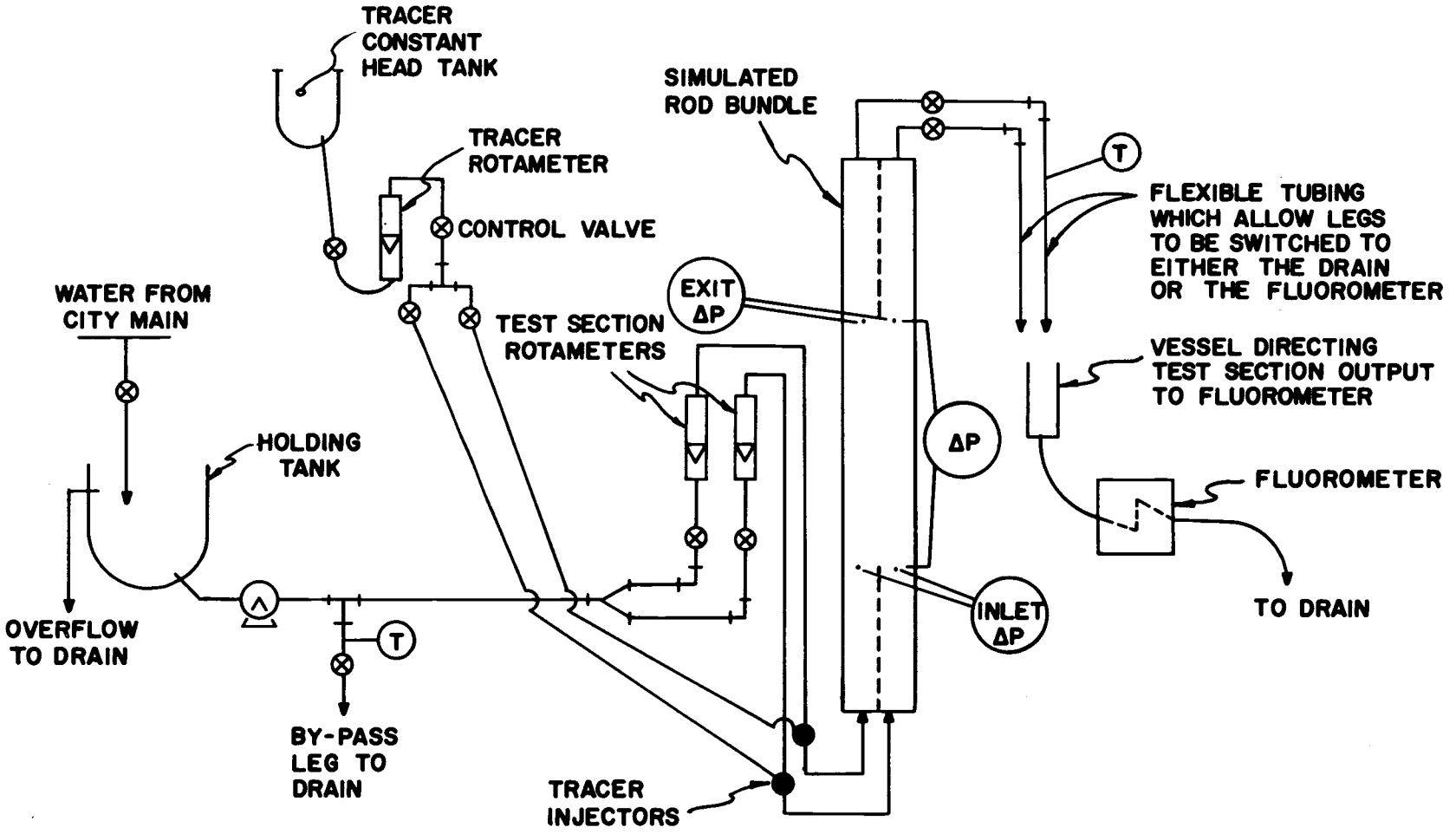

Figure 6. Schematic of the experimental test loop.

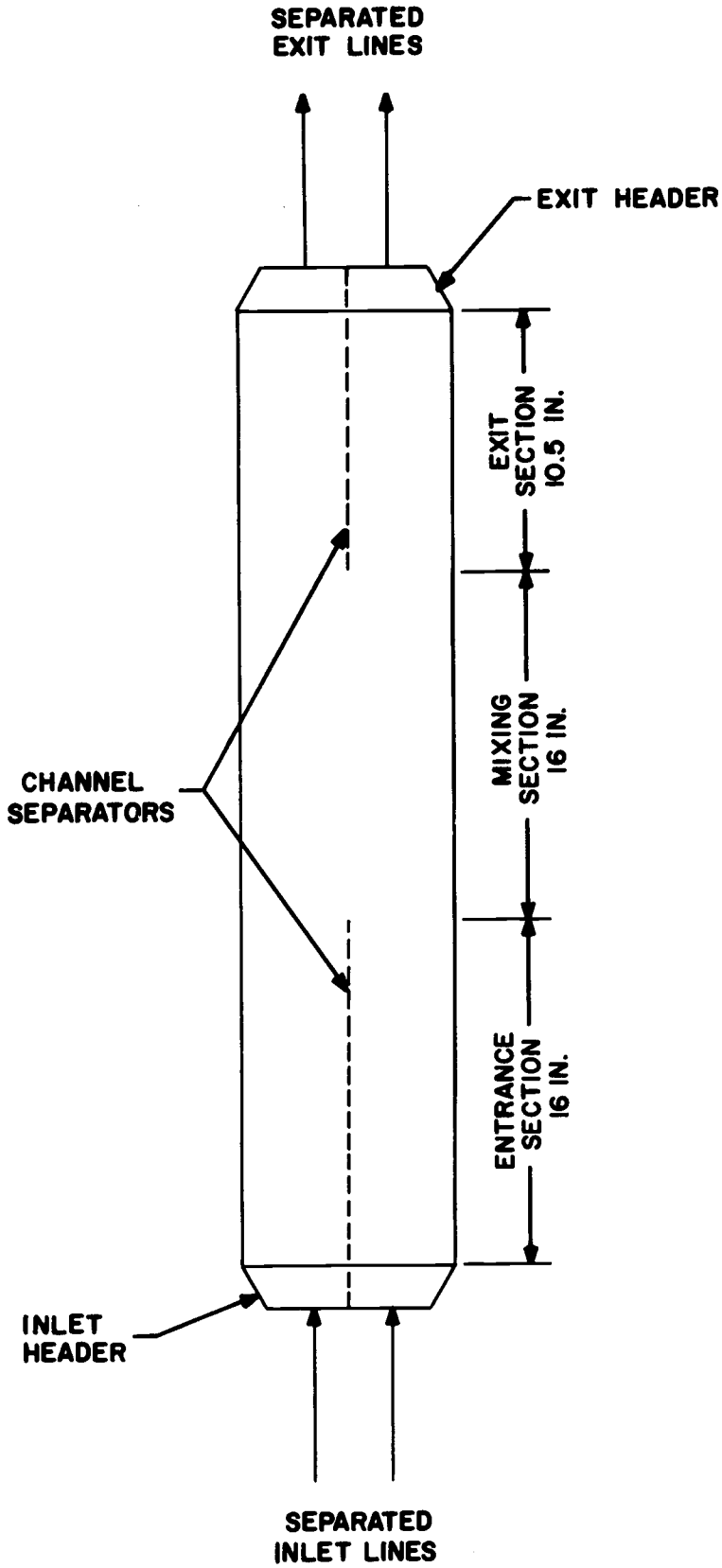

Figure 7. Schematic of the experimental test section.

functions: (1) to allow a smooth transition between the inlet plumbing and the simulated rod bundle geometry and (2) to increase the system entrance length. The exit header allowed a smooth transition between simulated rod bundle geometry and the exit plumbing. Figure 8 shows the exit face of the inlet header and Figure 9 shows a close-up of this header. Note that both headers are geometrically similar and dimensionally the same except for the separator tongue length.

Each header was constructed of eight 1-inch nominal outside diameter brass rods 3.5 inches in length, two 3/4-inch male connector Swagelok fittings, two pieces of 3/4-inch diameter refrigerator copper tubing 18 inches in length, a 1/8 x 7 1/2 x 6 1/4-inch brass kick plate, and a 316 stainless steel separating tongue. The separator was 1/32 x 1 7/16 x 19 1/2 inches for the inlet header and 1/32 x 1 7/16 x 14 inches for the exit header. The exit header had two 3/4-inch gate valves for back pressure control as fittings on the copper tubing lines.

The construction of each header was accomplished by silver soldering the various materials into the desired unit. The initial step was to silver solder four brass rods together such that the exit face of the inlet header (inlet face of the exit header) had a rod spacing of 0.100 ± 0.010 inches and the inlet face had the four rods touching one another. This design represented the average dimensions of the geometries to be investigated. The two faces were then machined on

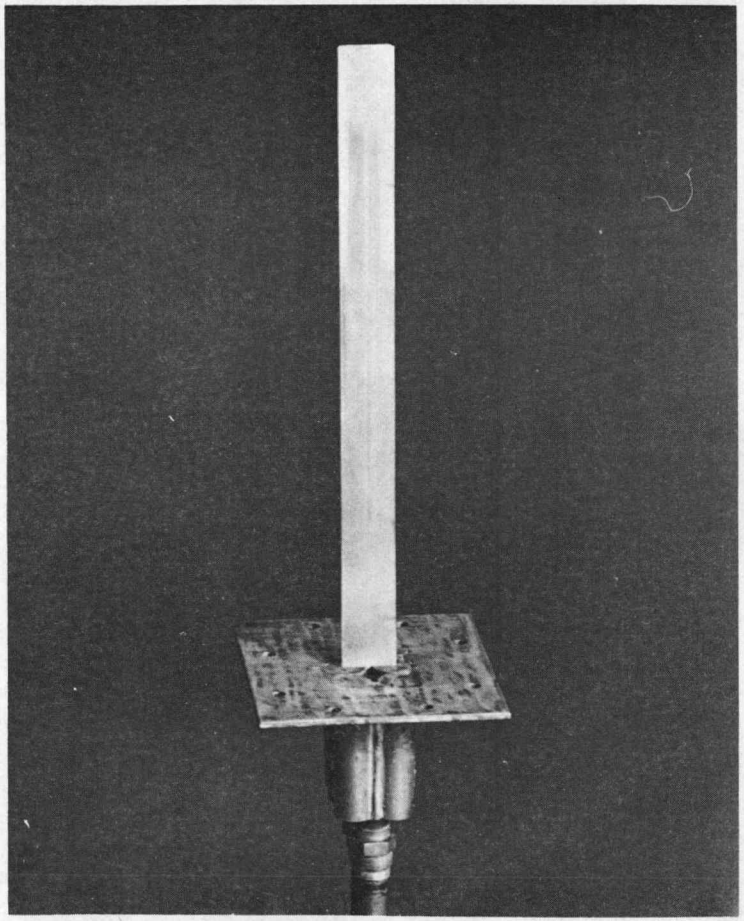

Figure 8. Inlet header.

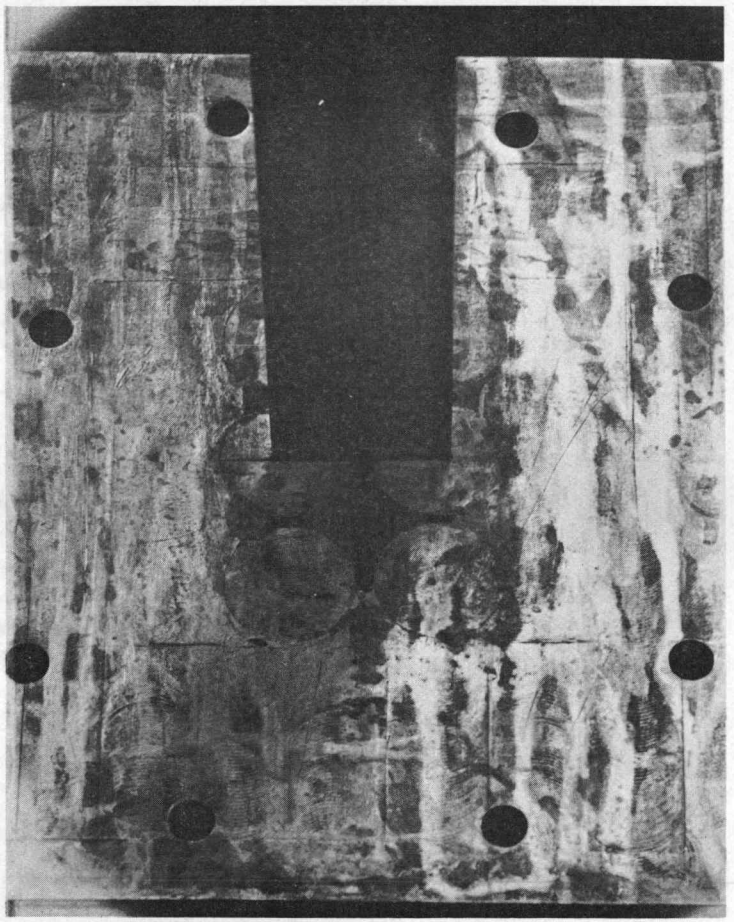

Figure 9. Close-up of the inlet header.

a milling machine such that the two faces were square and parallel to one another. This four rod arrangement was further machined to the geometry shown in Figure 10. Two such pieces, with the addition of the separator tongue, were then silver soldered together to make the main body of the headers. Each tongue was honed to a knife edge at the edge exposed to the flowing fluid.

The inlet of the inlet header (exit of the exit header) was then reamed to 9/16 inches at each of the inlet ports. The Swagelok male connectors, with the tubing legs already soldered in place, were then soldered to the header geometry. The header design was completed with soldering of the kick plate. The finished header allowed the brass rods to fit flush to the simulated rod bundle section (see Figure 11).

The eight 5/16-inch holes through the face of each kick plate were for the 5/16-inch cold rolled steel tension rods that were used to tighten the headers to the rod bundle section (see Figures 8 and 9).

Simulated Rod Bundle

The simulated rod bundle section was constructed of plexiglass (acrylic plastic). Figure 12 shows the cross-section of the system. Note that sides A and C (see Figure 12) were used for all rod spacings or gaps considered in this investigation while the particular design dimensions for sides B and D were used to control the

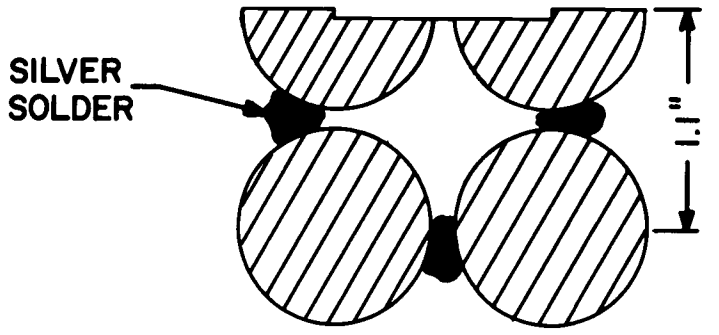

END VIEW
FACING TEST SECTION

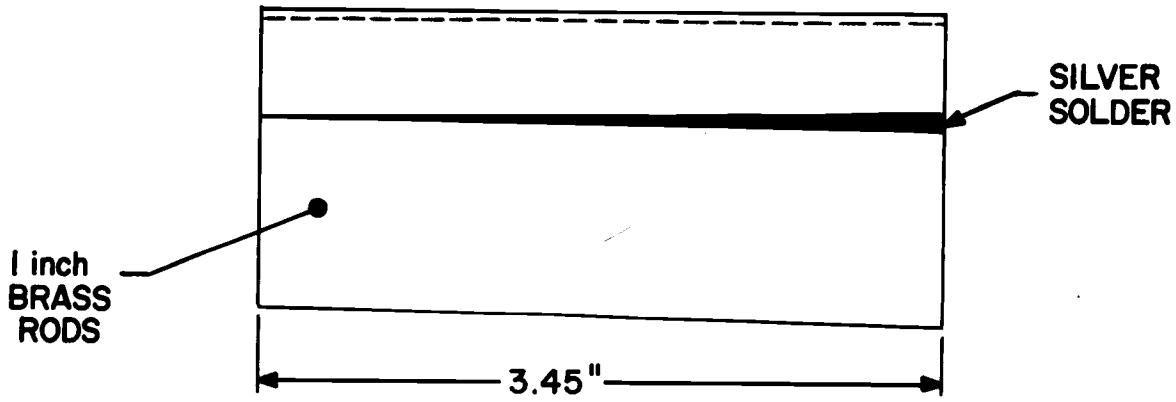

SIDE VIEW

Figure 10. Partial construction of the flow header.

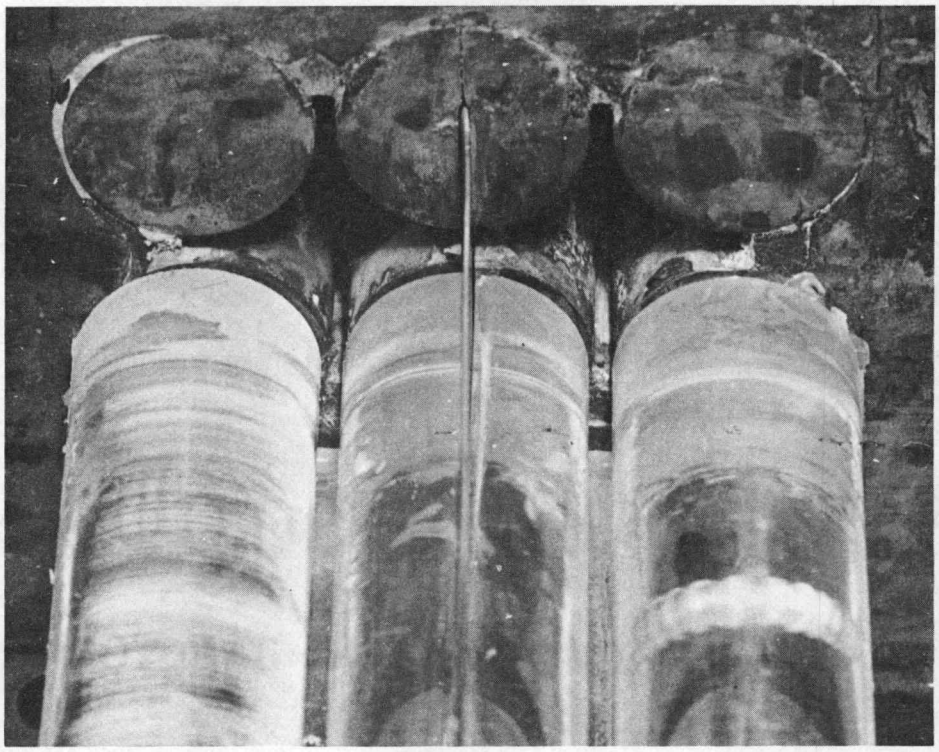

Figure 11. Partial assembly of the test section.

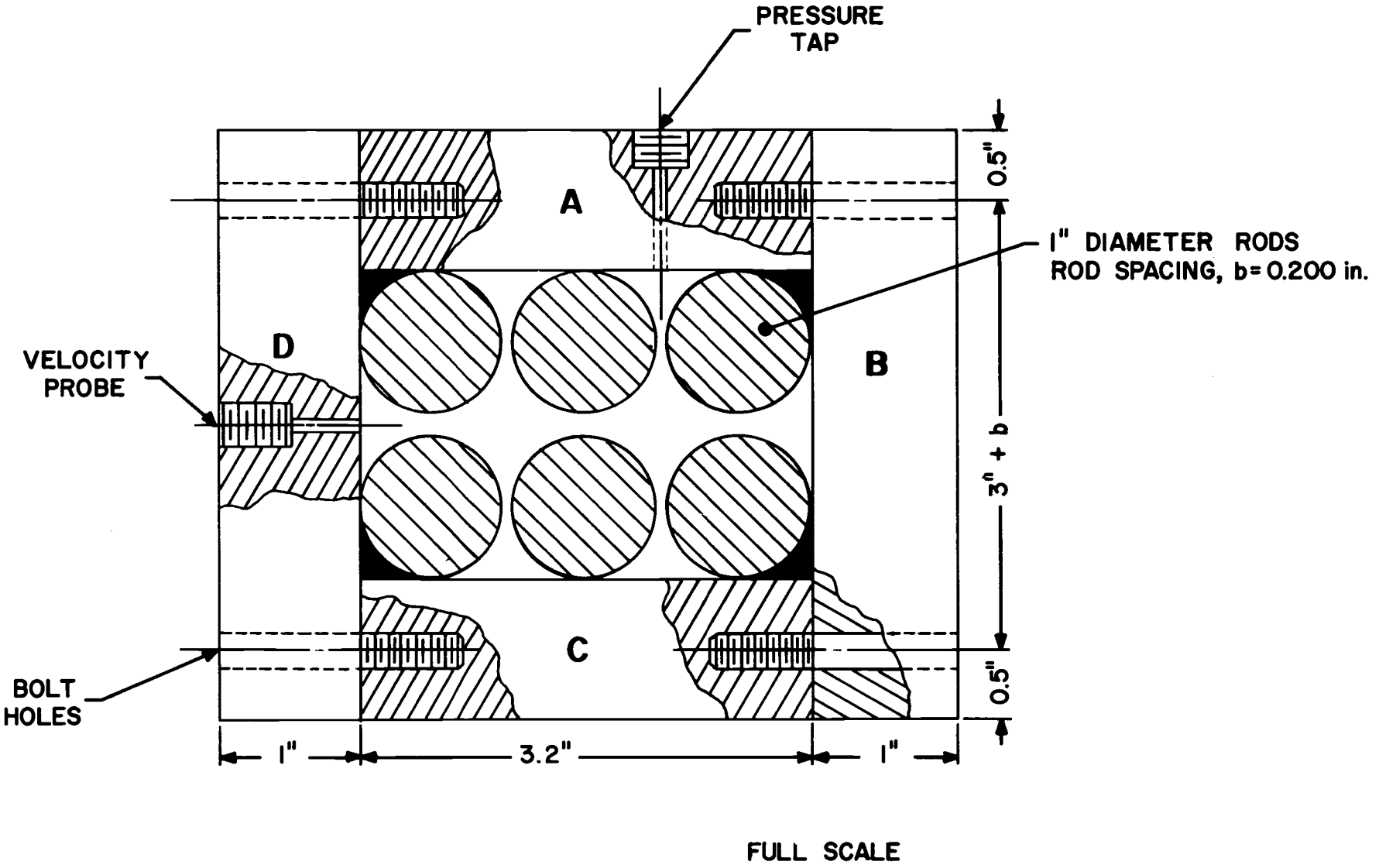

Figure 12. Cross-section of the experimental test section.

various gap spacings.

Construction of sides A and C was obtained by welding (gluing) three 1-inch nominal outside diameter plexiglass rods to a 1-inch thick piece of plexiglass flat stock. The side (three rods and flat stock) was then machined to the desired width. Since the dimensions of the flow channels were a major concern with this project, much care was taken in the selection of materials and methods of construction.

The rod separation for sides A and C was obtained by placing two pieces of shim stock that measured 0.097 ± 0.003 inches between the three rods for the entire length of the side. The shim stock was placed at the sides of the center rod and then the outside rods were snugged up with C-clamps. The three rod, two shim stock system was then held flush to the flat stock surface with heavy lead bricks. One end of this system was then elevated and the three rods were welded with methyl-ethyl-ketone solvent to the flat stock surface. The machined width of the side was 3.200 ± 0.005 inches. This width allowed sides B and D to fit flush to the surface of the outside rods.

The rod spacing between sides A and C was another dimension of major concern. Since the initial rod spacing (gap) would set the general integrity of all later gaps, the method used to set this particular dimension will be considered.

Even though a careful choice of materials was made, the tolerances of the flat stock and the gluing depth variation required that some unusual technique be used for the initial design. The first step was the measurement of the distance between the center rod and the exterior face of sides A and C. The four sides of the simulated rod bundle were then placed in the desired shape and held in place with mechanical clamps. The rod gap was set by placing shim stock between the center rods of sides A and C. When the desired gap tolerances were obtained (this required some pressure on sides A and C) the holes for the 1/4-20 coarse thread 1 1/2-inch bolt holes were drilled and tapped. Note the system was dismantled only after all the bolt holes had been drilled.

Table 3 shows the results of these efforts plus the results of other designs.

Table 3. Rod spacings for the mixing section.

Mean Rod Spacing	Standard Error
0.011	0.0005
0.028	0.0008
0.063	0.0005
0.127	0.0005
0.228	0.0006

The bolt holes were tapped only in sides A and C so that sides B and D could be tightened to them. The bolts were placed

three inches from each end and approximately every six inches thereafter. This design provided the necessary compression between the sides to insure the sealing of the system. When the system was put together, one inch diameter washers were used between the bolt heads and the plexiglass walls.

The final steps in the system construction was the machining of the header tongue slots in the center rods of sides A and C and the machining of the test section to the desired length, 42.5 ± 0.010 inches.

The separator tongue slots were cut on a milling machine with a 1/32 x 3-inch diameter slitting saw blade to a depth of one inch. The depth of the cut allowed for the full range of rod spacings without further adjustments to the system.

The flow separators of the two headers marked the beginning and end of various flow sections within the plexiglass test section. The entrance region was 16.0 ± 0.03 inches in length, which was a sufficient length for the full development of the velocity (53) and concentration (7) profiles. The inlet header was an entrance length safety factor. The separator provided a physical barrier to channel contact and thus eliminated any mixing until the mixing section (see Figure 11).

The end of the inlet separator tongue marked the beginning of the channel mixing section. This section was 16.0 ± 0.03 inches in

length and was where the turbulent mixing between channels took place.

The beginning of the exit separator marked the beginning of the exit section. This section terminated the turbulent mixing between channels and provided sufficient length to minimize the effects of exit flow disturbances on the mixing results. The exit section was 10.5 ± 0.03 inches in length and also split the channel flow so that the exit concentrations from the channels could be measured.

As implied above, the initial rod spacing was the only design for which the outlined construction steps were followed. All the other designs required that sides B and D of the original design be used as a pattern. The new rod spacings were obtained by using shim stock of the desired thickness between the original and new side. The procedure offered a very effective method of increasing or decreasing the bolt hole separation and thus varying the rod spacing. Although the method was very tedious and time consuming, the result was very successful.

Several methods of sealing the test section were attempted but none proved as effective as General Electric Silicone clear glue. A thin bead of the glue was applied to all contact surfaces moments before the test section was put together (tightening of all bolts and tension rods). The glue was allowed to cure for 24 hours before the system was used. The glue was easily removed after being used and

as such all surfaces were clean before construction of each new test section.

Dye Injection System

This system operated by gravity feed from a constant head tank elevated approximately 40 feet above the injection point to the test section. The dye flow rate was measured with a Fisher-Porter Tri-Flat 1/16-20 rotameter with a tantalum float. This rotameter had a flow range of 0-20 ml/min which was controlled with a Nupro-S micro-metering valve.

As Figure 6 indicates the dye could be injected into either side of the test section. This was controlled by two off-on 1/4-inch Whitey brass ball valves.

The inline injection system (one for each inlet leg of the header) was designed with a downstream inline mixing zone to insure complete mixing of the dye. The inline mixer was a small mesh screen placed normal to the flow. The dye was injected through a single 1/16-inch diameter stainless steel tube located in the center of the flow area.

The flow lines from the constant head tank to the injection rotameter and from the switching valves to the injectors was 1/4-inch outside diameter black polyethylene tubing. The black tubing was used to assure that there would not be any photochemical effects on the dye.

With a constant head tank, an even (unpulsed) flow of dye could

be injected into the system.

Gear Pump and Motor

The water for this study was taken from the city main and held in a constant head tank (holding tank). The primary function of this tank was to eliminate line pressure surges that often occur in the city main and as a heating vessel to bring the water to the desired temperature. The gear pump was driven by a General Electric AC induction motor that provided water at 31 gal/min at a maximum head of 50 psi. The inlet and outlet lines to the pump were 1 1/2-inch nominal outside diameter copper piping. The total flow was split with a 1 1/2-inch copper tee before it entered the flow lines leading to the test section rotameters.

The volume flow to the test section was controlled with a by-pass leg to the system (see Figure 6).

Measurement Systems

Fluid Flow Measurement

Two Fisher-Porter 1 1/2-27 (tube number) rotameters were used to measure the mass flow rates to the test section. Although the by-pass leg offered the secondary flow control to the test section, each rotameter had an upstream gate valve for primary control. Each

rotameter was calibrated for a flow range of 17 lb_m/min to 140 lb_m/min (see Appendix B). The exit from each rotameter was necked down from 1 1/2 to 3/4-inch such that the plumbing from rotameters to test section was 3/4-inch tubing.

The dye injection system rotameter was used to measure the volume flow rate of the dye to the system and was calibrated for a flow range of 1 ml/min to 20 ml/min (see Appendix B).

Pressure Gradient Measurement

Three manometers inclined at 15° from the horizontal were used to measure various test section pressure gradients. Two of the manometers measured static pressure gradients between the adjacent channels and were used to pressure balance the flow rates within the mixing section of the test section. The third manometer measured the pressure drop for the mixing section. This measured value was used later to calculate the friction factor.

The inclined manometers were used because the pressure gradients measure were between zero and five inches of water head and a high sensitivity was needed. As a means of further increasing the sensitivity of the two fluid (water over manometer fluid) inclined manometers, 2.96 specific gravity manometer fluid was used as the measuring fluid.

The pressure lines were 1/4-inch outside diameter polyethylene

tubing leading from the static pressure taps on the test section to surge pots that were elevated above the pressure taps.

The pressure balance taps were 1/4 of an inch above and below the inlet and exit channel separators for each channel in the mixing section. The same static taps were used to measure the pressure drop for one of the channels. Figure 12 shows the tap location on the cross-section.

Temperature Measurement

The temperature measurement of the fluid was accomplished with two mercury filled thermometers. The temperature measurements were made both up and down stream of the test section.

Dye Concentration Measurement

The dye or tracer, rhodamine B, was detected with a G. K. Turner model 111 fluorometer (see Appendix C). The split flow leaving the test section passed through a holding tank before it entered the fluorometer. The holding tank was built such that either or both exit test section streams could be analyzed. The fluorometer was operated continuously and the resulting tracer concentration measurement was the exit mixing-cup concentration for the analyzed flow.

The tracer used for this experimental study was DuPont

Rhodamine TLX-670 solution that has the following composition as reported by the E. I. DuPont Company:

DuPont Rhodamine B Base	20 ± 1%
Ethyl Alcohol SD-3A	28
Ethylene Glycol	20
Water	32

Because of the fluorescent property of rhodamine B, it can be detected with quantitative accuracy in concentrations less than 1 part/billion (4, 16).

This particular system operates on a continuous basis and as such the common sampling train was eliminated from the experimental routine.

Bias Pressure Measurement

Since diversion cross-flow was an important consideration in this investigation, some pressure biased experiments were considered. To insure that all investigations were consistent, a Pace pressure transducer (model KP15) and indicator (model CD25) were used. This equipment was also used in some velocity profile work considered in this study (see Appendix D).

Velocity Profile Measurement

A pitot tube was used to measure impact pressures at the

midpoint of the mixing section which was sensed with a Pace pressure transducer. The pitot tube was made of 0.028-inch outside diameter stainless steel tubing. A 0.010 ± 0.003-inch diameter hole was drilled in the side of the tubing which was the pressure sensing point of the pitot tube. The end exposed to the fluid was sealed.

The pitot tubes position in the test section was adjusted with a screw device that was mounted directly to the test section. The position was measured with a micrometer which was mounted on the screw device.

EXPERIMENTAL PROGRAM

The objective of this investigation was to determine the effect of rod spacing (subchannel gap spacing) and subchannel flow rates on the turbulent cross-flow mixing. The literature survey and theoretical section indicate that both of the afore mentioned parameters play an important role in the cross-flow mixing. The importance of pressure gradients between channels and subchannel geometry was also pointed out. Although the above mentioned system variables are common ones for most fluid dynamic studies, the use of the dye tracer system increased the complexity of this system by the addition of some new variables. Since the volume of water to be used in this work eliminated the use of distilled or even de-ionized water because of the associated cost, the general stability of the tracer in the water supply had to be considered before the final choice of tracer material could be made.

System Geometry

It is impractical to consider the rod spacing independent of the overall channel cross-sectional flow area. The geometrical considerations involve the accurate measurement of the channel and subchannel cross-sectional area and wetted surface. From these two geometrical values a hydraulic diameter can be found and in turn

through the use of Equation 19 the subchannel average velocity determined. The importance of the rod spacing is obvious when Equations 12 and 13 are considered.

Prior to the construction of the simulated rod bundle system, a diameter measurement of each of the plexiglass rods was made at 20 locations along the rod length with a caliper type micrometer. The rods had an average rod diameter of 1.001 ± 0.003 inches. It has already been noted that the separation between the rods glued to the flat stock was 0.097 ± 0.003 inches. With these measurements plus the rod gap spacing measurement, the subchannel cross-sectional areas and wetted parameters could be calculated.

The rod gap spacing was measured in triplicate with a variable anvil Starret micrometer (224A-R1) at nine positions along the mixing section.

The distance between the center rod and the exterior face of sides A and C of Figure 12 was measured at the centerline of the rod. Note that the position of the measurement along the mixing section was marked so that the same points could be used in all later measurements. The next step was the assembly of the test section and the measurement of the distance between the exterior test section faces of sides A and C. The above measurement minus the sum of the distance measurements of sides A and C gave the gap spacing for each design and completed the geometrical description of the

test sections.

Before and after each set of measurements the micrometer was compared against a standard length. Table 4 lists the various geometrical lengths used in this work.

Water Mass Flow Rates

The mass flow rates entering each half of the test section were measured with two calibrated rotameters. The mass flow rate range considered gave a three fold range of Reynolds numbers.

Channel Pressure Gradients

The diversion cross-flow between channels can be obtained when pressure gradients between the channels exist. The elimination of this possible pressure imbalance is necessary if accurate turbulent mixing measurements are to be obtained. The measurement of the static pressure gradient between subchannels 7 and 8 at the inlet and exit of the mixing section has been a means of determining if pressure imbalances exist. The elimination of such imbalances have been made through inlet and exist flow adjustments and thus the accuracy of the experimental results depends to some extent upon the pressure gradient measuring device. Because of the continuous tracer analysis routine used in this investigation, an additional method of pressure balancing the system was available which gave the experimental

Table 4. Geometrical lengths for the experimental simulated rod bundles.

Rod Spacing (gap) Inches	Ac_I Square Inches	Ac_7 Square Inches	Ac_2 Square Inches	Ac_1 Square Inches	de_I Inches	de_7 Inches	de_2 Inches	de_1 Inches
0.011	0.748	0.323	0.156	0.113	0.270	0.411	0.234	0.175
0.028	0.775	0.342	0.156	0.122	0.280	0.435	0.234	0.187
0.063	0.831	0.380	0.156	0.139	0.299	0.484	0.234	0.211
0.127	0.934	0.450	0.156	0.171	0.334	0.573	0.234	0.253
0.228	1.095	0.561	0.156	0.222	0.388	0.714	0.234	0.316

results increased impetus.

Rhodamine B Dye

The primary requirement for the tracer system was that some method of continuous analysis be applicable. This requirement eliminated most of the experimental systems used by earlier investigators. It did suggest the possible use of various spectrophotometer or colorimeter analysis techniques. These methods were soon eliminated from consideration because of their limited range of concentration detection, turbidity or background effects and the potentially high cost of the tracer needed for the investigation.

The use of fluorescent dyes as tracers has been in wide use by various investigators of basic hydrological studies (time of travel, turbulent dispersion and etc. of rivers, streams and etc. (19)) but has had limited use by other fields of research. The fluorescent material was sensed by a fluorometer which had a reported dye detection capability of 0.1 parts/billion (4). The versatility of the equipment was such that it could be set up for batch or continuous operation. The high detection capabilities plus the continuous analysis made the system ideal for the present investigation and as such the tracer technique was reduced to finding a suitable fluorescent material for the system.

Several fluorescent materials were examined but rhodamine B

was chosen because it was readily available and exhibits a high degree of stability. Fenerstein and Selleck (16) have made an extensive investigation of the effects of pH, temperature, storage time degradation and photochemical effects of fluorescence. The fluorescence of rhodamine B in distilled water is as follows:

1. It is independent of pH in the range of $5 < pH < 10$.
2. It is decreased by 1 percent/°F with increasing temperature. The reverse holds for decreasing temperatures.
3. It is not affected by storage time unless exposed to sunlight.
4. It is degraded by 50 percent after direct exposure to sunlight for 31 hours.

All of the above effects were accounted for in this work either physically or by choice of materials. There still remained a question as to the effect the chosen fluid (city water) system would have on the tracer.

Possible pH effects could be eliminated simply by not operating on those days when the limits of the pH stability range were exceeded. However the pH never varied appreciably from 7.0 during the entire experimental program as determined by a Beckman pH meter.

Temperature was a controlled variable and remained constant throughout a series of runs. The difference between the systems fluid temperature and tracer temperature was never more than 3°F. This was the maximum temperature difference in the ambient and

system fluid conditions.

The dye constant head tank was shielded from all light sources, natural and artificial, thus eliminating possible photochemical degradation. The tracer solution for the constant head tank was also made up with distilled water to eliminate possible chemical degradation.

The possible chemical degradation of the dye from impurities in the city water system was studied through a batch analysis of several tracer samples.

A sample of dye and city water were mixed and the fluorescence was immediately measured with the fluorometer and the time and temperature were noted. The fluorescence was measured at regular time intervals and recorded. This procedure was followed for several dye sample sizes (tracer concentrations) before and during the experimental program. The tracer never showed a fluorescence decrease greater than 2 percent and this resulted after a time elapse of 30 to 40 minutes after the first fluorescence reading. Since the dye residence time (the time between injection and analysis) would be of the order of a minute, the water-tracer system was considered satisfactory.

EXPERIMENTAL PROCEDURE

The following preliminary procedures were performed before each experimental run:

1. The fluorometer was turned on and allowed to warm up for 30 to 40 minutes.
2. The water holding tank was filled and the pump started with the by-pass valve open and the valves to the system rotameters closed. The city water main feed line to the holding tank was adjusted so that the water level remained constant in the holding tank.
3. The live steam was added to the water in the holding tank. The steam flow rate was adjusted to give a water temperature at the by-pass between 67 and 69° F.
4. The valves to the test section were fully opened.
5. The purge valves to all the manometers were opened and the pressure lines were purged for 30 to 40 minutes.
6. The flow of water to and through the fluorometer was checked and adjusted if necessary.
7. The tracer injection was momentarily operated to insure that it was working correctly.
8. At the end of the warm-up period for the fluorometer, all the manometer purge valves were closed and the fluorometer was

balanced to read zero fluorescence.

The following procedure was used in recording the necessary data for each gap spacing:

1. The rotameters were adjusted to the same scale readings and the exit pressure gradient was zeroed. The rotameters were checked again and the inlet pressure gradient checked and rezeroed if necessary by adjusting the inlet and exit valves to the test section.
2. The ambient temperature and the pH of the water were measured.
3. A series of tracer inlet concentration runs were made before and after the actual mixing runs. These runs considered 6 to 10 inlet mass flow rates that would cover the mass flow range to be investigated and a range of tracer flow rates. The following variables were recorded at each mass flow rate: (a) test section rotameter scale readings, (b) tracer scale rotameter readings, (c) fluorometer sensitivity, (d) fluorescence reading, (e) channel traced and (f) temperature of the water.
4. The turbulent mixing runs were not accepted until the exit fluorescence from both channels were within ±3 percent for the same rotameter settings for the tracer injection into either channel. Only one channel was traced at a time and

the recorded fluorescence was for the initial untraced channel. The recorded variables included those of step 3 plus the high and low leg readings from the mixing length pressure gradient manometer.

5. The pressure biased runs were operated under the same techniques used for the turbulent mixing runs (steps 1 through 3) but required that a constant pressure bias be maintained for the mass flow rate ranges considered. The pressure bias was maintained by adjusting the exit valves to the test section.

6. The velocity measurements were made with a balanced system. The general data recorded included: (a) system rotameter scale readings and (b) fluid temperature. The pitot tube position and transducer reading for each measured position was also recorded. As a general rule only the high and low mass flow rates for a particular geometry were considered.

CALCULATIONS

The observed data from this study are shown in Appendix E. These were reduced with a digital computer to the results shown in Appendix F. The tracer concentration from the constant head tank although shown as observed data was actually a calculated result that was made with a desk calculator.

Calculations Using Observed Data and Calculated Data

In order to calculate cross-sectional flow areas and corresponding hydraulic diameters the rod spacing must be used (see Figures 5 and 12). The following equations were used to calculate the various cross-sectional flow areas:

$$Ac_I = Ac_{1,2,6,7} = Ac_{II} = Ac_{3,4,5,8}$$

$$= (2d+b)(1.5d+0.097) - 2.5(\frac{\pi}{4}d^2) - 0.5d^2 \qquad (35)$$

$$Ac_7 = Ac_8 = (d+0.097)(d+b) - \frac{\pi}{4}d^2 \qquad (36)$$

$$Ac_1 = Ac_4 = (d+b)\frac{d}{2} - \frac{\pi}{8}d^2 \qquad (37)$$

$$Ac_2 = Ac_3 = Ac_5 = Ac_6 = (d+0.097)\frac{d}{2} - \frac{\pi}{8}d^2 \qquad (38)$$

The following equations were used to calculate the wetted surface for each subchannel:

$$Pw_I = Pw_{1,2,6,7} = Pw_{II} = Pw_{3,4,5,8} = (2.5\pi+3)d + 2(0.097) + b \tag{39}$$

$$Pw_7 = Pw_8 = \pi d \tag{40}$$

$$Pw_1 = Pw_4 = 1.5\pi d + b \tag{41}$$

$$Pw_2 = Pw_3 = Pw_5 = Pw_6 = 1.5\pi d + 0.097 \tag{42}$$

Equation 17 was used to calculate the hydraulic diameter for each subchannel, i.e.,

$$de_i = \frac{4Ac_i}{Pw_i} \tag{43}$$

The total mass flow rate, m, to the test sections was calculated from the calibration curves for the test section rotameters (see Appendix B). The average velocity for each half of the test section was then calculated from the measured mass flow rate for that half of the test section, i.e.,

$$m = m_{1,2,6,7} + m_{3,4,5,8} \tag{44}$$

and

$$U_I = U_{1,2,6,7} = \frac{m_{1,2,6,7}}{\rho A_{1,2,6,7}} \tag{45}$$

The average velocities for each subchannel was then calculated by Equation 19. The simple subchannel average velocity relationship of Equation 21 was not applicable for this system (see Analysis of Data)

and the following equation was used:

$$U_7 = \left[\frac{0.65}{0.079} U_i^{1.44} \frac{de_7^{1.25}}{de_i^{1.56}} \left(\frac{\rho}{\mu}\right)^{-0.31}\right]^{-1.75} \quad (46)$$

where

i = 1, 2 and 6 subchannels.

The same form of this equation was also applicable to subchannel 8 and its peripheral subchannels 3, 4 and 5. The continuity equation, Equation 47, was then used to calculate each average subchannel velocity with Equation 46 used to equate the various subchannel average velocities.

$$\rho Ac_{1,2,6,7} U_{1,2,6,7} = \rho[Ac_7 U_7 + Ac_1 U_1 + 2Ac_2 U_2] \quad (47)$$

The test section pressure drop was measured with a manometer inclined at 15°. The manometer fluid used had a specific gravity of 2.96, thus the following equation gives the pressure drop:

$$\Delta P = \frac{g}{g_c} 1.96 \rho \frac{(15.3 - \Delta s)}{30.5} \sin(15°) \quad (48)$$

where

Δs = the manometer reading in centimeters

ρ = density of water at the ambient temperature.

The friction factor for the test section was calculated from

Equation 18 with $\frac{dP}{dx}$ replaced by the finite difference of the pressure gradient, $\frac{\Delta P}{\Delta x}$; therefore, the following equation gives the friction factor for the test section:

$$f = \frac{g_c}{2} \left(\frac{\Delta P}{\Delta x}\right) \frac{de_{1,2,6,7}}{\rho U^2_{1,2,6,7}} (3600)^2 \tag{49}$$

where

Δx = distance between pressure taps = 1.23 ft.

All concentration calculations were made from the measured fluorescence and the calibration curves (see Appendix C). The exit fluorescence was for the initially untraced channel, subchannels 1, 2, 6 and 7 or subchannels 3, 4, 5 and 8, and was therefore the mean mixing-cup concentration for the channel. The inlet tracer concentration was calculated from an overall tracer mass balance for the test section, i.e.,

$$COT = \frac{(\text{exit tracer concentration})\ m}{m_t} \tag{50}$$

where

m_t = tracer mass flow rate (see Appendix B)

COT = inlet dye concentration

and the initial tracer concentration to the test section was calculated as follows:

$$C_o = COT \frac{m_t}{m_{1,2,6,7}} \tag{51}$$

This was for subchannels 1, 2, 6 and 7 being initially traced. As was indicated in the experimental program, the tracer concentration was checked at regular intervals during a set of runs.

Calculation of the turbulent cross-flow was made after the above calculations were made. The two-channel model allowed the turbulent cross-flow to be calculated explicitly from Equation 26. This was not the case for the system of equations used for the eight-channel model.

The set of linear ordinary differential equations developed for the eight-channel model were numerically integrated with a Runge-Kutta-Merson numerical algorithm. Since the cross-flow mixing was implicit in the set of equations, an iterative scheme was necessary to calculate the turbulent cross-flow for this model. The following sequence of events for the calculation of the cross-flow for the eight-channel model was followed:

1. The two-channel model cross-flow was used as the initial guess for the cross-flow.
2. The system of equations were numerically integrated.
3. The tracer mass balance was used as the check point for the iterative scheme. The measured exit tracer mass was compared against the calculated exit tracers mass and the

difference between the two values was used for the acceptance or rejection of the calculated results. The difference was calculated as follows:

$$DIFF = (m_{1,2,6,7}) \text{ (measured exit tracer concentration)} \tag{52}$$

The cross-flow used in the calculation was accepted if

$$DIFF = \pm(m_{1,2,6,7}) \text{ (measured exit tracer concentration)}(0.05) \tag{53}$$

4. If the calculation was rejected the value of the cross-flow was linearly adjusted so as to given a DIFF value equal to zero. This new value of the cross-flow was thus used for the numerical integration of the system of equations.
5. Steps 2, 3 and 4 of this sequence were continued until Equation 53 was satisfied.

The point velocities were calculated from the measured impact pressure. The pressure transducer calibration was used to adjust the transducer output to the true impact pressure (see Appendix D). The point velocities were then calculated as follows:

$$u = 60\sqrt{288\, g_c \frac{P_I}{\rho}} \tag{54}$$

ANALYSIS OF DATA

The subchannel mixing data were considered with two mixing models, the two-channel model and the eight-channel model. Both models represent an attempt at describing the mixing phenomena that occurs between connected flow channels and differs only in the manner in which each uses the measured exit dye concentration.

Previous investigators of simulated rod bundle systems have used the two-channel analysis scheme because of the nature of the simulated rod bundle design (32, p. 3; 40; 41; 52, p. 3). This type of an approach has afforded the experimentalist a method of isolating various rod bundle configurations. Rowe and Angle (41) and Walton (52, p. 64) have noted that the system configuration (see Figures 4c, 4d and 4e) results in different mixing rates.

For the simulated rod bundle configuration used in this study (see Figure 5) the transport between subchannels 7 and 8, a square-square geometry, was of prime interest. Although the peripheral subchannels 1 through 6 increase the complexity of the system, this design was considered advantageous opposed to a simple two-channel square-square system in more closely simulating rod bundle flow. Hetsroni, Leon and Hakim (23) considered the same geometry as a two-channel system and evaluated the mixing from the average conditions for each half of the geometry, channel I and channel II (see

Figure 5).

Independent of the particular model (two-channel or eight-channel) chosen to describe a particular system, the mass flow rate and inlet and exit concentration must be known. Equation 19 may be used to calculate the average subchannel velocity and in turn the mass flow rate while the total mass flow, the inlet and the exit concentrations are measured quantities.

Friction Factor

Figure 13 is a plot of the overall or test section Fanning friction factor as a function of the Reynolds number for channel I, $Re_{1,2,6,7}$, for three rod spacings. The remaining rod spacings fall within these results as indicated by Table 5.

Table 5. Friction factor versus Reynolds number for the test section.

Rod Spacing (Inches)	Fanning Friction Factor for Channel I
0.011	$f = 0.21\ Re^{-0.404}$
0.028	$f = 0.23\ Re^{-0.416}$
0.063	$f = 0.34\ Re^{-0.459}$
0.127	$f = 0.15\ Re^{-0.37}$
0.228	$f = 0.22\ Re^{-0.417}$

The von Karman-Nikuradse equation is also shown for

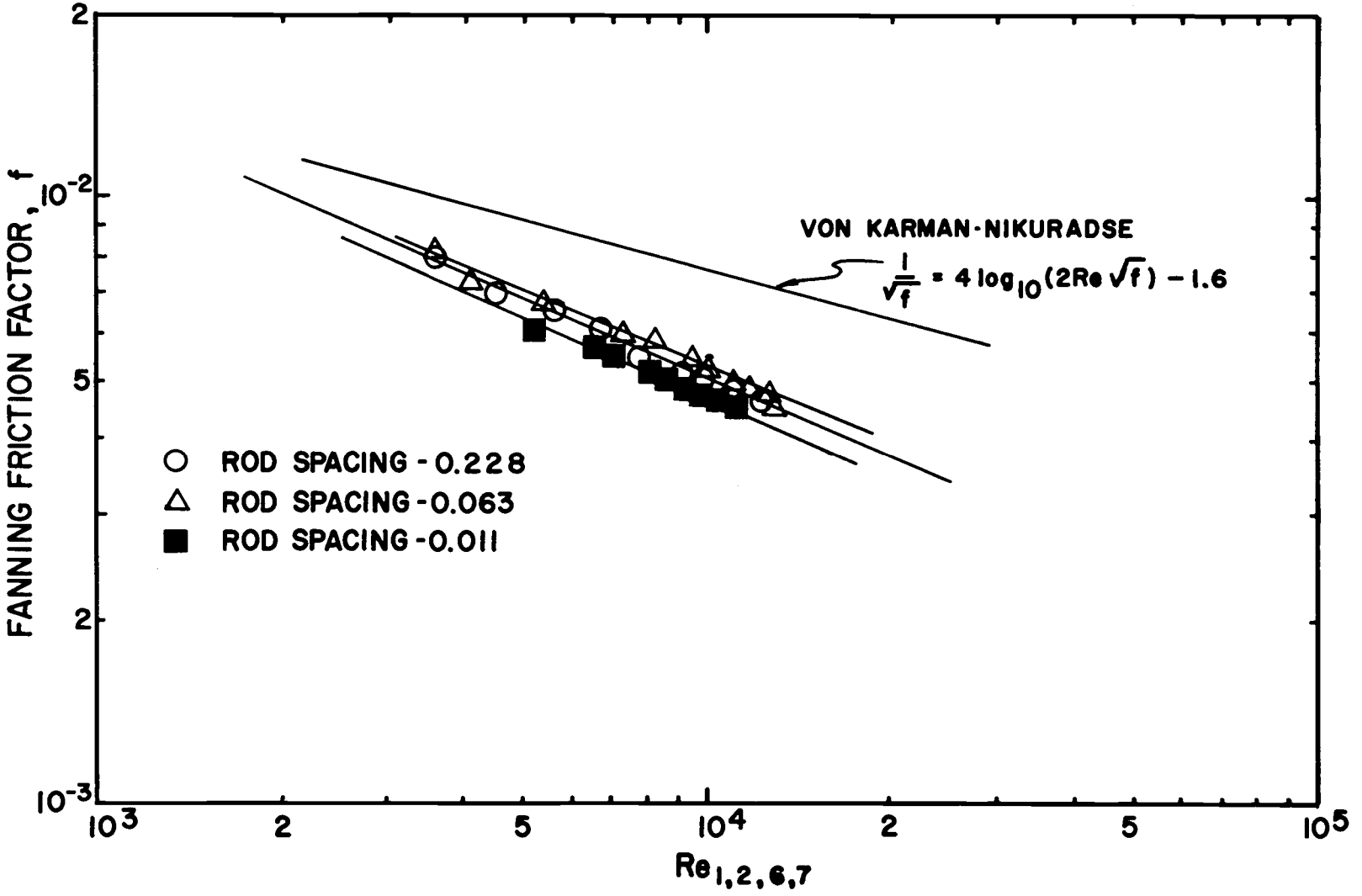

Figure 13. Fanning friction factor versus Reynolds number for the test section.

comparison since it represents the best fit for turbulent flow in smooth tubes. For the Reynolds number range considered in this study, the Blasius equation is nearly identical to the von-Karman-Nikuradse equation but is a much simpler expression, i.e.,

$$f = 0.079\ Re^{-0.25} \tag{55}$$

The experimental results for each gap fall below the Blasius equation and each has a slope (see Figure 13) that is greater than -0.25 (the slope of the Blasius equation). The experimental work of Eifler and Nijsing (13) and Walton (53) for the rod bundle geometries indicate that results lower than the Blasius equation could be expected but the slopes should be close to -0.25. Deissler's (11) analytical investigation shows a general agreement with the above mentioned experimental investigations.

It is important to note that each of these cited references consider Reynolds numbers that were greater than 1.6×10^4 which is above the upper limit for this study (see Figure 14). The experimental data of Eifler and Nijsing (13) showed an increase in slope for the low range Reynolds number data and also indicated that for a b/d ratio greater than 0.05 the Blasius equation could be used.

The other two-channel and multi-channel investigations have neglected to report or investigate pressure drop. They have used the Blasius friction factor result or other correlations that give results

to within ±5 percent of the Blasius equation (2, 6, 7, 31, 35, 38).

Waggener (51) reports the friction factor results for several rod bundle designs in current use and suggests that for smooth rod bundles Equation 55 can be used for a Reynolds number range of 4×10^3 to $1. \times 10^5$.

When Equation 21 was used with the experimental friction factor results, it was noted that the continuity equation for the complete bundle was not satisfied. This suggested that these friction factor relationships when used in Equation 21 did not describe the friction loss in all, if any, of the subchannels. This implies that each subchannel in the simulated rod bundle may have its own unique friction factor-Reynolds number relationship. Thus to calculate the average velocity in each subchannel, this relationship must be known. This could also explain the position of the experimental curves shown in Figure 13, both with respect to the Blasius curve and the results of other investigators.

For laminar flow in a duct the exponent on the Reynolds number is equal to -1.0, while for fully developed turbulent flow the exponent is -0.25 (see Equation 55). The experimental exponents in Table 5 indicate that some transition flow regime, a combination of laminar and turbulent flow, might be occurring in the test section. Eckert and Irvine (12) noted that for triangular passages, laminar flow and turbulent flow can exist side by side near the corners of these noncircular

ducts.

Since the subchannels 1, 2, 3, 4, 5 and 6 of the whole bundle have well defined corner areas in their cross-section, the combined laminar-turbulent flow pattern is conceivable for these subchannels. It was thus assumed that Equation 55 describes the friction factor relationship for subchannels 7 and 8 and based on this assumption the friction factor relationship for subchannels 1, 2, 3, 4, 5 and 6 could be determined from the experimental data and Equation 19. This assumption is consistent with the findings of Eifler and Nijsing (13) except for the 0.011-inch rod spacing.

On the basis of the above assumption, and using Equations 19 and 55, the experimental results indicated that the friction factor-Reynolds number relationship for subchannels 1, 2, 3, 4, 5 and 6 could be expressed by the following single relationship for all rod spacings including the 0.011-inch rod spacing, i.e.,

$$f = 0.65\ Re^{-0.56} \tag{56}$$

Table 6 shows the results of the continuity equation check for each geometry. The results are within the accuracy of the 2 percent error estimate for the cross-sectional areas of each subchannel.

Equation 55 and 56 were used to describe the flow in the various subchannels for both of the proposed mixing models. It is important to recognize that Equation 21 no longer applies, but application of

Equation 19 with the proper friction factor equation will give the subchannel velocities for each rod spacing.

Table 6. Mass balance for the simulated rod bundle geometries.

Rod Spacing (Inches)	$\frac{\text{Calculated mass flow-Measured mass flow}}{\text{Measured mass flow}} \times 100$
0.011	0.0 to 1.3%
0.028	-1.3 to 0.0%
0.063	-2.3 to 1.5%
0.127	-1.3 to 0.6%
0.228	-1.3 to 1.5%

Turbulent Mixing

Figures 14 through 18 show the results of both the two-channel and eight-channel turbulent mixing models. These figures also indicate which channel was initially traced. Each pair of points for a given Reynolds number were obtained for the same system conditions except for the changing of the traced channel. This change was made such that no other adjustments to the system were necessary.

The ordinate for these figures is the turbulent cross-flow, w_{78}^{t}, divided by the dynamic viscosity, μ, which could also be written as the effective or apparent eddy diffusivity, E, divided by the kinematic viscosity, ν. The abscissa is the Reynolds number for subchannels 7 or 8.

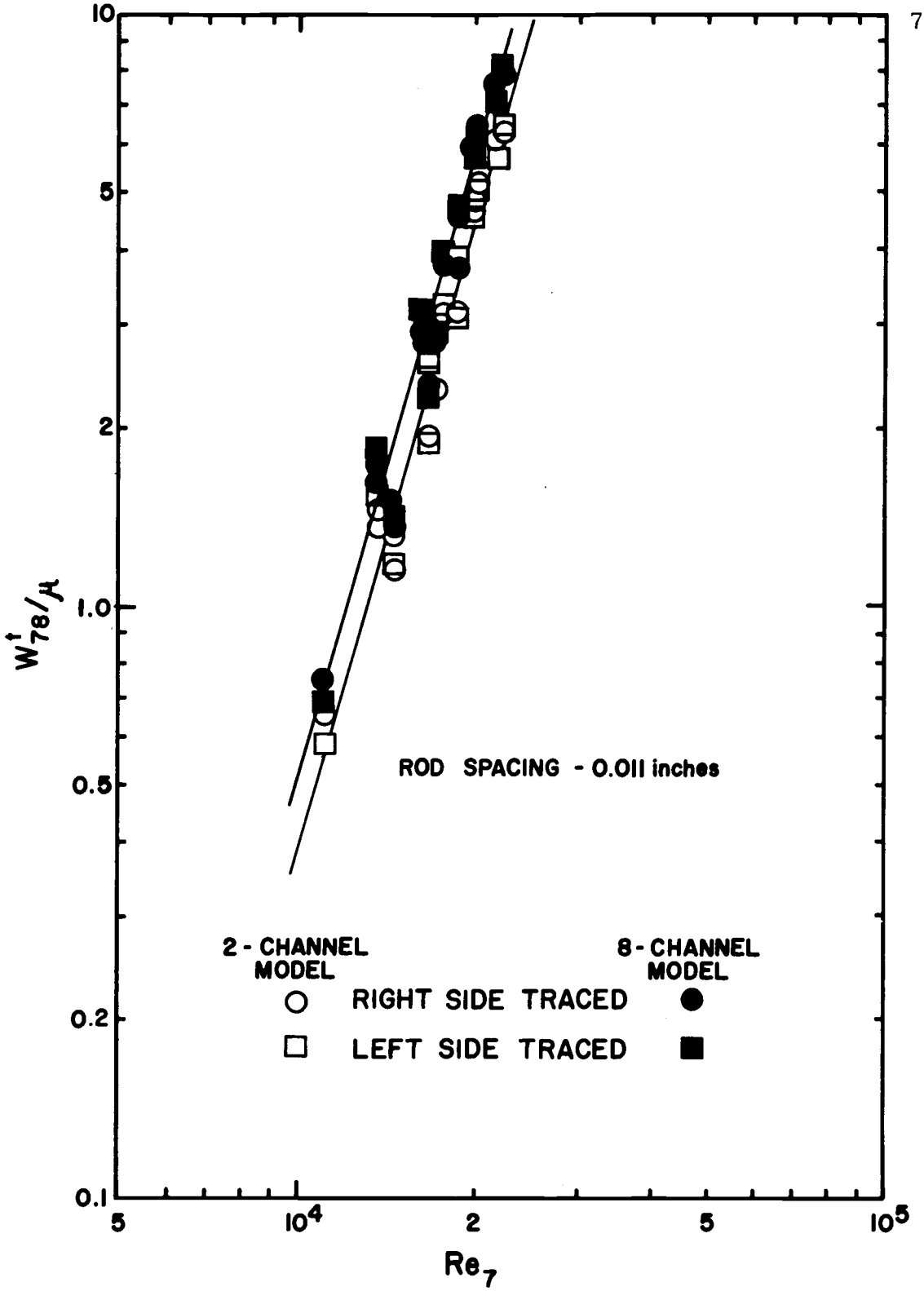

Figure 14. Two-channel and eight-channel mixing results versus subchannel 7 Reynolds number for the 0.011-inch rod spacing.

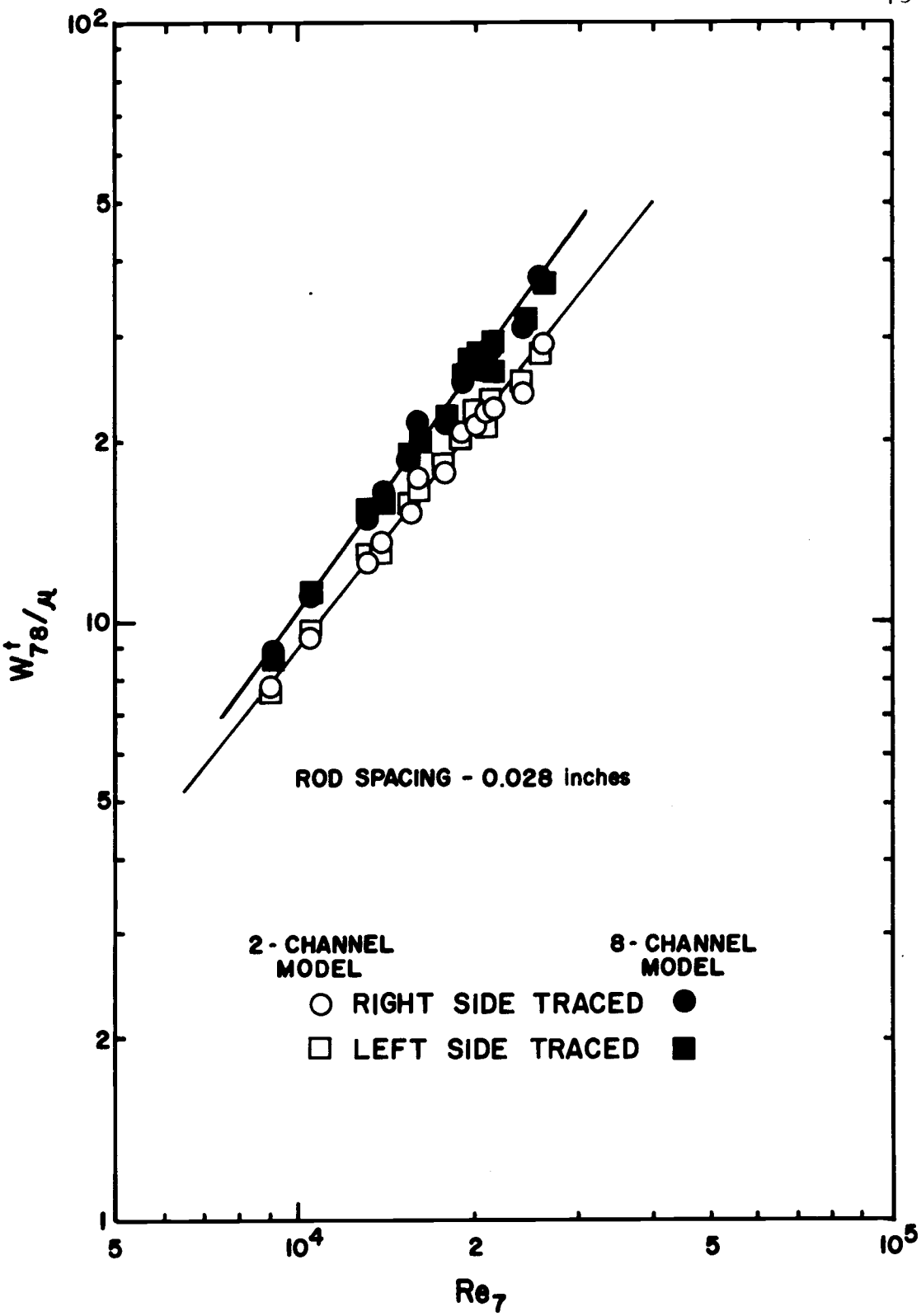

Figure 15. Two-channel and eight-channel mixing results versus subchannel 7 Reynolds number for the 0.028-inch rod spacing.

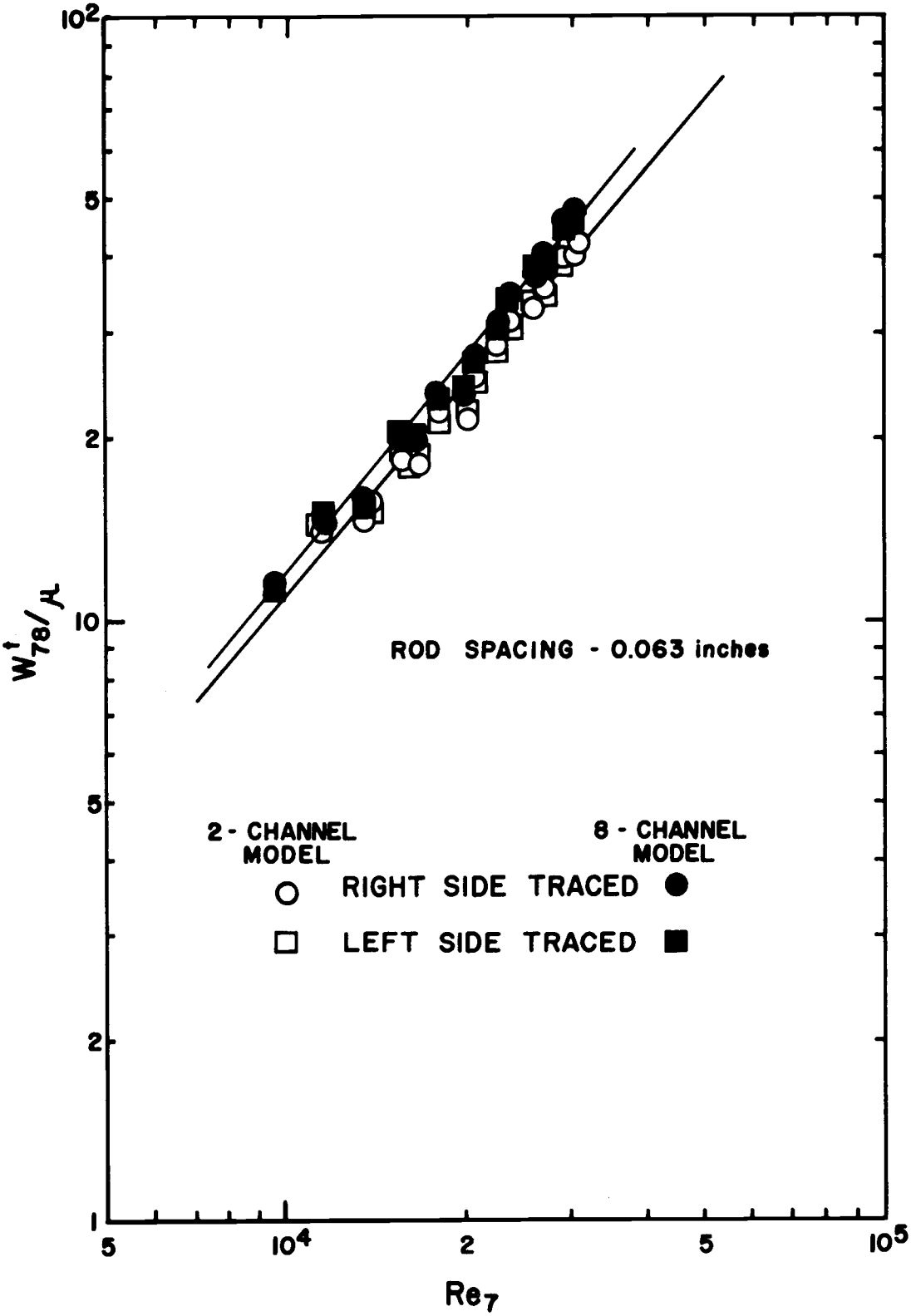

Figure 16. Two-channel and eight-channel mixing results versus subchannel 7 Reynolds number for the 0.063-inch rod spacing.

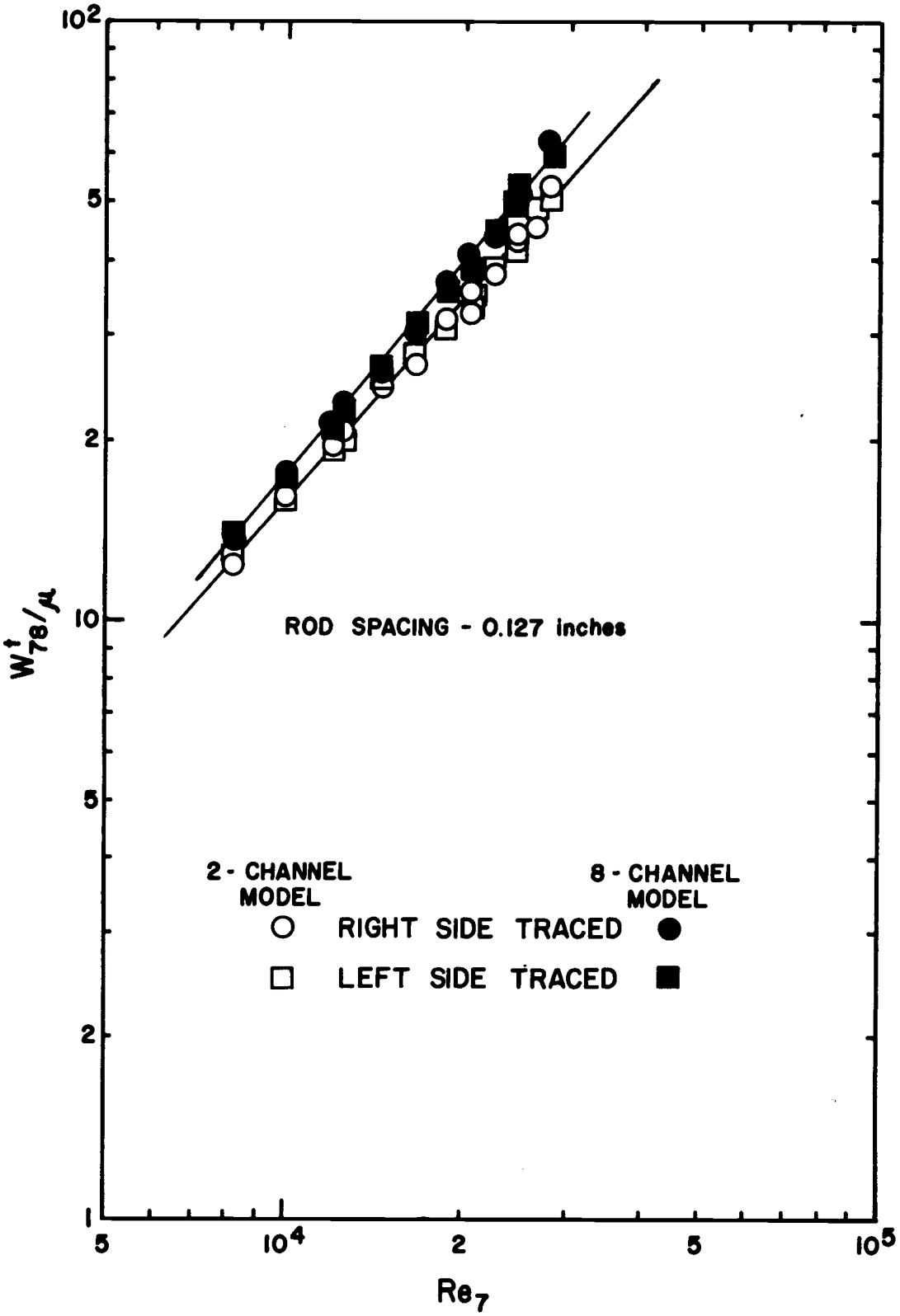

Figure 17. Two-channel and eight-channel mixing results versus subchannel 7 Reynolds number for the 0.127-inch rod spacing.

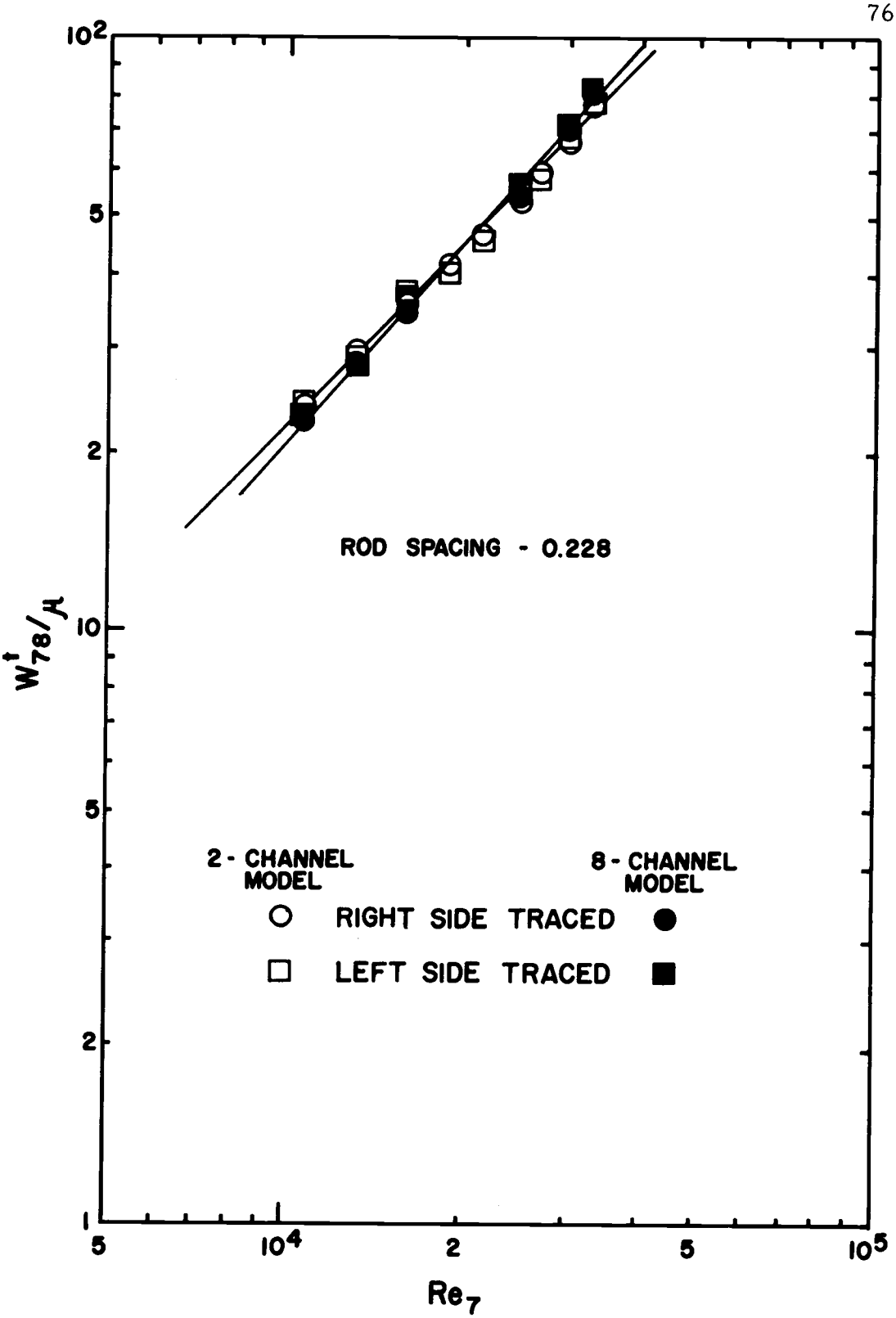

Figure 18. Two-channel and eight-channel mixing results versus subchannel 7 Reynolds number for the 0.228-inch rod spacing.

Two-Channel Analysis

Figure 19 shows w^t_{78}/μ versus the Reynolds number for subchannel 7, while Figure 20 shows the w^t_{78}/μ versus the Reynolds number for channel I, $Re_{1,2,6,7}$, for each of the rod spacings considered.

These figures indicate that for the two-channel model the rod spacing has a definite effect upon the turbulent cross-flow. Figure 20 is presented to show the effect an error in the mass flow rate calculation would have on the reported results and as such it shows that the mass flow rate is important to this model only if a definitive result is sought. Even though both methods of analyzing the observed data give the same general result, the analysis based upon the subchannel Reynolds number is of the greatest value since in considers the hydrodynamic conditions that are effecting the turbulent interchange between adjacent subchannels.

Figure 21 shows the comparison of experimental results from Hetsroni, Leon and Hakim (23) with this work for geometrically similar flow channels and the same turbulent mixing model. The difference in the two results is a result of the manner in which Hetsroni, Leon and Hakim evaluated the viscosity of their fluid. Since they were using a hot-cold channel (enthalpy balance) scheme, they chose to report the results as for the hot channel. Their experimental program

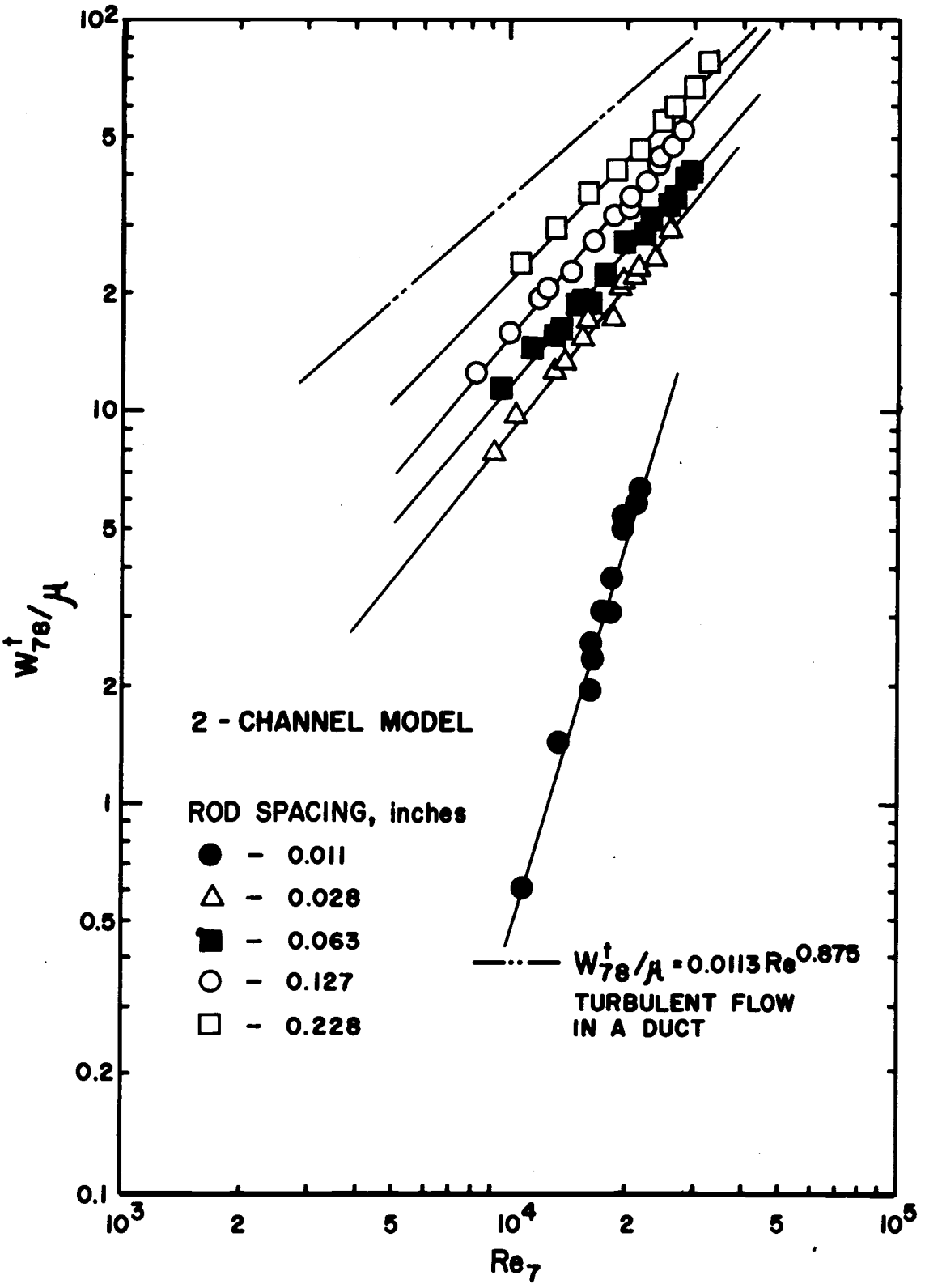

Figure 19. Mixing results for the two-channel model for each rod spacing versus subchannel 7 Reynolds number.

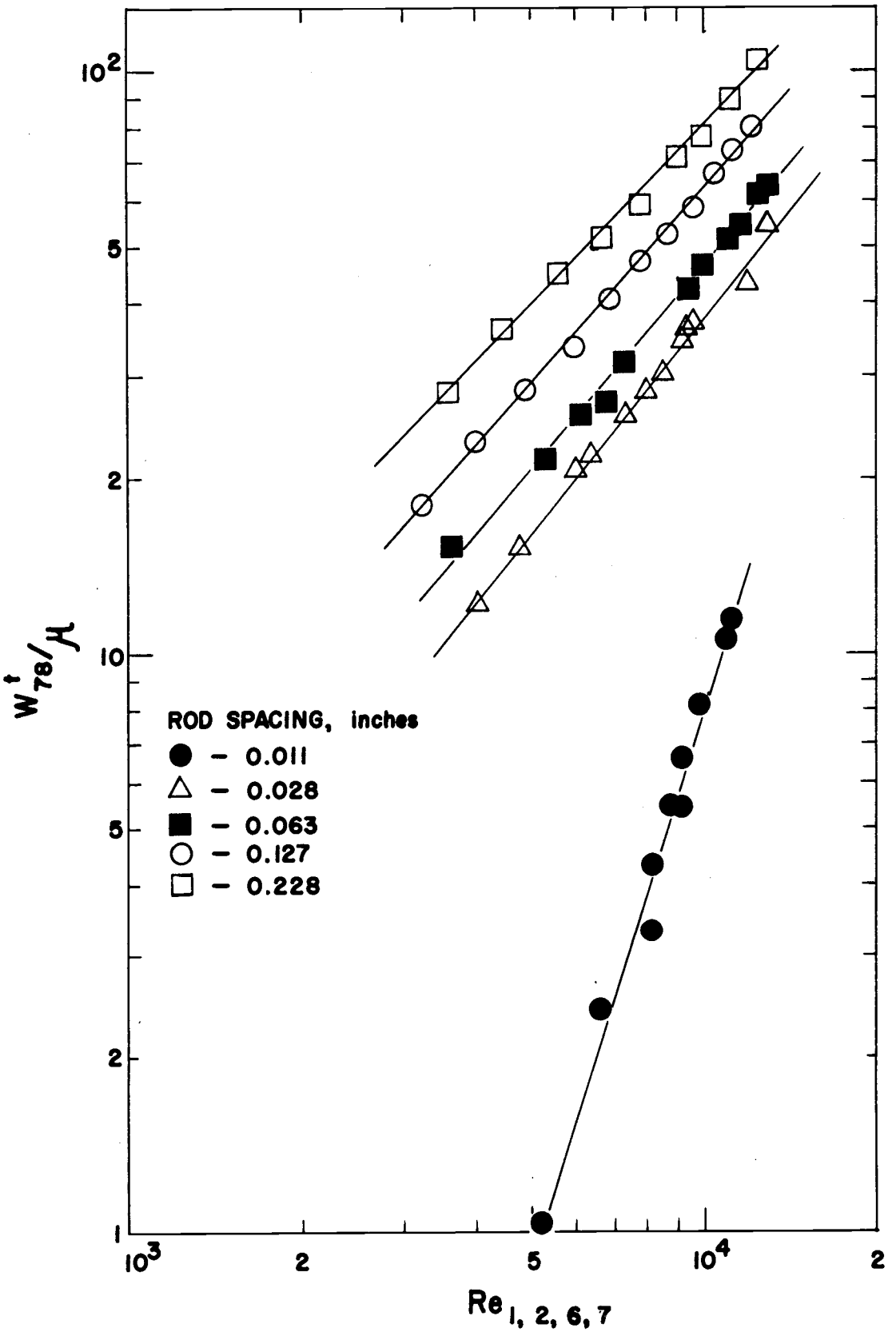

Figure 20. Mixing results for the two-channel model for each rod spacing versus channel I Reynolds number.

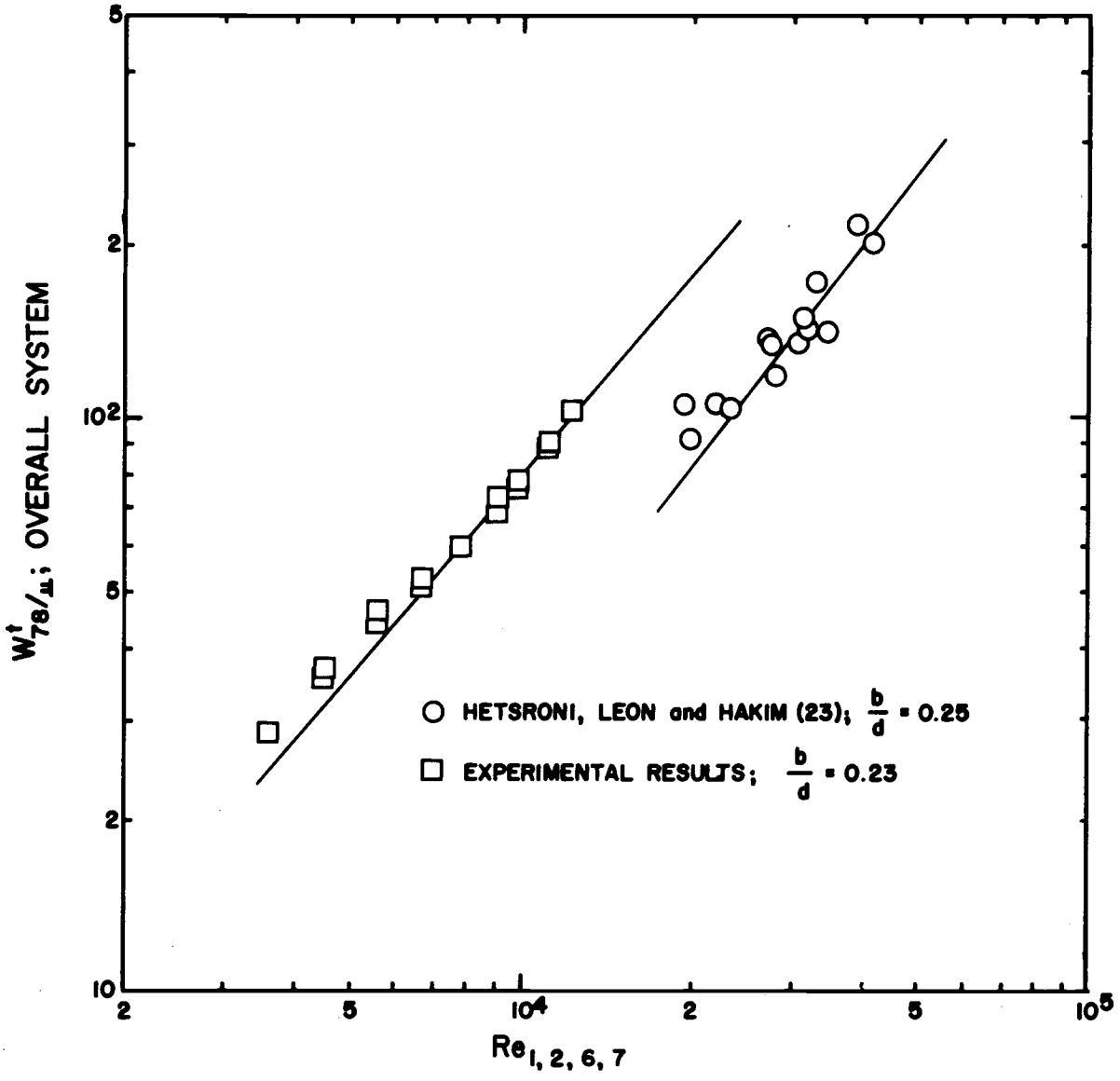

Figure 21. Comparison of experimental results with mixing results of Hetsroni, Leon and Hakim (23).

considered average channel temperature differences from 30 to 70° F which would give a two fold difference in viscosities between the hot and the cold channels. Even so, the two results exhibit similar Reynolds number effects and a viscosity adjustment to the data of Hetsroni, Leon and Hakim would close the relative difference in the two results.

Eight-Channel Analysis

Figure 22 shows w_{78}^{t}/μ versus subchannel Reynolds number for each rod spacing considered. This method of analyzing the observed data is an attempt to account for all possible subchannel interaction. It should therefore offer the most realistic approach of describing the experimental system.

Figures 14 through 18 show that this model gives higher turbulent cross-flow rates for the same Reynolds number and rod spacing than the two-channel model with the exception of the 0.288-inch rod spacing. This was thought to be a result of the exit concentration used by the two-channel model and the convergence criteria used for the eight-channel model.

Since the measured exit concentration is the mean mixed-cup concentration for the channel I or channel II cross-section, and the actual exit concentration of subchannel 7 or 8 should be higher than this result, the two-channel model would thus give a conservative

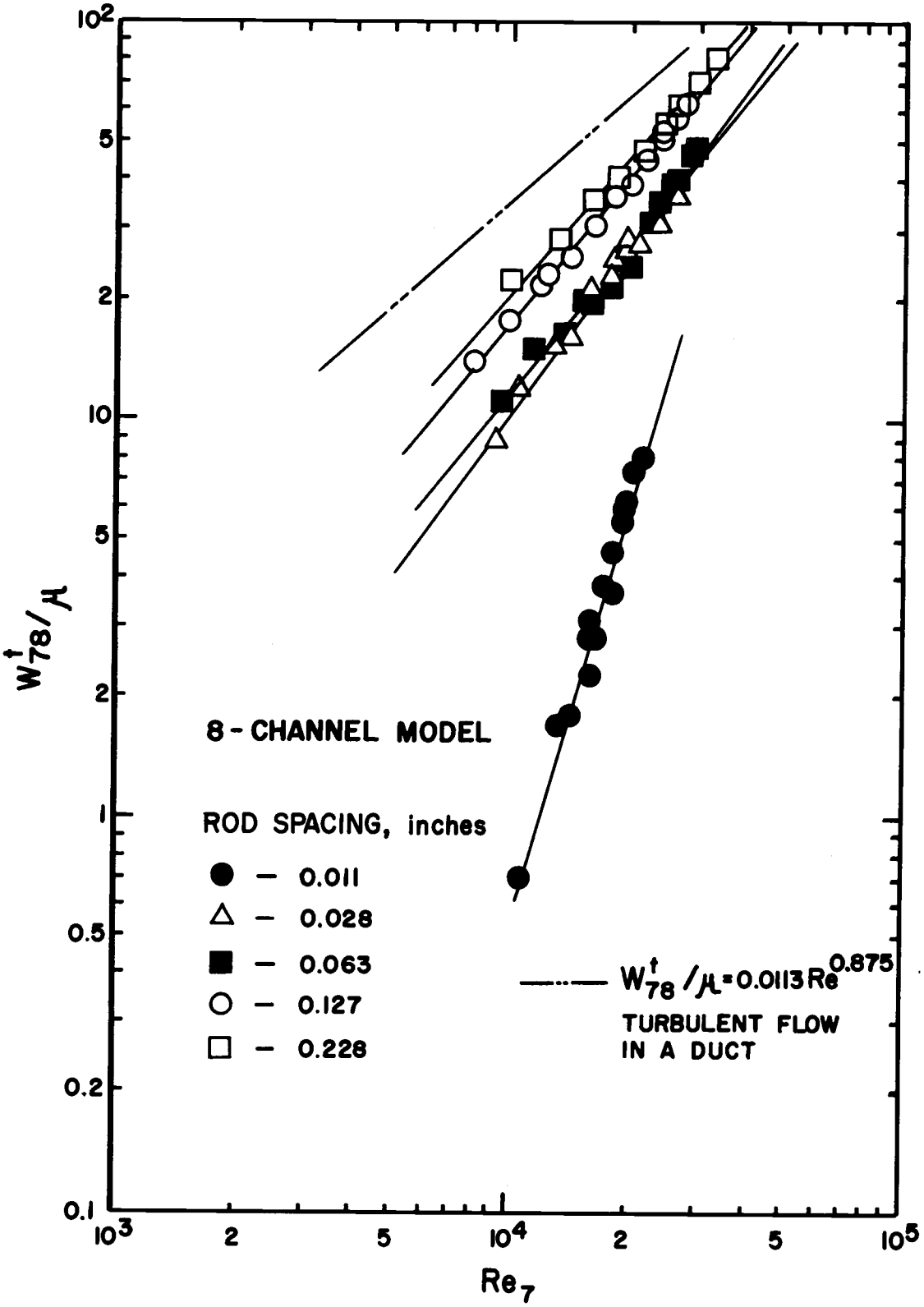

Figure 22. Mixing results for the eight-channel model for each rod spacing versus subchannel 7 Reynolds number.

estimate of the turbulent mixing.

This may be seen from the following analysis of the two-channel model. If $2(C_7^f/C_o)$ from Equation 26 is very much smaller than 1 $(2(C_7^f/C_o) \ll 1)$ then Equation 26 may be written as follows:

$$w_{78}^t \simeq \frac{m_7}{L} \frac{C_7^f}{C_o} \tag{57}$$

When the effect of rod spacing upon turbulent interchange is considered, it is apparent why the two models give very nearly the same results for larger rod spacings.

The convergence criteria used for the eight-channel model could cause the calculated turbulent mixing to be either high or low depending upon the rod spacing. Equation 58 is the mathematical representation of the criteria.

$$\left| \frac{1 - \Sigma\, m_i\,(\text{exit dye concentration})_i}{\left(\begin{matrix}\text{measured mass}\\ \text{flow rate}\\ \text{channel I}\end{matrix}\right)\left(\begin{matrix}\text{mean mixing-cup}\\ \text{exit dye concentration}\\ \text{channel I}\end{matrix}\right)} \right| = \begin{cases} \geq 0.05 \text{ accept} \\ < 0.05 \text{ reject} \end{cases} \tag{58}$$

where

$$i = 1,\ 2,\ 6 \text{ and } 7 \text{ subchannels}$$

and it has been assumed that channel II was initially traced. The rod spacing effects the criteria by how well the mass balance of channel I

was satisfied.

If the sum of the subchannel mass flow rates for channel I is less than the measured mass flow rate for channel I, the calculated exit subchannel dye concentration will be higher than the true value. This will result in a calculated turbulent cross-flow mixing rate that will be higher than the true value. The opposite effect is also true for the sum of the subchannel mass flow rates greater than the measured mass flow rate for channel I.

Table 7 gives an estimate of the error of the two models from the true results independent of the possible errors in measured concentrations, mass flow rates and geometrical lengths. These estimates of the error are for the maximum possible error in both cases.

Table 7. Error estimate for the mixing models.

Rod Spacing (Inches)	Two-Channel Model	Eight-Channel Model
0.011	-34%	5 to 10% low
0.028	-31%	5 to 10% high
0.063	-20%	± 10%
0.127	- 9%	± 10%
0.228	0%	± 10%

The error estimate for the two-channel model was made by assuming none of the dye was transported to the peripheral subchannels for the initially untraced channel. The resulting exit

concentrations were then put on a relative scale that assumed the exit mean mixing-cup concentration for the 0.228-inch rod spacing was the true value.

The error estimate for the eight-channel model was made by considering the mass balance error (see Table 6) for each rod spacing times the maximum error in the convergence criteria.

Effect of Pressure Bias on Turbulent Mixing

When the turbulent cross-flow mixing divided by the sum of the mass flow rates for subchannels 7 and 8 was plotted against subchannel 7 or 8 Reynolds number, the results showed that w'_{78}/m increased with increasing Reynolds number. This result was unexpected in view of the experimental studies of Rowe and Angle (40, 41) and Walton (52, p. 82-83).

The initial operation of the test section had indicated that the inlet and exit pressure gradient measurement was not sensitive enough to insure the test section was pressure balanced, zero pressure gradients between subchannels 7 and 8. This result initiated the thought to operate under a known pressure bias or gradient between the two subchannels. The mixing results for the 0.011-inch rod spacing under this condition gave higher mixing than for the pressure balanced case and a decrease in mixing for an increase in Reynolds number. Figure 23 shows the difference in results for the balanced and unbalanced

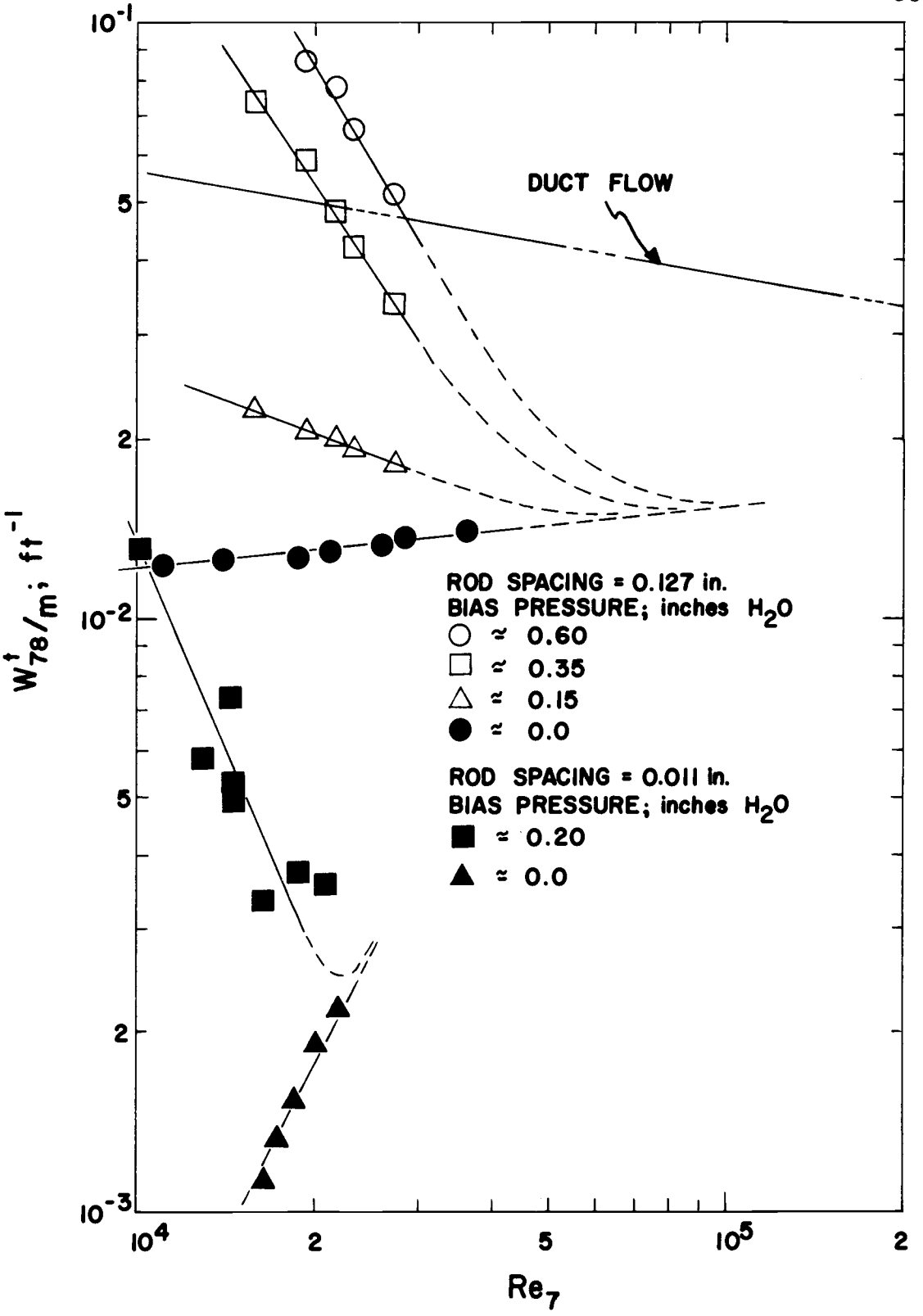

Figure 23. Biased pressure mixing results for the 0.011 and 0.127-inch rod spacings.

pressure conditions for this rod spacing.

The extreme sensitivity of the 0.011-inch rod spacing geometry to the imposed pressure bias made it difficult and impractical to consider the bias pressure effects beyond the range shown. This was not the case for the 0.127-inch rod spacing geometry.

Figure 23 shows the results for three bias pressure gradients and the balanced pressure gradient at the exit for subchannels 7 and 8 for the 0.127-inch rod spacing. The results exhibit the same trends as the pressure biased 0.011-inch rod spacing results. In Figure 23 the bias mixing results have been extended such that they approach the balanced mixing condition. The dashed lines are a qualitative estimate of the effects of a pressure gradient upon the mixing as the Reynolds number increases.

Figure 24 shows the experimental results of Rowe and Angle (41) and Walton (52, p. 82-83). These results indicate that the experimental systems of the cited references could be pressure biased or that diversion cross-flow had not been eliminated. This might also account for the fact that the Rowe and Angle results showed that rod spacing had no effect upon the turbulent mixing.

Correlations of the Mixing Results

The 0.011-inch rod spacing gave the same general results for both the two-channel and eight-channel mixing models. This

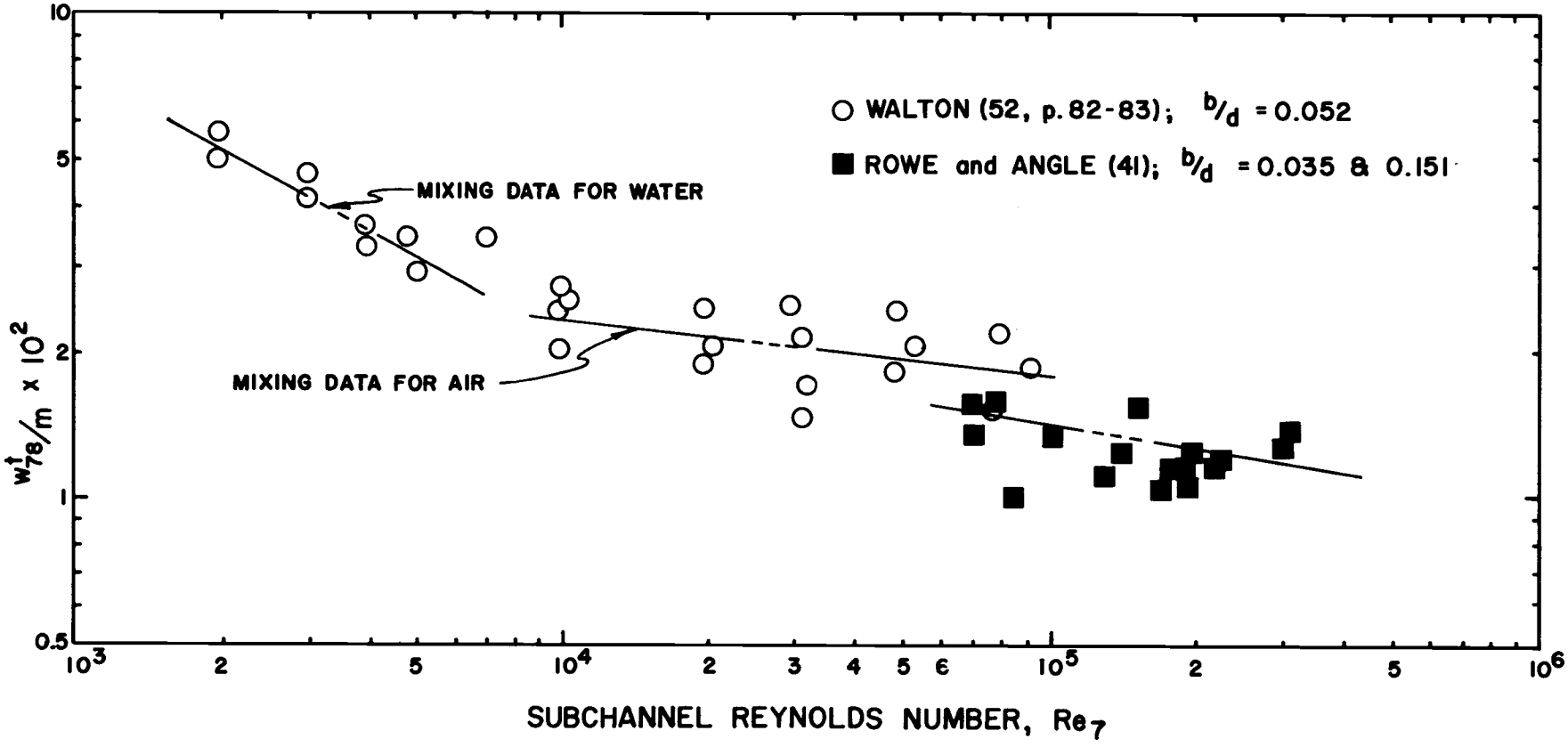

Figure 24. Mixing results from Rowe and Angle (41) and Walton (52) versus subchannel Reynolds number.

configuration supports the hypothesis that turbulent mixing between adjacent subchannels is a function of rod spacing and indicates that the mixing approaches zero for very small rod spacings.

The mixing results for rod spacings 0.028, 0.063, 0.127 and 0.228 inches were used to develop a general mixing correlation. The 0.011-inch rod spacing was not considered since the results for this system exhibited mixing characteristics very different to the other geometries investigated which is consistent with variations in turbulent flow near the wall and turbulent flow away from the wall.

Equation 11 which is theoretically derived relates the measured turbulent mixing for the simulated rod bundle to the eddy diffusivity, i.e.,

$$w'_{ij} = \frac{\rho b}{z_{ij}} E$$

For the turbulent mixing or cross-flow between subchannels 7 and 8 and assuming that E in Equation 11 may be replaced by the turbulent core eddy diffusivity equation for flow in a duct, Equation 8, the following equation is obtained:

$$w'_{78} = \frac{\rho b}{z_{78}} (0.04\ Re_7 \sqrt{f}\ \nu) \tag{59}$$

If the Blasius equation for the friction factor, Equation 55, is applied

to Equation 59 the following results:

$$w_{78}^{t} = \frac{\rho b}{z_{78}} (0.0113 \, Re_{7}^{0.875} \nu)$$

or

$$\frac{w_{78}^{t}}{\mu} = \frac{b}{z_{78}} (0.0113 \, Re_{7}^{0.875}) \qquad (60)$$

where

z_{78} = a mixing distance between subchannels 7 and 8.

The importance of using Equation 8 to describe the turbulent core eddy diffusivity is that it represents the ultimate value for the turbulent mixing, w_{78}^{t}. This concept is consistent with the works of Schlichting (42, p. 468) and Szablewski (50) when the test section is compared to either duct or channel flow which are the physical limits of the system.

The mixing results for each rod spacing were correlated with the subchannel 7 Reynolds number for both of the mixing models with the results shown in Table 8. These results imply that for the scope of this work the mixing distance between subchannels 7 and 8 is a function of the subchannel Reynolds number when compared to Equation 60. This further suggests that assuming z_{78} to be a constant and equal to some characteristic dimension of the subchannel is incorrect as has been done in the past (2, 30, 36, 49, 53).

Table 8. Empirical correlations for subchannel mixing; $w^t_{78}/\mu = a\ Re^b_7$.

Rod Spacing (Inches)	Two-Channel Model		Eight-Channel Model	
	a x 10^5	b	a x 10^5	b
0.011	7.5 x 10^{-10}	3.43	2.9 x 10^{-10}	3.55
0.028	10	1.23	4.5	1.34
0.063	37	1.12	10	1.26
0.127	50	1.12	17	1.20
0.228	190	1.01	66	1.12

When the mixing distance, z_{78}, is considered as some mixing length comparable to the Prandtl mixing length its dependence on the Reynolds number becomes apparent. For Reynolds numbers less than 1 x 10^5 the mixing length, ℓ, for turbulent flow is a function of the Reynolds number because the velocity profile is not independent of the Reynolds number as is the case for turbulent flow above Re = 1 x 10^5 (42, p. 568-569).

The b/z_{78} term in Equation 60 is thus a correction factor for the mixing in the rod bundle geometry that approaches unity for high Reynolds number flow.

In considering the general correlation of the mixing results for the 0.028, 0.063, 0.127 and 0.228-inch rod spacings, Equation 60 was used as the starting point. This required that some function for the b/z_{78} term be developed that satisfied the following conditions:

1. As b becomes large (approaching the hydraulic diameter

of the subchannel) b/z_{78} must approach unity.

2. As Re_7 becomes large (the velocity profile becomes independent of Re) b/z_{78} must approach unity.
3. As b becomes small (approaching zero) b/z_{78} must approach zero.

The function

$$1 - \exp(-f(b, Re_7)) \tag{61}$$

would satisfy these requirements provided

$$f(b, Re_7) \propto b \quad \text{and} \quad Re_7 \tag{62}$$

replacing b/z_{78} by Equation 61 in Equation 60, i.e.,

$$\frac{w_{78}^t}{\mu} = [1 - \exp(-f(b, Re_7))](0.0113\ Re_7^{0.875}) \tag{63}$$

Note that the left hand side of Equation 63 is a result of the experiment and thus $f(b, Re_7)$ may be found for each rod spacing. The individual expressions for each rod spacing were then correlated to give a general expression for both the two-channel and the eight-channel models.

Figures 25 and 26 are plots of the predicted versus the actual w_{78}^t/μ values. The estimate of the variance of the correlation was

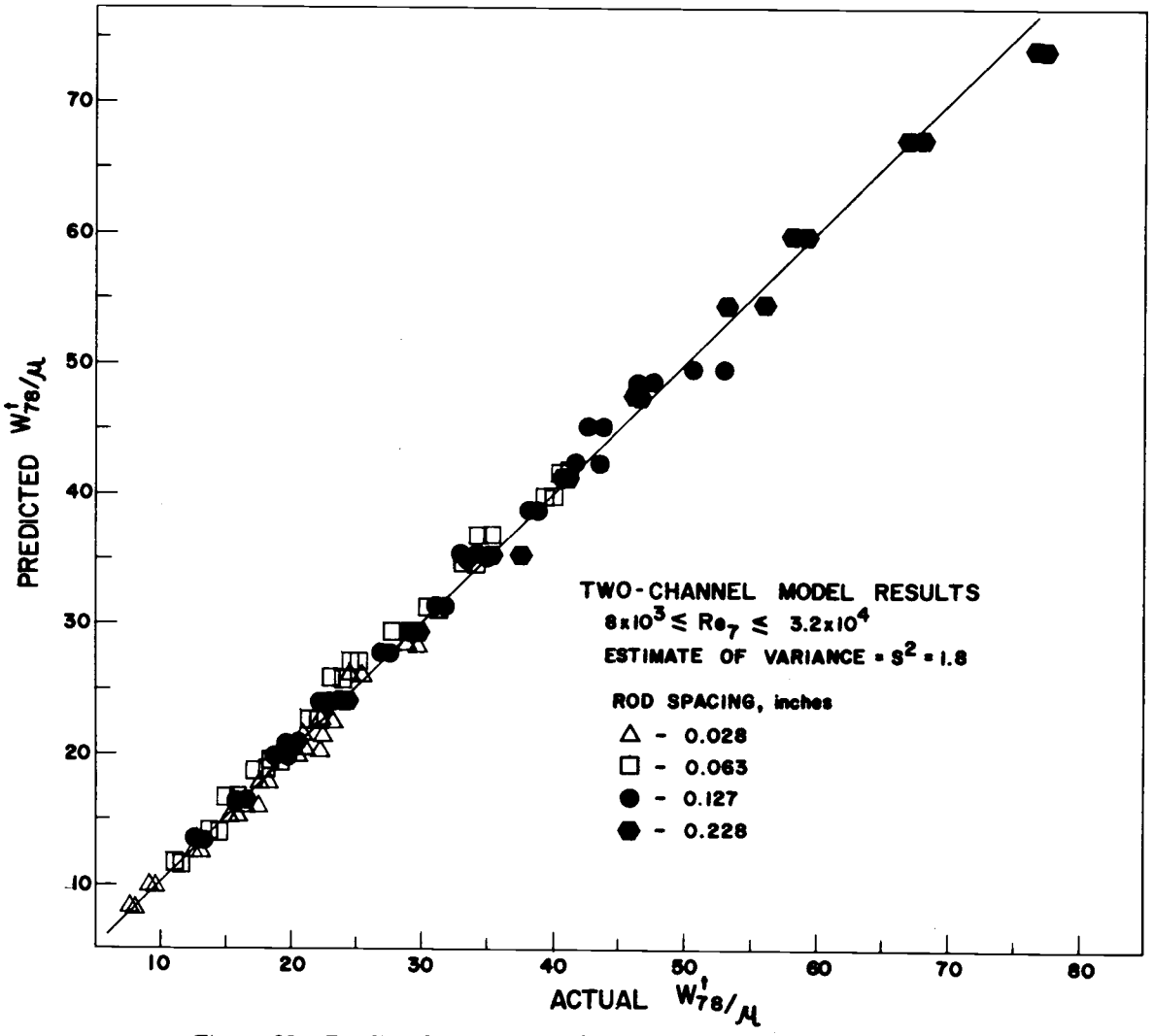

Figure 25. Predicted versus actual mixing for the two-channel model.

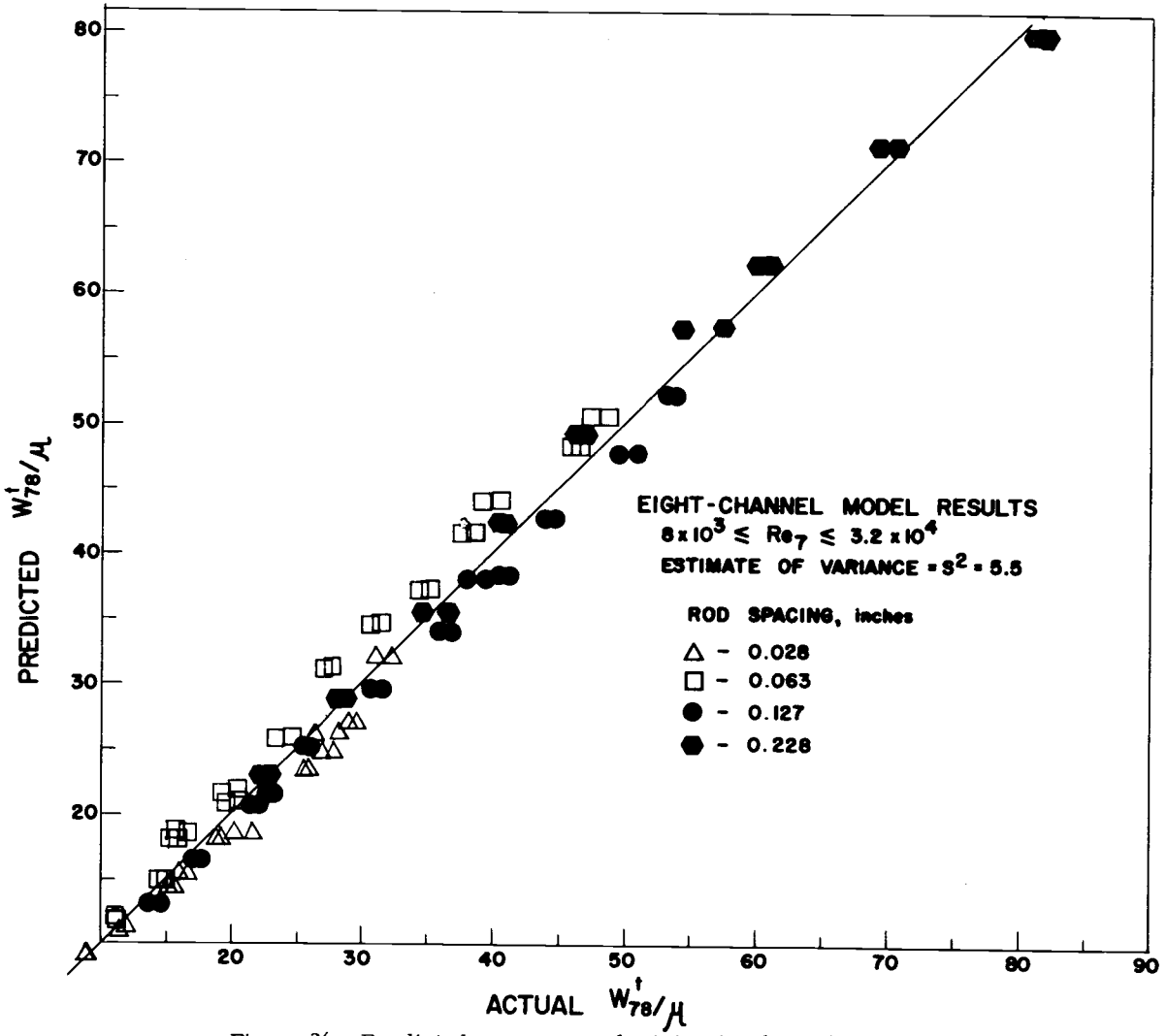

Figure 26. Predicted versus actual mixing for the eight-channel model.

made with the following expression:

$$\left(\begin{matrix}\text{estimate of}\\ \text{variance}\end{matrix}\right) \triangleq \frac{\sum_{k}^{N} \left(\text{predicted } \frac{w_{78}^{t}}{\mu} - \text{actual } \frac{w_{78}^{t}}{\mu}\right)_{k}}{N}$$

where

k = a data point or result

N = total number points

and the $f(b, Re_7)$ equations for each mixing model are

two-channel model

$$f(b, Re_7) = 0.158 \exp(5.17\frac{b}{de_7}) + 10^{-5}(0.618+2.34\frac{b}{de_7})Re_7 \quad (65)$$

eight-channel model

$$f(b, Re_7) = 0.14 \exp(4.75\frac{b}{de_7}) + 10^{-5}(1.1+4.7\frac{b}{de_7})Re_7 \quad (66)$$

These results are consistent with the general restriction of Equation 62.

Subchannel Velocity Profiles

Figures 27 and 28 show the axial velocity profile measured along the centerline of the rod bundle cross-section through the center of the rod spacing in the z direction (see Figure 29) where the fluid motion is normal to the paper.

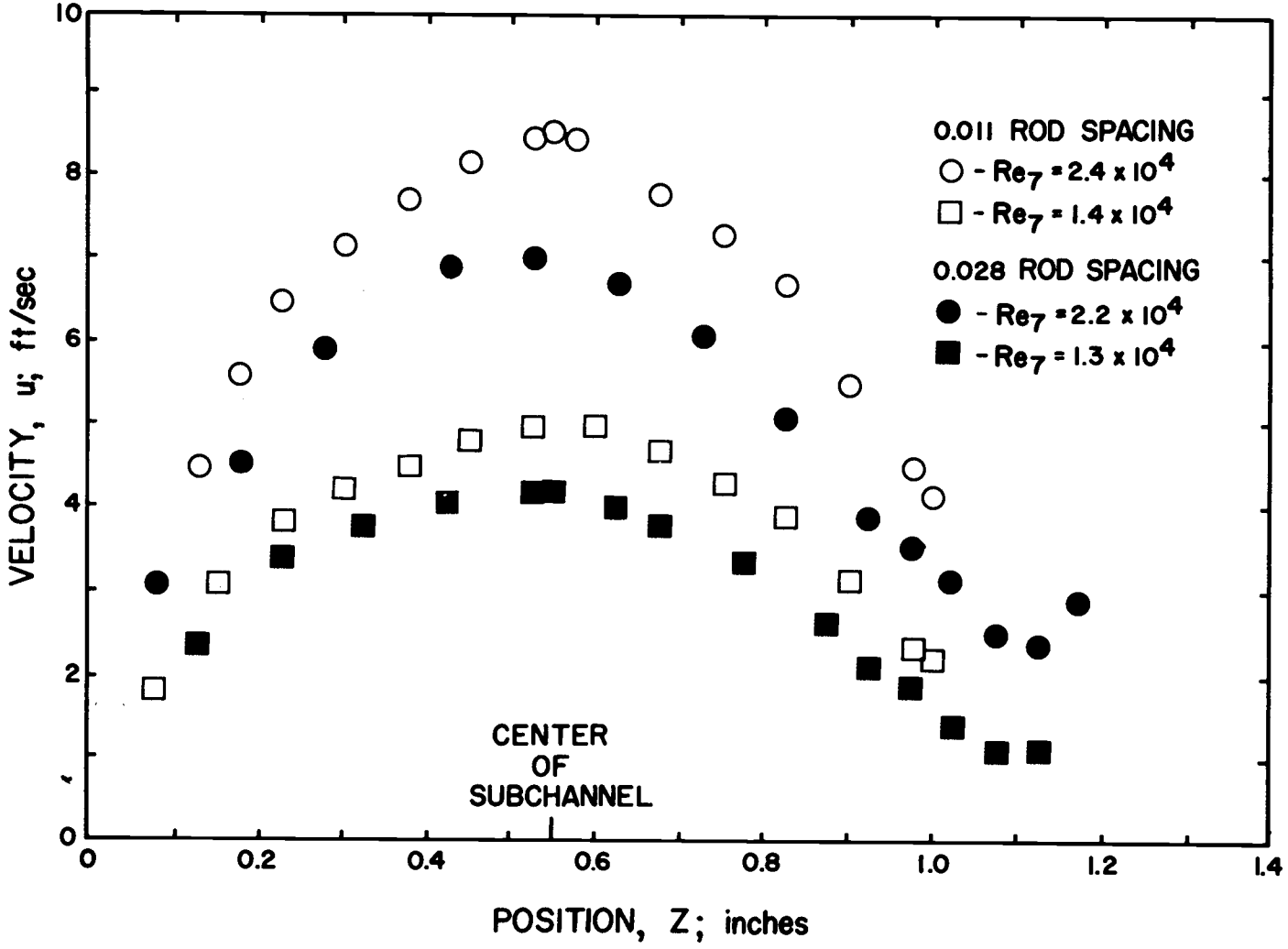

Figure 27. Velocity profiles for the 0.011 and 0.028-inch rod spacings for subchannel 7.

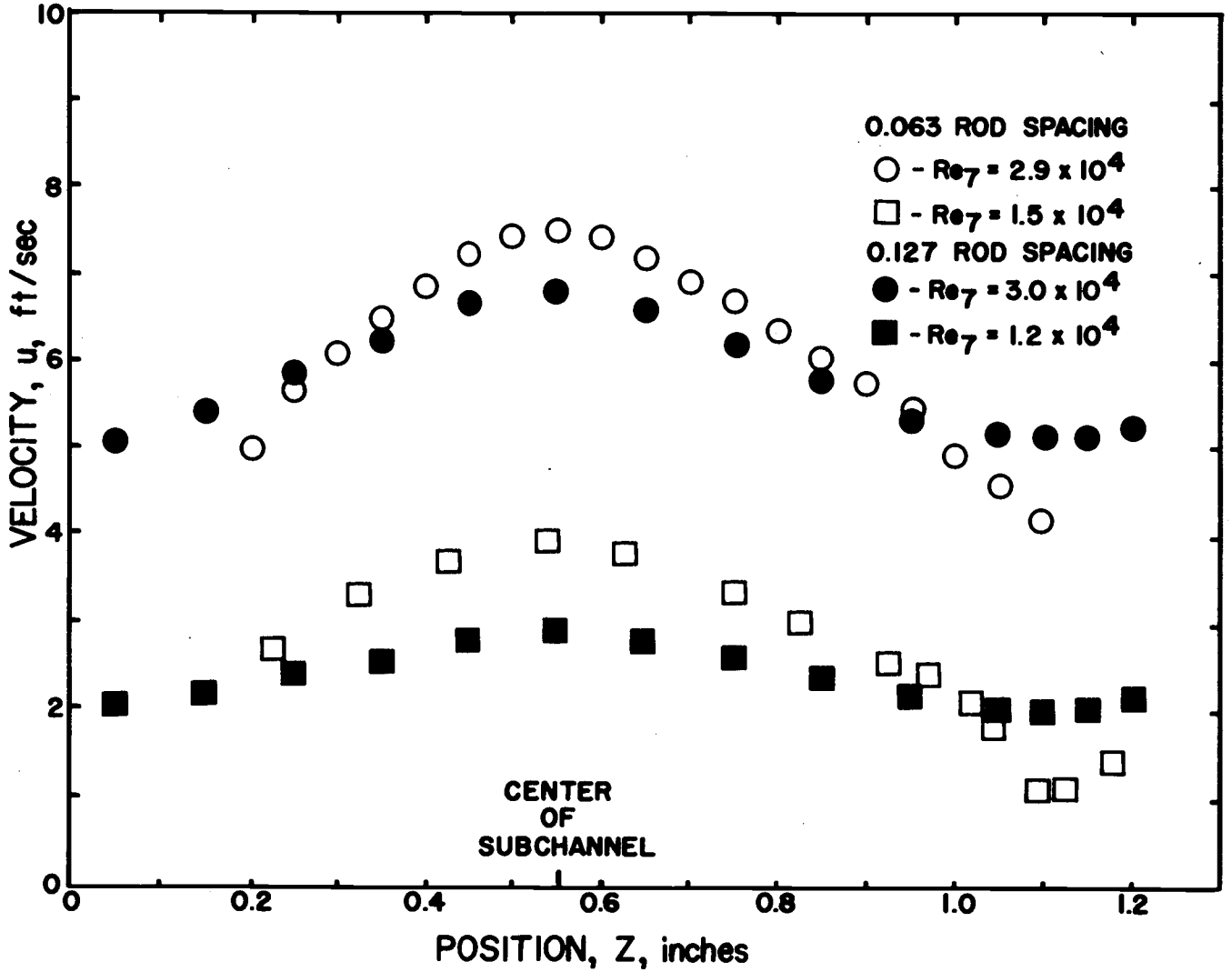

Figure 28. Velocity profiles for the 0.063 and 0.127-inch rod spacings for subchannel 7.

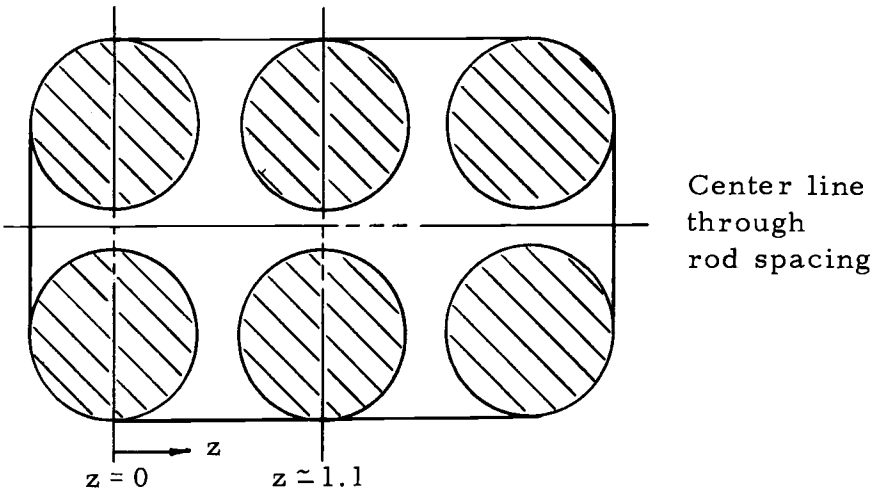

Figure 29. Rod bundle cross section.

Since the probe used to measure the impact pressure had an outside diameter of 0.028 inches, the velocity results in the gap are considered to be of a qualitative value only. Even so, the results are consistent with the idea that the velocity profile in the vicinity of the gap is a function of the Reynolds number. This is particularly evident for the 0.011, 0.028 and 0.063-inch rod spacings. The Reynolds number effect also appears to decrease with increasing rod spacing which is consistent with the turbulent mixing correlation for the various rod spacings shown in Table 8.

Since the rod spacing has been shown to have a measurable effect upon the transport between adjacent subchannels, a gap Reynolds number was calculated using the measure point velocities in the gap.

The gap Reynolds number was defined as

$$Re_g = \frac{2bu_g(0.8)}{\nu}$$

where

u_g = point velocity at the geometric center of the gap

b = rod spacing

ν = kinematic viscosity.

The gap was considered as being formed by two flat plates for which the plate separation was the rod spacing and thus the hydraulic diameter was 2b, as calculated from Equation 17.

Figure 30 shows the gap Reynolds number, Re_g, plotted as a function of the subchannel 7 Reynolds number, Re_7. This figure implies that at the gap the fluids motion could be laminar.

As a means of additional description for the fluid motion within the gap, an estimation of the laminar sublayer thickness was made with the following equation:

$$\delta = \frac{y^+_{max} de_7}{Re_7} \sqrt{\frac{2}{f}} \qquad (68)$$

where

y^+_{max} = represents the thickness of the laminar sublayer and is assumed equal to 5 based on turbulent flow in tubes.

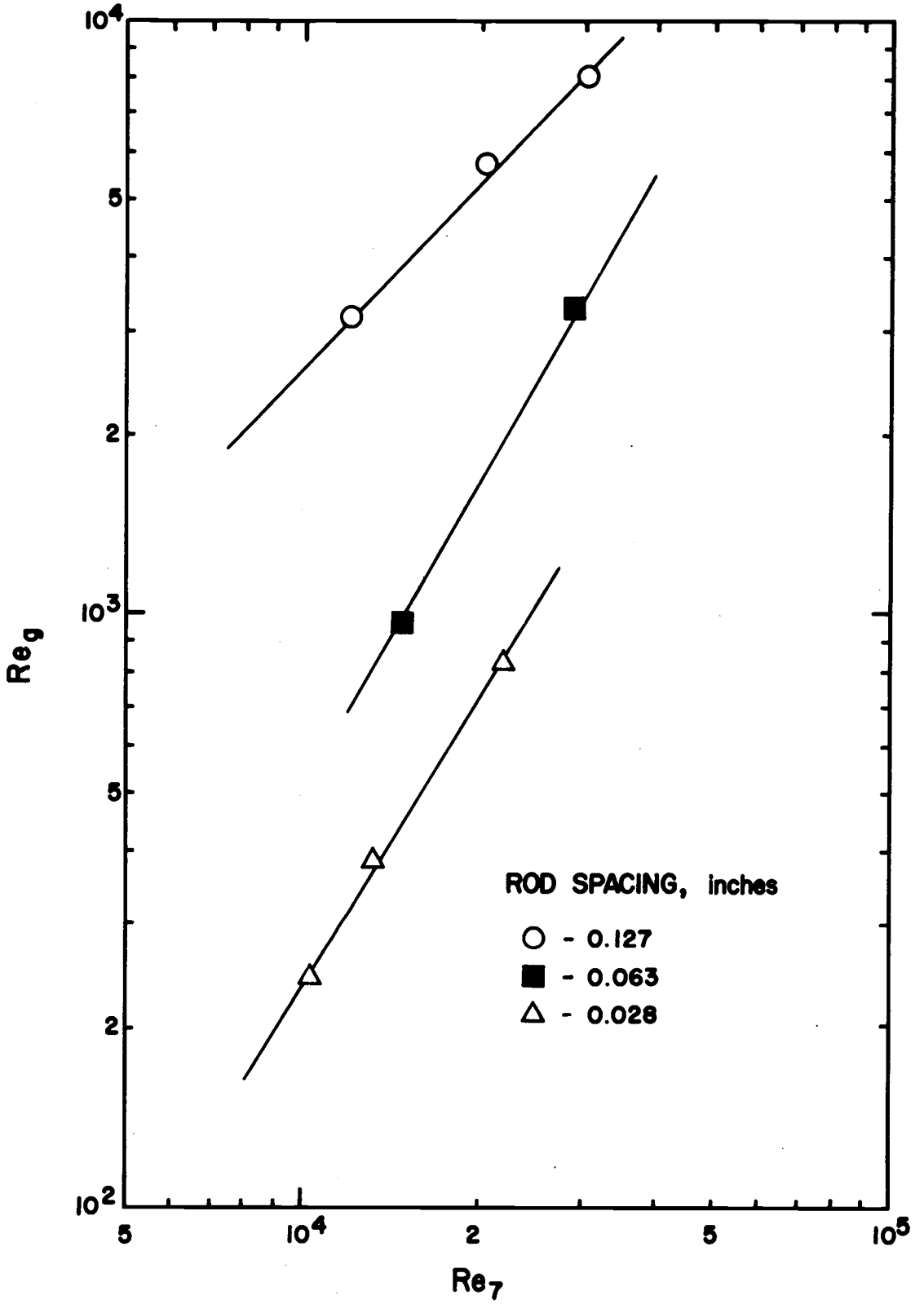

Figure 30. Gap Reynolds number versus subchannel 7 Reynolds number for the 0.028, 0.063 and 0.127 inch rod spacings.

Using the Blasius equation for the friction factor, Equation 55, evaluated for subchannel 7, Equation 67 can be written as follows:

$$\delta = 5\, de_7\, Re_7^{-0.875} \sqrt{\frac{2}{0.079}} \qquad (69)$$

If Equation 68 is divided by half the rod spacing, $b/2$, the resulting expression when plotted as a function of Re_7 gives the results shown in Figure 31.

This figure indicates that even though the gap may be near a complete laminar flow condition for the smaller rod spacing, turbulence could still exist in a portion of the gap.

Equation 68 will give an estimate of the average sublayer thickness in subchannels 7 or 8. In the region between the gap the layer could conceivably be thicker. Figure 31 indicates that the sublayer could fill at least one-half the gap at the 0.011 rod spacing and probably almost completely fills the gap under actual conditions. As the gap increases the effect of the laminar sublayer decreases. Hence for gap spacing greater than 0.028 inches the turbulent mixing correlations obtained appear reasonable.

This analysis indicates the reason why the 0.011-inch rod spacing did not fit the correlations. It appears that in the gap region between 0.011 and 0.028 inches the influence of the laminar sublayer is decreased significantly and does not provide a major resistance to cross channel mixing.

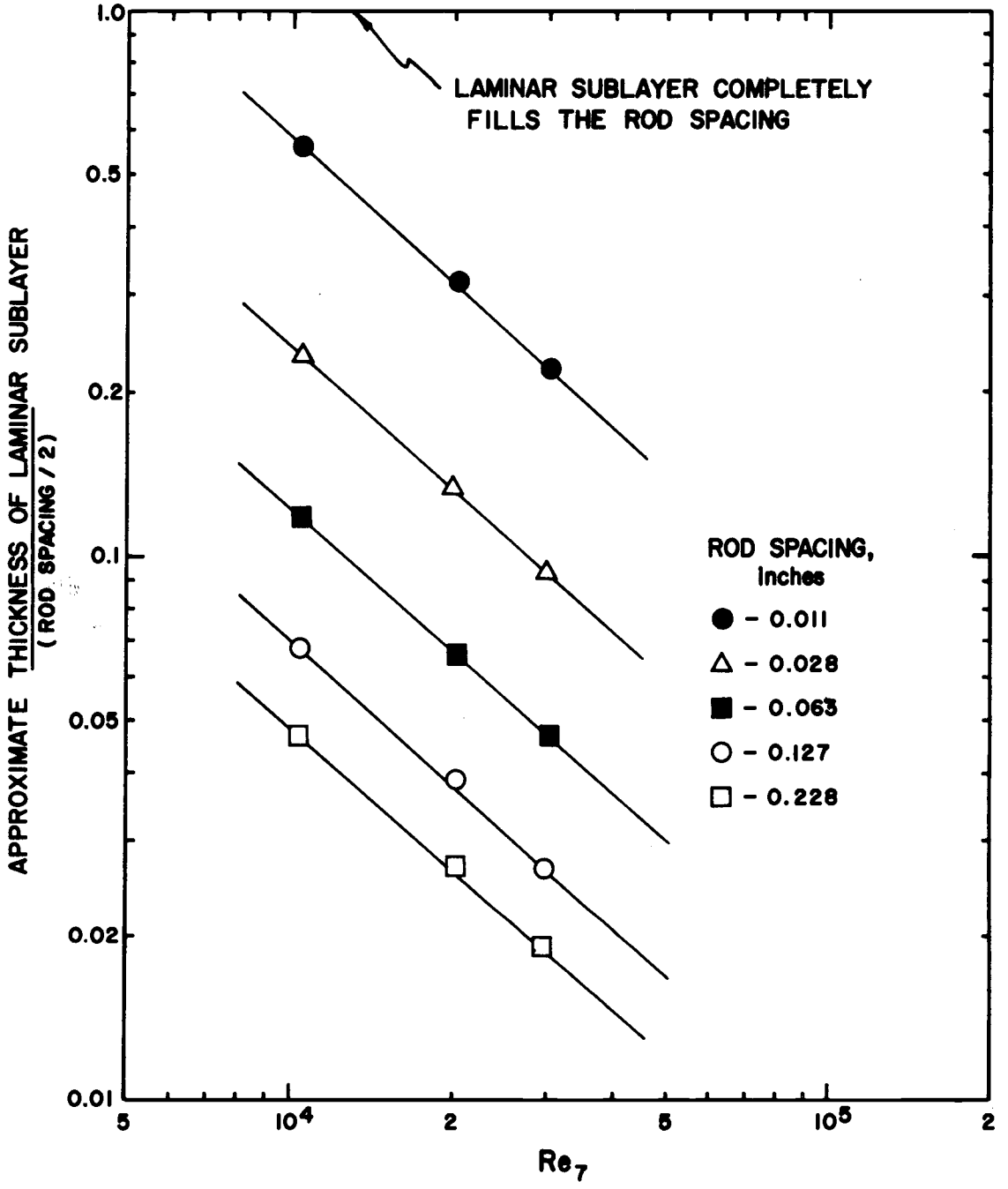

Figure 31. Estimated laminar sublayer thickness divided by one-half of the rod spacing versus subchannel 7 Reynolds number.

ESTIMATION OF EXPERIMENTAL AND CALCULATION ERRORS

Although a general estimate of the error for the two-channel and eight-channel mixing models was presented previously, a more formal approach will be presented here through the use of the error estimates of the various measured quantities.

Experimental Errors

System and Tracer Flow Rates

The flow rates of interest were calculated from the recorded rotameter readings which were converted to the desired mass flow rate through the calibration curves of Appendix B.

The system rotameters could be read to ±0.25 of the scale reading. For the range of scale readings considered, this gave mass flow rate results of ±1 percent. The tracer rotameter could be read to ±0.1 of the scale reading which gave the tracer flow rates of ±1 percent.

Concentration

The recorded tracer fluorescence was used with the calibration curves in Appendix C to calculate the dye concentration. The fluorometer could be read to ±0.5 percent fluorescence and checks of the

calibration curve at various times during the experimental procedure showed that the concentrations could be consistently reproduced to ±2 percent.

Pressure Drop

The inclined manometer could be read to ±0.2 cm which would give a calculated pressure gradient of ±2 percent. Since the pressure lines were always bled prior to making an experimental run, the presence of air in the manometer leads was not considered a problem.

Geometrical Lengths

The subchannel cross-sectional areas and wetted parameters were considered to be accurate within ±2 percent while the lengths measured in the axial direction for the test section were considered to be accurate within ±1 percent.

Calculated Errors

The estimate of error propagation as cited by Mickley, Sherwood and Reed (29, p. 53) was used for the error analysis of the mixing models and the other calculated results.

Two-Channel Mixing Model

The turbulent mixing between subchannels is defined for this

model by Equation 26, i.e.,

$$w_{78}^{t} = -\frac{m_7}{2L}\log_e\left(1-2\left(\frac{C_7^f}{C_o}\right)\right)$$

Taking the differential of the variable w_{78}^{t}

$$dw_{78}^{t} = \frac{\partial w_{78}^{t}}{\partial m_7}dm_7 + \frac{\partial w_{78}^{t}}{\partial L}dL + \frac{\partial w_{78}^{t}}{\partial C_7^f}dC_7^f + \frac{\partial w_{78}^{t}}{\partial C_o}dC_o \qquad (70)$$

where

$$\frac{\partial w_{78}^{t}}{\partial m_7} = -\frac{\log_e\left(1-2\left(\frac{C_7^f}{C_o}\right)\right)}{2L} \qquad (71)$$

$$\frac{\partial w_{78}^{t}}{\partial L} = \frac{m_7\log_e\left(1-2\left(\frac{C_7^f}{C_o}\right)\right)}{2L^2} \qquad (72)$$

$$\frac{\partial w_{78}^{t}}{\partial C_7^f} = -\frac{m_7\left(-\frac{2}{C_o}\right)}{2L\left(1-2\left(\frac{C_7^f}{C_o}\right)\right)} \qquad (73)$$

$$\frac{\partial w_{78}^{t}}{\partial C_o} = -\frac{m_7\left(2\left(\frac{C_7^f}{C_o^2}\right)\right)}{2L\left(1-2\left(\frac{C_7^f}{C_o}\right)\right)} \qquad (74)$$

If the total derivatives in Equation 70 are approximated by finite increments, i.e.,

$$dw_{78}^{t} = \Delta w_{78}^{t}$$

and both sides of the equation divided by w_{78}^{t} with Equations 71, 72, 73 and 74 replacing the partial derivative terms, the following equation results:

$$\frac{\Delta w_{78}^{t}}{w_{78}^{t}} = \frac{\Delta m_7}{m_7} - \frac{\Delta L}{L} - \frac{2\left(\frac{C_7^f}{C_o}\right)}{\left(1-2\left(\frac{C_7^f}{C_o}\right)\right)\log_e\left(1-2\left(\frac{C_7^f}{C_o}\right)\right)}\left(\frac{\Delta C_7^f}{C_7^f} - \frac{\Delta C_o}{C_o}\right) \tag{75}$$

Before the value of $\Delta w_{78}^{t}/w_{78}^{t}$ can be evaluated the terms C_7^f/C_o, $\Delta m_7/m_7$ and $\Delta C_o/C_o$ must be evaluated, i.e.,

$$\frac{\Delta C_o}{C_o} = \frac{\Delta(\text{measured concentration})}{\text{measured concentration}} + \frac{\Delta m}{m} - \frac{\Delta m_t}{m_t} \tag{76}$$

$$\frac{\Delta C_o}{C_o} = \pm 4\%$$

where the various experimental errors have been used to replace the terms in Equation 76 such that the maximum possible error is obtained.

The evaluation of $\Delta m_7/m_7$ was made by considering Equation

45 and an equation similar to Equation 46 which related U_7 and U_I and using the error propagation technique, i.e.,

$$\frac{\Delta U_7}{U_7} = \frac{1.6}{1.75}\frac{\Delta U_I}{U_I} + \frac{1.25}{1.75}\frac{\Delta de_7}{de_7} - \frac{1.4}{1.75}\frac{\Delta de_I}{de_I} \qquad (77)$$

where

$$\frac{\Delta U_I}{U_I} = \pm 3\%$$

$$\frac{\Delta de_7}{de_7} = \frac{\Delta de_I}{de_I} = \pm 2\%$$

Therefore the maximum possible error for Equation 77 is ±7 percent. Using this result the value of $\Delta m_7/m_7$ was found to be accurate within ±10 percent. All of the values needed for evaluation of Equation 71 are now known with the exception of C_7^f/C_o which changes for each experimental run. If the two extreme cases for C_7^f/C_o are considered

1. 0.011 inch rod spacing, run 29; $\frac{C_o}{C_7^f} = 936.1 \left\{ \frac{\Delta w_{78}^t}{w_{78}^t} = \right. \begin{matrix} \pm 17\% \\ \pm 11\% \end{matrix}$
2. 0.228 inch rod spacing, run 14; $\frac{C_o}{C_7^f} = 22.2$

Eight-Channel Mixing Model

This model does not lend itself to the analysis routine used for

determination of the error for the two-channel mixing model since the cross-flow, w'_{78}, is not an explicit result of the analysis. Since the RKM algorithm had a constant error criteria of 10^{-5}, the subchannel concentrations were considered to be as accurate as the measured exit concentrations. When this approximation is used with the convergence criteria which actually controls the accuracy of the calculated value of w'_{78}, an error estimate equal to the acceptance criteria is obtained, ±5 percent.

Friction Factor

The experimental friction factor was calculated for the half of the total flow cross-section and used the measured pressure drop for the mixing length. The error propagation technique was used with Equation 49 to give the following error estimate:

$$\frac{\Delta f}{f} = \pm 12\%$$

Subchannel Reynolds Number

The turbulent mixing data was correlated as a function of the subchannel Reynolds number. An estimate of the error gave the following results for the Reynolds numbers used in the various correlations:

$$\frac{\Delta Re_7}{Re_7} = \pm 11\%; \qquad \frac{\Delta Re_I}{Re_I} = \pm 7\% .$$

RESULTS AND CONCLUSIONS

The effects of rod spacing and mass flow rates on the turbulent interchange between adjacent subchannels in a simulated rod bundle were investigated and both were found to be significant parameters effecting the turbulent interchange.

Both the two-channel model and the eight-channel model gave results that were sensitive to the rod spacing. This was particularly true when the 0.011-inch rod spacing mixing results were compared to the other rod spacing results for both models. At the higher rod spacings 0.028, 0.063, 0.127 and 0.228, the two-channel model gave results that increased with an increase in rod spacing. The same general results were obtained for the eight-channel model except that the resolution between the various rod spacings was not as pronounced. The cause of the overlapping of the mixing results for various rods spacings for this model was considered to be related to the convergence criteria for the model and the subchannel mass velocity fit to the continuity equation. Even so, the mixing results for this model also indicated that transport between adjacent subchannels was a function of the rod spacing for the scope of this investigation.

Independent of the mixing model used to evaluate the observed experimental results, the significant difference in the subchannel mixing between the 0.011 and 0.028-inch rod spacing was considered to

be a result of the fluid dynamic conditions within the gap. It was estimated qualitatively that the 0.011-inch rod spacing was filled or very nearly filled by the laminar sublayer which would subject the turbulent transport mechanism to direct viscous dissipation (3, p. 258). The turbulent transport results for the other rod spacings indicated that the effects of the laminar sublayer were nominal when considered relative to the 0.011-inch turbulent transport results.

The turbulent mixing for all the rod spacings investigated increased as the subchannel mass flow rate was increased. This is consistent with the fact that as the mass flow rate increases the thickness of the laminar sublayer decreases thus the area of viscous dissipation of the eddies is reduced which enhances the turbulent transport. At the same time, the fluid motion in the vicinity of the gap approaches the fluid conditions in the turbulent core of the subchannel and the maximum transport condition for the geometry is approached.

The turbulent mixing results were correlated with the duct or channel eddy diffusivity which was considered as the ultimate value possible for the interchannel transport. This approach led to the fact that the dimensionless length, b/z_{78}, may be considered a correction factor for subchannel turbulent mixing when the mixing results are correlated with the duct eddy diffusivity.

The subchannel mixing length, z_{78}, was found to be a function

of the subchannel Reynolds number and rod spacing. This result was found to be consistent with the experimental subchannel velocity profiles and the concepts associated with the duct mixing length for turbulent flow for the range of Reynolds numbers investigated in this study.

The above results were for the system void of lateral pressure gradients between adjacent subchannels. The effects of a pressure bias (lateral pressure gradient) in the test section were studied for the 0.011 and 0.127-inch rod spacings. This investigation indicated that the smaller rod spacing was more sensitive to small pressure gradients than was the larger rod spacing.

This study also gave mixing results that decreased with an increase in the mass flow rate which was the reported result of earlier investigators (23; 32, p. 3; 41; 52, p. 3). This implied that the experimental systems of the cited references could be pressure biased or that diversion cross-flow had not been eliminated. These results thus indicate the importance of a balanced system when turbulent mixing between subchannels is to be measured.

The following conclusions were thus drawn from this investigation of turbulent mixing between adjacent subchannels for the Reynolds number and rod spacings considered:

1. The mixing between subchannels is a function of the rod spacing and the subchannel mass flow rate.
2. Small pressure gradients between adjacent subchannels have

a significant effect upon the interchannel mixing.

3. The subchannel mixing can be compared to turbulent mixing in the turbulent core of a duct.

4. The rod spacing when nondimensionalized with a subchannel mixing length may be considered a correction factor to the turbulent mixing for a duct.

5. The gap flow conditions seem to control the subchannel mixing for the 0.011-inch rod spacing but have a lesser effect for the 0.028, 0.063, 0.127 and 0.228-inch rod spacings.

6. The two-channel mixing model results can be predicted by the following semi-empirical relationship:

$$\frac{w^t_{78}}{\mu} = \left[1-\exp\left(-0.158\ \exp\left(5.17\frac{b}{de_7}\right) - 10^{-5}\left(0.618+2.34\frac{b}{de_7}\right)Re_7\right)\right]\frac{E}{\nu}$$

where

$$\frac{E}{\nu} = 0.0113\ Re_7^{0.875}$$

This result predicted the actual results with a standard relative error of $\pm$ 5 percent, when the 0.011-inch rod spacing results are excluded.

7. The eight-channel mixing model results can be predicted by the following semi-empirical relationship:

$$\frac{w^t_{78}}{\mu} = \left[1-\exp\left(-0.14\ \exp\left(4.75\frac{b}{de_7}\right) - 10^{-5}\left(1.1+4.7\frac{b}{de_7}\right)Re_7\right)\right]\frac{E}{\nu}$$

where

$$\frac{E}{\nu} = 0.0113\ Re_7^{0.875}$$

This result predicted the actual results with a standard relative error of ±8 percent, when the 0.011-inch rod spacing results are excluded.

RECOMMENDATIONS FOR FURTHER STUDY

1. The investigation of turbulent mixing for other geometrical forms such as triangle-triangle and triangle-square should be considered so that the complete description of turbulent mixing in a rod bundle may be made.
2. It is recommended that the range of Reynolds numbers and rod spacings of this investigation be extended to further substantiate the results and conclusions of this study.
3. A study of the effects of mechanical mixing devices such as warts, wire wraps and spacers is recommended. An investigation of this nature could provide valuable pressure drop data and mixing results for various design configurations for such devices.
4. More experimental information on the pressure drop for axial flow through rod bundles is needed so that accurate subchannel mass velocity calculations may be made. This type of investigation should consider rod spacing as one of the parameters of interest since it does appear to have an effect. The simulated rod bundle design or rod bundle design should not have the rods touching the rod bundle housing.
5. It is recommended that a point velocity investigation in the vicinity of the rod spacing be made with a device capable of

measuring the turbulent intensities. A study of this nature could yield significant information as to the mechanism of turbulent transport between adjacent subchannels.

BIBLIOGRAPHY

1. Armistead, R. A., Jr. and J. J. Keyes, Jr. A study of wall-turbulence phenomena using hot-film sensors. Journal of Heat Transfer 90:13-21. 1968.

2. Bowring, R. W. HAMBO: A computer program for the subchannel analysis of the hydraulic and burnout characteristics of rod clusters. 1968. 60 p. (Atomic Energy Establishment. AEEW-R-582) (Microfiche)

3. Brodkey, Robert S. The phenomena of fluid motions. Reading, Massachusetts, Addison-Wesley Publishing Company, 1967. 736 p.

4. Carpenter, J. H. Tracer for circulation and mixing in natural waters. Public Works 91:110-112. 1960.

5. Churchill, R. V. Operational mathematics. 2d ed. New York, McGraw-Hill, 1958. 337 p.

6. Clarke, G. J. Mixing studies of types C19A14B, C19A14C and C19X8D fuel bundles. 1961. 96 p. (Atomic Energy of Canada. Nuclear Plant Division. TCVI-19)

7. Clayton, C. G., A. M. Ball and R. Spackman. Dispersion and mixing during turbulent flow of water in a circular pipe. 1968. 33 p. (United Kingdom Atomic Energy Authority. AERE-R5569) (Microfiche)

8. Dean, R. A. Coolant mixing in open lattice reactor cores. 1963 50 p. (Westinghouse Electric Corporation. Atomic Power Division. WCAP-3735) (Microcard)

9. Deissler, R. G. Analytical and experimental investigation of adiabatic turbulent flow in smooth tubes. Washington, D. C., 1950. 41 p. (U. S. National Advisory Committee for Aeronautics. Technical Note NACA TN 2138)

10. Deissler, R. G. Analysis of turbulent heat transfer, mass transfer, and friction in smooth tubes at high prandtl and schmidt numbers. Washington, D. C., 1955. 14 p. (U. S. National Advisory Committee for Aeronautics. NACA Report 1210)

11. Deissler, R. G. and M. F. Taylor. Analysis of axial turbulent flow and heat transfer through banks of rods or tubes. Presented at Reactor Heat Transfer Conference, Cleveland, Ohio. 1957.

12. Eckert, E. R. G. and T. R. Irvine. Flow in corners of passages with noncircular cross sections. American Society of Mechanical Engineers, Transactions 78:709-718. 1956.

13. Eifler, W. and R. Nijsing. Experimental investigation of velocity distribution and flow resistance in a triangular array of parallel rods. Nuclear Engineering and Design 5:22-42. 1967.

14. Elder, J. W. The dispersion of marked fluid in turbulent shear flow. Journal of Fluid Mechanics 5:544-560. 1959.

15. Elzy, E. Assistant Professor, Oregon State University, Department of Chemical Engineering. Personal communication. Corvallis, Oregon. May, 1969.

16. Fenerstein, D. L. and R. E. Selleck. Fluorescent tracers for dispersion measurements. Proceedings of the American Society of Civil Engineers, Journal of the Sanitary Engineering Division 89(SA4):1-21. 1963.

17. Flint, D. L., H. Kada and T. J. Hanratty. Point source turbulent diffusion in a pipe. American Institute of Chemical Engineers, Journal 6:325-331. 1960.

18. Gessner, F. B. and J. B. Jones. On some aspects of fully developed turbulent flow in rectangular channels. Journal of Fluid Mechanics 23:689-713. 1965.

19. G. K. Turner Associates. Fluorometry in studies of pollution and movement in fluids. Palo Alto, 1968. 19 p. (Flurometry Reviews. Accession number 9941)

20. G. K. Turner Associates. Turner laboratory instruments. Catalogue. Palo Alto, 1967. 27 p.

21. Hamming, R. W. Numerical methods for scientists and engineers. New York, McGraw-Hill, 1962. 411 p.

22. Harlow, F. H. and P. L. Nakayama. Turbulence transport equations. The Physics of Fluids 10:2323-2332. 1967.

23. Hetsroni, G., J. Leon and M. Hakim. Cross flow and mixing of water between semiopen channels. Nuclear Science and Engineering 34:189-193. 1968.

24. Hinze, J. O. Turbulence. New York, McGraw-Hill, 1959. 586 p.

25. Kays, W. M. Convective heat and mass transfer. New York, McGraw-Hill, 1966. 387 p.

26. Knudsen, J. G. The effect of mixing on burnout in multirod bundles. 1964. 51 p. (Hanford Atomic Products Operation. HW-84525)

27. Knudsen, J. G. and D. L. Katz. Fluid dynamics and heat transfer. New York, McGraw-Hill, 1958. 576 p.

28. McCarter, R. J., L. F. Stutzman and H. A. Kock, Jr. Temperature gradients and eddy diffusivities in turbulent fluid flow. Industrial and Engineering Chemistry 41:1290-1295. 1949. (Microfiche)

29. Mickley, H. S., T. K. Sherwood and C. E. Reed. Applied mathematics in chemical engineering. 2d ed. New York, McGraw-Hill, 1957. 413 p.

30. Moyer, C. B. Coolant mixing in multirod fuel bundles. 1966. 37 p. (Danish Atomic Energy Commission. RISO-125)

31. Nijsing, R., W. Eifler, F. Delfau and J. Composilvan. Studies on fluid mixing between subchannels in a bundle of finned tubes. Nuclear Engineering and Design 5:229-253. 1967.

32. Petrunik, K. J. Turbulent mixing measurements for single-phase air, single-phase water and two-phase air-water flows in adjacent rectangular subchannels. Master's thesis. Windsor, Ontario, University of Windsor, 1968. 74 numb. leaves.

33. Prandtl, L. Über die ausgebildete turbulenz. Zeitschrift für angewandte Mathematik und Mechanik 5:136-139. 1925.

34. Reynolds, O. On the experimental investigation of the circumstances which determine whether the motion of water shall be direct or sinuous, and the law of resistance in parallel channels. The Royal Society, Philosophical Transactions 174:945-982. 1883. (Cited in: Foust, A. S. et al. Principles of Unit Operations. 2d ed. New York, John Wiley and Sons, Incorporated, 1962. p. 140)

35. Rogers, J. T. and W. R. Tarasuk. A generalized correlation for natural turbulent mixing of coolant in fuel bundles. Presented at the American Nuclear Society Meeting, Toronto, Ontario. 1968.

36. Rogers, J. T. and W. R. Tarasuk. Inter-sub-channel coolant mixing in close-packed reactor fuel bundles. Part I. Natural Mixing. 1966. 104 p. (Canadian General Electric Company. CGE Report R64CAP29-I)

37. Rowe, D. S. A mechanism for turbulent mixing between rod bundle subchannels. Presented at the American Nuclear Society Meeting, San Francisco, California. 1969.

38. Rowe, D. S. COBRA-II: A digital computer program for thermal-hydraulic subchannel analysis of rod bundle nuclear fuel elements. 1970. 60 p. (Battelle Memorial Institute. Pacific Northwest Laboratories. BNWL-1229)

39. Rowe, D. S. Cross-flow mixing between parallel flow channels during boiling. Part I. COBRA-computer program for coolant boiling in rod arrays. 1967. 87 p. (Battelle Memorial Institute. Pacific Northwest Laboratories. BNWL-371-PTI)

40. Rowe, D. S. and C. W. Angle. Cross-flow mixing between parallel flow channels during boiling. Part II. Measurement of flow and enthalpy in two parallel channels. 1967. 55 p. (Battelle Memorial Institute. Pacific Northwest Laboratories. BNWL-371-PTII)

41. Rowe, D. S. and C. W. Angle. Cross-flow mixing between parallel flow channels during boiling. Part III. Effect of spacers on mixing between channels. 1968. 69 p. (Battelle Memorial Institute. Pacific Northwest Laboratories. BNWL-371-PTIII)

42. Schlichting, Hermann. Boundary layer theory. 6th ed. New York, McGraw-Hill, 1968. 747 p.

43. Schubert, G. and G. M. Coros. The dynamics of turbulence near a wall according to a linear model. Journal of Fluid Mechanics 29:113-135. 1967.

44. Sherwood, T. K. Heat transfer, mass transfer, and fluid friction. Industrial and Engineering Chemistry 42:2077-2084. 1950.

45. Sherwood, T. K. and W. L. Towle. Eddy diffusion, mass transfer in the central portion of a turbulent air stream. Industrial and Engineering Chemistry 31:457-462. 1939.

46. Sherwood, T. K. and B. B. Wortz. Mass transfer between phases. Industrial and Engineering Chemistry 31:1034-1041. 1939.

47. Singleton, N. R. Mixing due to eddy diffusion between parallel open flow channels. Master's thesis. Pittsburgh, University of Pittsburgh, 1963. 85 numb. leaves.

48. Skinner, J. R., A. R. Freeman and H. G. Lyall. Gas mixing in rod clusters. International Journal of Heat and Mass Transfer 12:265-278. 1969.

49. St. Pierre, C. C. Subchannel analysis for the steadystate. 1966. 84 p. (Atomic Energy of Canada. SASS Code I. APPE-41) (Microfiche)

50. Szablewski, Von W. Turbulente parallel stromungen. Zeitschrift für angewandte Mathematik und Mechanik 48:35-50. 1968.

51. Waggener, J. P. Friction factors for pressure-drop calculations. Nucleonics 19:145-147. 1961.

52. Walton, F. B. Turbulent mixing measurements for single-phase air, single-phase water and two-phase air-water flows in adjacent triangular-triangular subchannels. Master's thesis. Windsor, Ontario, University of Windsor, 1969. 97 numb. leaves.

53. Walton, F. B., K. J. Petrunik and C. C. St. Pierre. Two phase air-water turbulent mixing between parallel flow channels. Presented at the American Institute of Chemical Engineers National Meeting, Portland, Oregon. 1969.

54. Wilson, J. F. Fluorometric procedures for dye tracing. Washington, D. C., 1968. 44 p. (U. S. Department of the Interior. Chapter A12)

APPENDICES

APPENDIX A

NOMENCLATURE

NOMENCLATURE

Symbol	Definition	Dimension
a	empirical constant	
Ac	cross-sectional area	ft^2
A_T	mixing coefficient	$lb_m/ft\text{-}hr$
b	rod spacing	ft
c	empirical constant	
C	tracer concentration	ppb
C^f	final tracer concentration	ppb
COT	tracer concentration in holding tank	ppm
Cp	heat capacity	$Btu/lb_m\text{-}°F$
d	rod diameter	ft
de	hydraulic diameter	ft
D	circular duct diameter	ft
DIFF	difference between measured and calculated channel tracer mass balance	parts/hr
E	apparent eddy diffusivity for flow in a duct	ft^2/hr
E_h	eddy diffusivity of heat	ft^2/hr
E_m	eddy diffusivity of mass	ft^2/hr
E_M	eddy diffusivity of momentum	ft^2/hr
f	Fanning friction factor	dimensionless

Symbol	Definition	Dimension
$f(b, Re_7)$	empirical correlation function	dimensionless
g	acceleration due to gravity	ft^2/sec^2
g_c	gravitational constant	$lb_m\text{-}ft/lb_f\text{-}sec^2$
ℓ	Prandtl mixing length	ft
$\log_e$	natural logrithm	
L	axial mixing length in test section	ft
m	total mass flow rate to test section	lb_m/hr
m_t	tracer mass flow rate	lb_m/hr
n	empirical constant	
N	number of subchannels	dimensionless
P	pressure	lb_f/ft^2
ΔP	finite pressure difference	lb_f/ft^2
P_I	impact pressure	lb_f/in^2
Re	Reynolds number	dimensionless
Δs	manometer reading	cm
$\overline{T}$	average temperature	°F
u	point velocity	ft/sec
U	average velocity	ft/hr
w_{ij}^t	turbulent cross-flow mass flow rate per unit length between subchannels i and j	$lb_m/ft\text{-}hr$
x	distance along duct or subchannel axis	ft
Δx	finite axial position difference	ft

Symbol	Definition	Dimension
y	distance from wall of duct	ft
y	universal dimensionless length	
z	length normal to axis of flow and through the center line of the rod spacing	in
z_{ij}	semi-empirical mixing distance between adjacent subchannels i and j	ft

Greek symbols

α, γ	correction factor for cross-flow mixing to peripheral subchannels	
ρ	fluid density	lb_m/ft^3
μ	dynamic viscosity	$lb_m/ft\text{-}hr$
ν	kinematic viscosity	ft^2/hr
τ_o	wall shear stress	lb_f/ft^2

Subscripts

i, j	subchannel notation; 1-8
I, II	channel notation
o	initial condition

APPENDIX B

CALIBRATION OF THE ROTAMETERS

CALIBRATION OF THE ROTAMETERS

The test section rotameters and the tracer rotameter were calibrated by measuring the mass and volume flow rates respectively.

Test Section Rotameters

The channel rotameters used for this investigation were calibrated while they were on-line by measuring the time required to discharge a 50 or 100 lb_m sample to a holding tank. The rotameter discharge was passed directly to a holding tank that was on a previously calibrated scales. The holding tank discharge was controlled with a quick action ball valve. A Lab-Chron electric timer was used as the timing device. The general technique was such that the timer was started and stopped with the movement of the weighing scale arm for 50 to 100 lb_m samples.

The measured variables were the rotameter scale readings (10-80), the water temperature, the mass change and the time required for the mass change. The results were plotted as rotameter scale readings versus the measured mass flow rates (see Figure 32). The results were reproducible to ±1 percent.

Tracer Rotameter

The tracer rotameter was calibrated using a volume

displacement technique because the small flow rates did not make mass measurements practical. The rotameter was discharged to a graduated cylinder and the volume displaced for a measured time was recorded. The Lab-Chron timer was used to measure the elapsed time for the volume displacement.

The results were plotted as rotameter scale readings versus the measured volume flow rate (see Figure 33). The results agreed with the calibration curve supplied by Fisher-Porter for water. This was expected in view of the dye concentration (1 to 2 grams per liter of water) and the temperature.

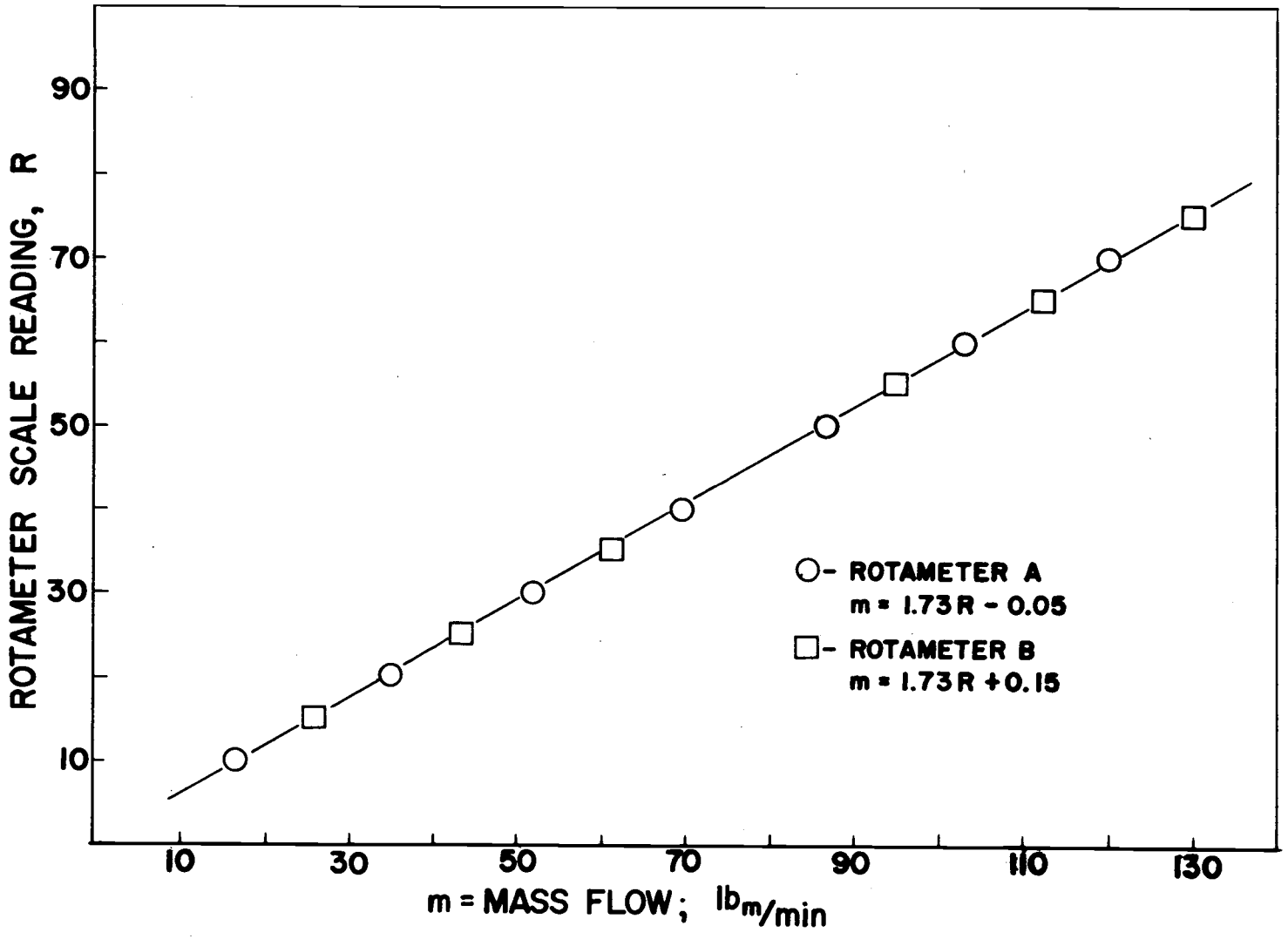

Figure 32. Test section rotameter calibrations.

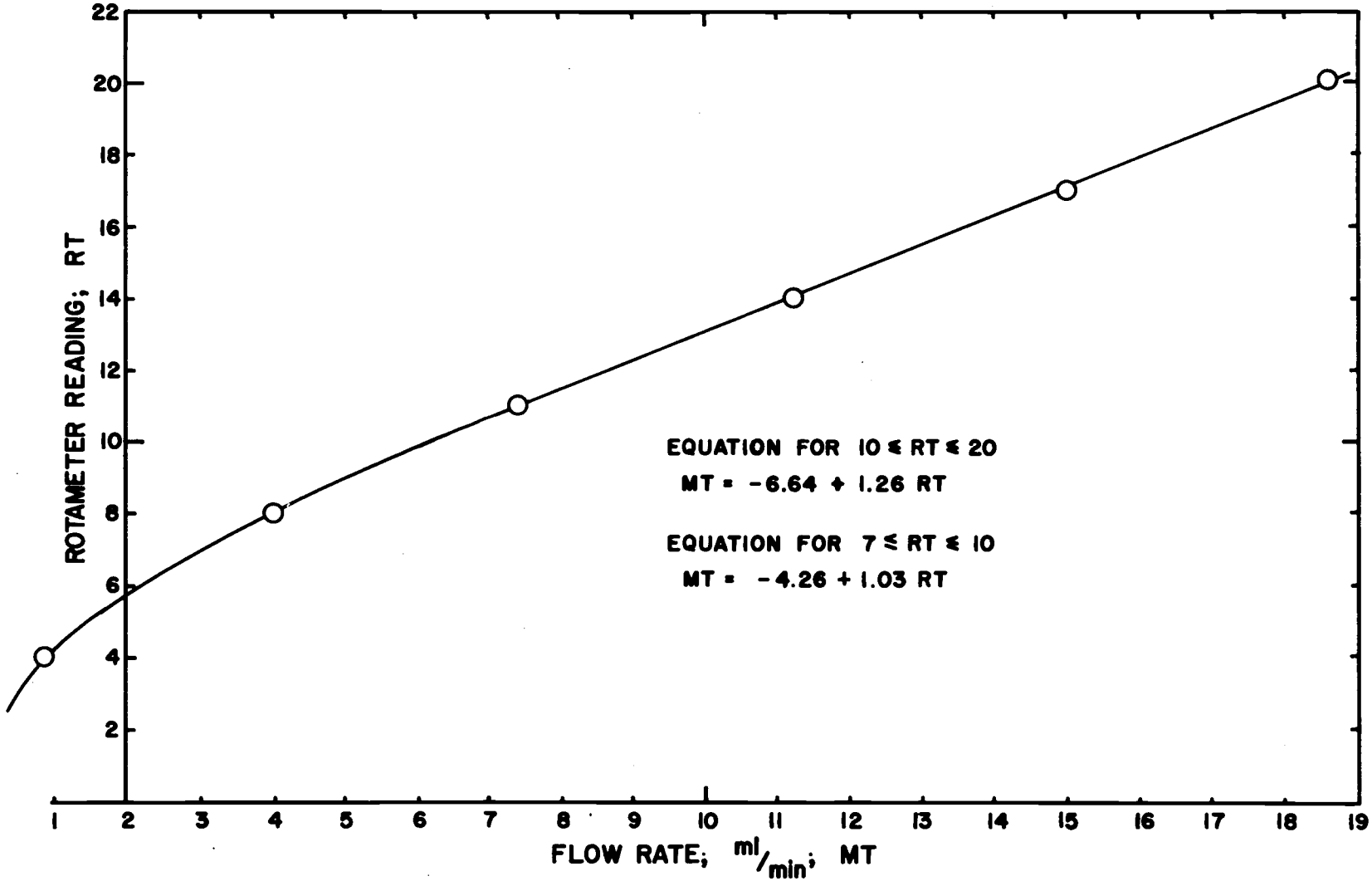

Figure 33. Tracer rotameter calibration.

APPENDIX C

CALIBRATION OF THE FLUOROMETER

CALIBRATION OF THE FLUOROMETER

The measurement of the rhodamine B dye concentration was made with a G. K. Turner F-111 fluorometer which can be used for batch or continuous analysis of the dye fluorescence. The fluorometer is a self balancing double beam instrument that measures the ratio of the intensities of the fluorescent light and a constant portion of the light from the light source. This method of operation eliminates the need to account for light source fluctuation due to line voltage variations, drift due to warmup or long term drift due to aging of the components.

Since the continuous analysis of the dye was used for the experimental program, the fluorometer was calibrated for continuous operation by using a simple closed system that included a 5 liter holding tank, centrifugal pump, mercury thermometer and a 50 ml burette.

The following procedure was used to calibrate the fluorometer at each of its four sensitivities:

1. The holding tank was filled with water from the city water main and the volume of water, Vw, added was recorded.
2. The fluorometer was zeroed (adjusted to read zero fluorescence).
3. The addition of measured quantities of a known concentration solution of rhodamine B was made with the burette.

4. The temperature of the solution was constantly monitored.
5. The total volume of material (dye plus water), quantity of dye added and the fluorescence reading were recorded for the volume of the dye added to the system.
6. The system concentration was calculated from the following equation:

$$C = C_s \frac{V_s}{V_t}$$

where

C = concentration of solution in the system

C_s = concentration of known added to the system

V_s = volume of known added to the system

$V_t = Vw + V_s$ = total volume of material in the system.

All runs were made at a fluid temperature of 68 to 69° F. The results were plotted as fluorometer reading versus dye concentration (see Figures 34 through 37).

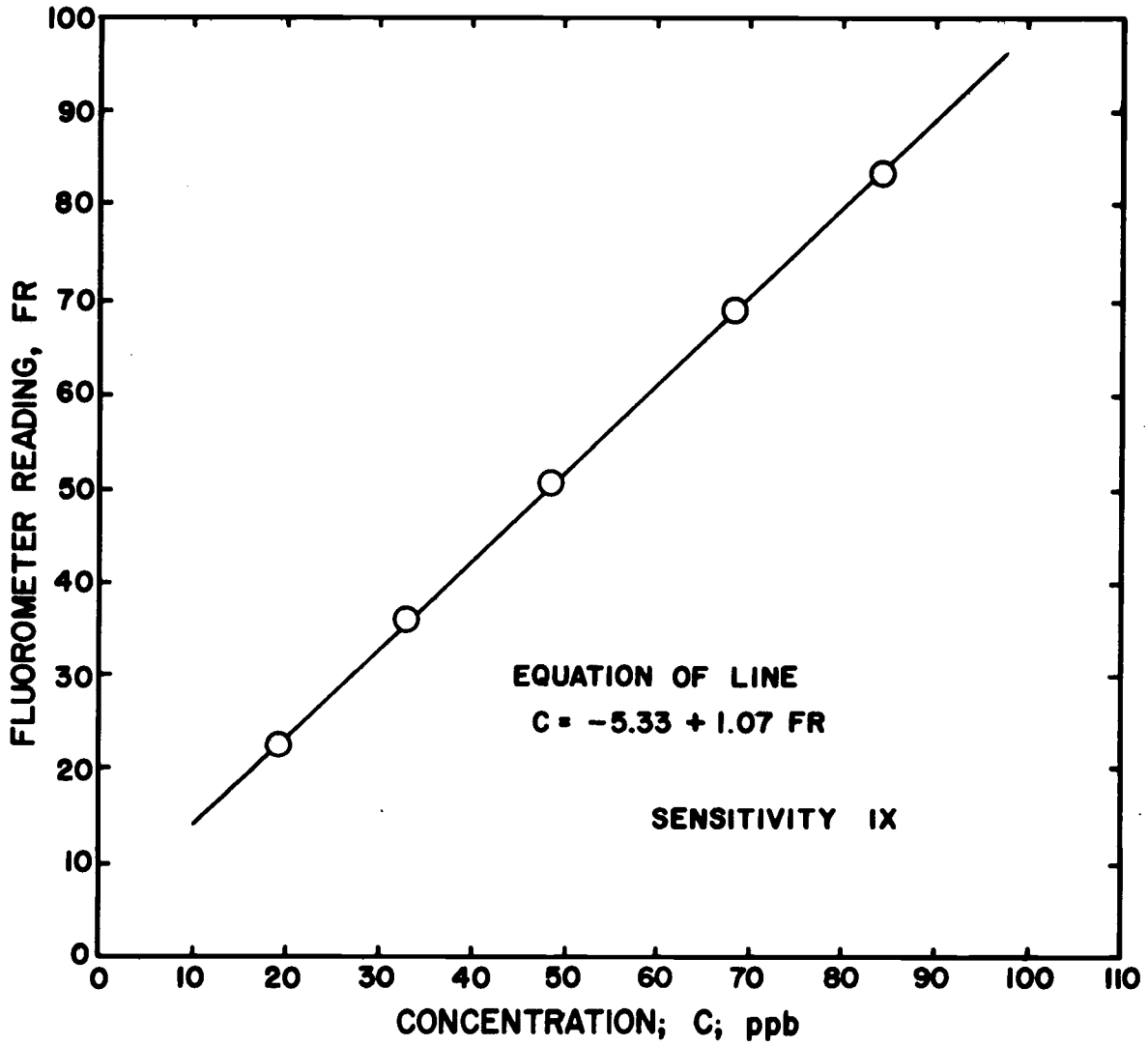

Figure 34. Fluorometer calibration for 1x sensitivity.

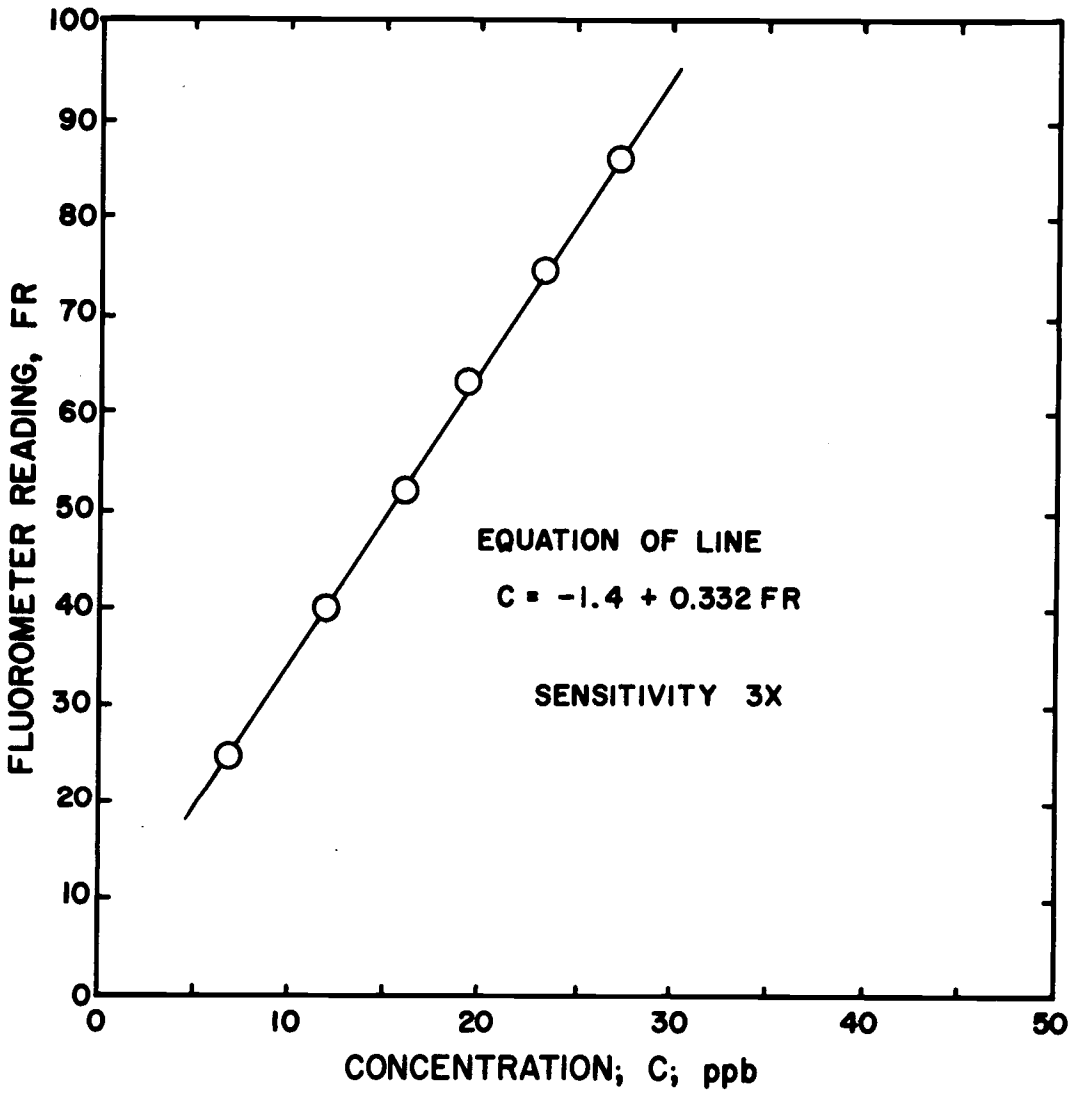

Figure 35. Fluorometer calibration for 3x sensitivity.

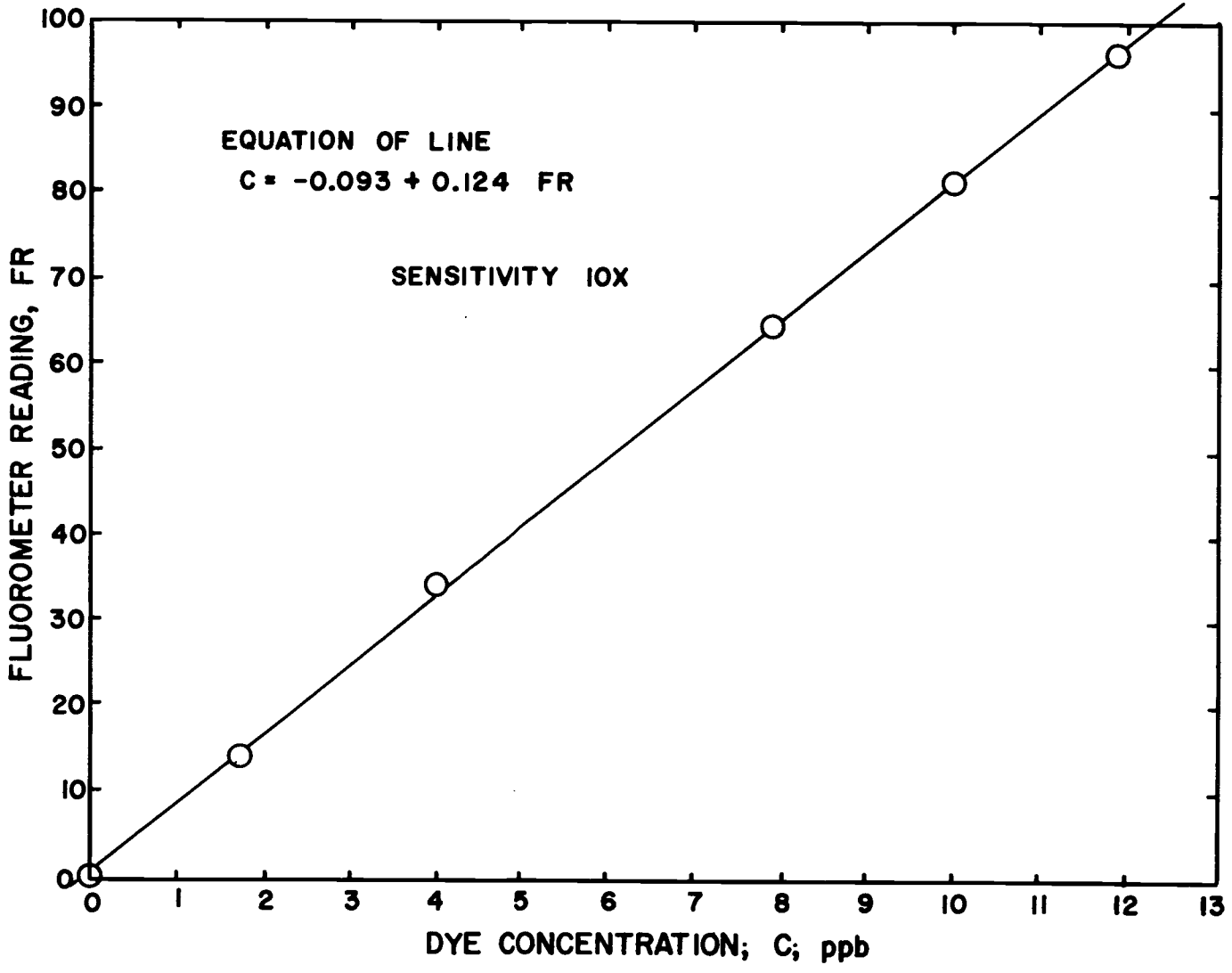

Figure 36. Fluorometer calibration for 10x sensitivity.

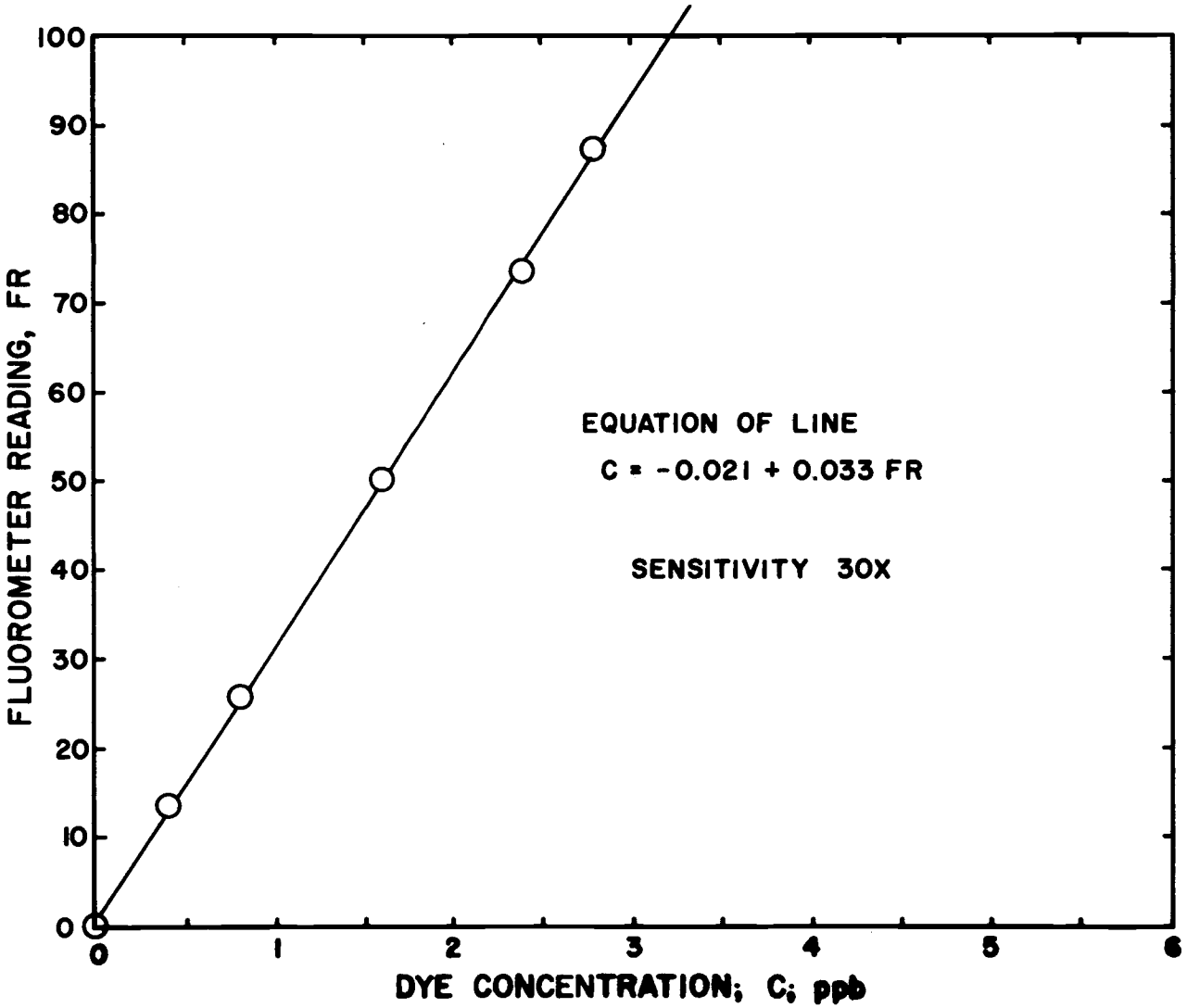

Figure 37. Fluorometer calibration for 30x sensitivity.

APPENDIX D

CALIBRATION OF THE PACE PRESSURE TRANSDUCER

CALIBRATION OF THE PACE PRESSURE TRANSDUCER

The pressure transducer was calibrated by using a static water head. The transducer was a Pace model KP15 in which the pressure is sensed through the deflection of a flat magnetic stainless steel diaphragm located between two magnetic pick off coil assemblies. The motion of the diaphragm results in a change in the inductance ratio between the pick off coils and through the appropriate bridge circuit producing an output voltage proportional to the pressure.

The transducer voltage output was sensed with a Pace model CD25 Transducer Indicator (TI) that gave the voltage as a meter indication or as a three digit dial reading. The digital reading was obtained by using the meter as a null balance indicator. The transducer indicator operated with 115 volt 60 cps power.

The following sequence of steps was followed to calibrate the pressure transducer:

1. The temperature of the water used for static calibration was recorded.
2. The transducer indicator span for maximum pressure gradient (1.0 psi) (maximum static head) was set.
3. The static head was brought to zero and the transducer read-out was zeroed.
4. Both the span and the zero settings were checked and reset

if necessary and then recorded.

5. The static head versus TI output was recorded for the entire pressure range of the transducer.

After the transducer was calibrated, it was tested in a dynamic field for the full pressure gradient range of the diaphragm. It was then rechecked with a static water head. There was no change in the calibration curve. The results were plotted TI dial reading versus the measured static water head (see Figure 38).

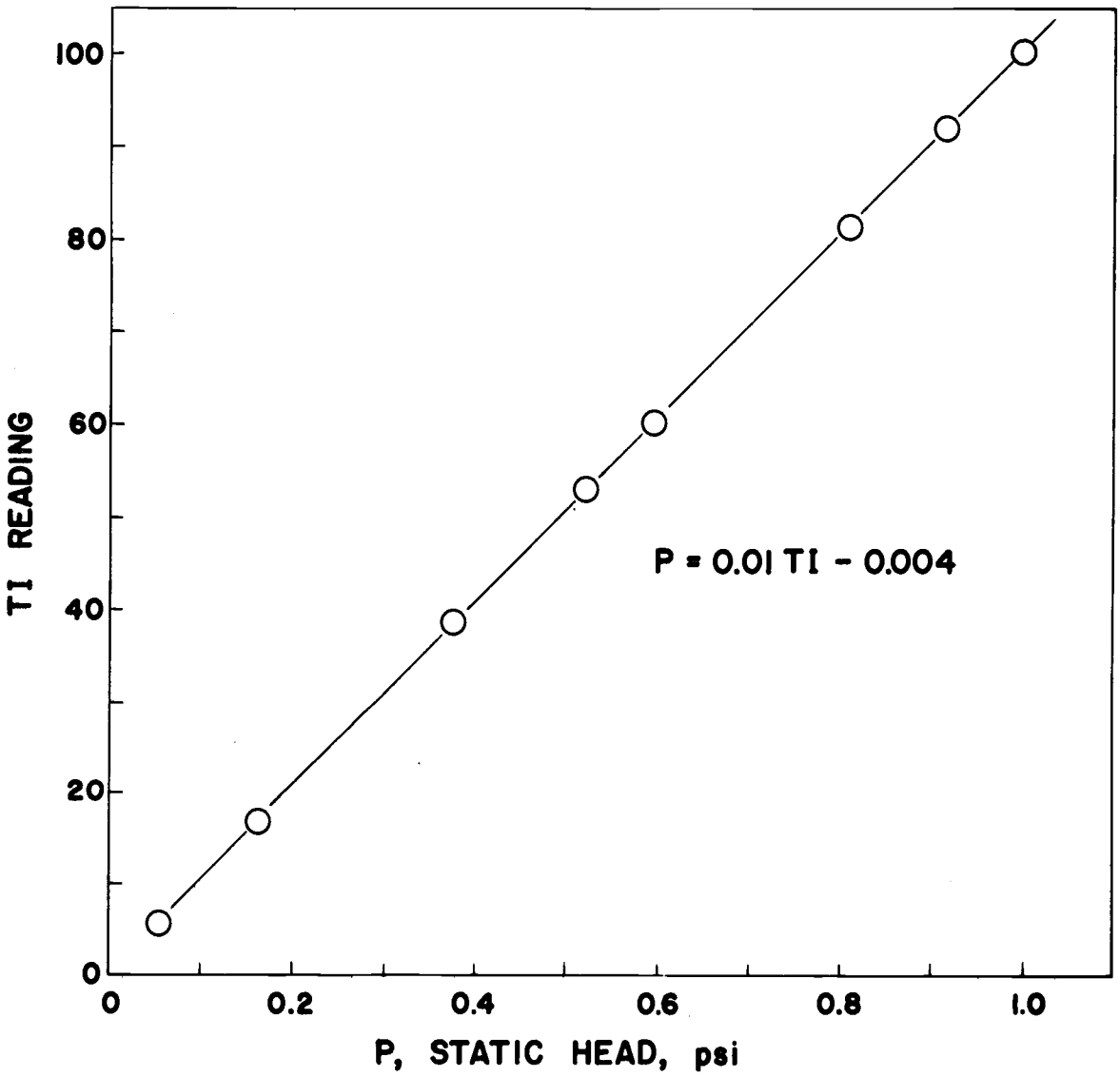

Figure 38. Transducer calibration.

APPENDIX E

OBSERVED DATA

NOMENCLATURE FOR OBSERVED DATA

Symbol	Definition	Dimension
RA, RB	test section rotameter readings	
RT	tracer rotameter readings	
HI, LO	leg readings for inclined manometer; Δs = (HI-LO)	cm
SEN	fluorometer sensitivity	
FLO	fluorescence readings for fluorometer	percent
T	fluid temperature	°F
CHT	channel initially traced 1 = subchannels 1, 2, 6 and 7	
COT	tracer concentration	ppb

OBSERVED PRESSURE BALANCED MIXING DATA

OBSERVED DATA FOR ROD SPACING = .011 INCHES

RUN	RA	RB	RT	HI	TC	SEN	FLO	T CHT	CCT
28	28.2	28.2	19.2	44.30	36.90	30	35.0	68 1	1.208E 06
29	28.2	28.2	19.2	44.30	36.90	30	33.0	68 2	1.259E 06
30	44.0	44.0	16.3	40.05	41.15	30	42.5	68 1	1.208E 06
31	44.0	44.0	16.3	40.05	41.15	30	40.0	68 2	1.259E 06
32	44.0	44.0	12.1	40.05	41.15	30	31.0	68 2	1.259E 06
33	44.0	44.0	12.1	40.05	41.15	30	28.0	68 1	1.259E 06
34	53.9	53.9	12.3	36.75	44.35	30	37.5	68 1	1.259E 06
36	53.9	53.9	10.1	36.75	44.35	30	26.0	68 2	1.259E 06
35	53.9	53.9	12.3	36.75	44.35	30	39.0	68 2	1.259E 06
37	53.9	53.9	10.1	36.75	44.35	30	27.0	68 1	1.259E 06
38	61.2	61.2	8.0	34.25	46.90	30	19.5	68 2	1.259E 06
39	61.2	61.2	8.0	34.25	46.90	30	19.0	68 1	1.259E 06
40	47.0	47.0	15.3	39.00	42.15	30	49.0	68 2	1.259E 06
41	47.0	47.0	15.3	39.00	42.15	30	47.0	68 1	1.259E 06
42	47.0	47.0	12.0	39.00	42.15	30	32.0	68 1	1.259E 06
43	35.5	35.5	15.0	42.35	38.80	30	34.0	68 1	1.259E 06
44	35.5	35.5	15.0	42.35	38.80	30	39.0	68 2	1.259E 06
45	35.5	35.5	13.3	42.35	38.80	30	53.0	68 1	1.259E 06
46	50.0	50.0	14.0	38.00	43.10	30	44.0	68 1	1.259E 06
47	50.0	50.0	14.0	38.00	43.10	30	45.0	68 2	1.259E 06
48	50.0	50.0	11.0	38.00	43.10	30	30.0	68 2	1.259E 06
50	44.0	44.0	17.1	39.95	41.15	30	39.0	68 2	1.286E 06
51	44.0	44.0	17.1	39.95	41.15	30	40.0	68 1	1.286E 06
67	50.0	50.0	14.1	38.20	42.90	30	37.0	68 1	1.286E 06
68	50.0	50.0	14.1	38.20	42.90	30	38.0	68 2	1.286E 06
70	60.0	60.0	8.1	34.65	46.45	30	20.0	68 1	1.286E 06
71	60.0	60.0	8.1	34.65	46.45	30	18.5	68 2	1.286E 06
72	55.0	55.0	11.9	36.35	44.70	30	38.0	68 2	1.286E 06
73	55.0	55.0	11.9	36.35	44.70	30	39.0	68 1	1.286E 06
74	45.0	45.0	17.0	39.65	41.45	30	45.5	68 1	1.286E 06
75	45.0	45.0	17.0	39.65	41.45	30	47.0	68 2	1.286E 06
76	38.0	38.0	19.7	41.60	39.50	30	38.0	68 2	1.332E 06
77	38.0	38.0	19.7	41.60	39.50	30	40.0	68 1	1.332E 06
78	38.0	38.0	15.1	41.60	39.50	30	28.0	68 2	1.332E 06
79	38.0	38.0	15.1	41.60	39.50	30	31.0	68 1	1.332E 06

OBSERVED DATA FOR ROD SPACING = .028 INCHES

RUN	RA	RB	PT	HT	LC	SEN	FLO	T CHT	COT
1	35.0	35.0	19.2	43.20	37.95	3	46.0	68 1	1.125E 06
2	35.0	35.0	19.2	43.20	37.95	3	45.0	68 2	1.125E 06
3	51.0	51.0	13.0			10	49.5	68 1	1.125E 06
4	51.0	51.0	13.0			10	48.0	68 2	1.125E 06
5	22.0	22.0	16.9	45.40	35.40	3	52.5	68 1	1.125E 06
6	22.0	22.0	16.9	45.40	35.40	3	53.0	68 2	1.125E 06
7	41.0	41.0	12.9	41.30	39.55	10	59.0	68 1	1.125E 06
8	41.0	41.0	12.9	41.30	39.55	10	56.0	68 2	1.125E 06
9	50.0	50.0	13.1	38.85	41.95	10	49.0	68 2	1.125E 06
10	50.0	50.0	13.1	38.85	41.95	10	49.5	68 2	1.125E 06
11	52.0	52.0	12.5	38.25	42.85	10	49.5	68 2	1.271E 06
12	52.0	52.0	12.5	38.25	42.85	10	51.0	68 1	1.271E 06
15	46.0	46.0	14.7	39.75	41.15	10	67.5	68 2	1.271E 06
16	46.0	46.0	14.7	39.75	41.15	10	69.0	68 1	1.271E 06
17	40.0	40.0	12.1	41.50	39.45	10	56.5	68 1	1.271E 06
18	40.0	40.0	12.1	41.50	39.45	10	56.0	68 2	1.271E 06
19	33.0	33.0	13.1	43.35	37.65	10	74.5	68 1	1.271E 06
20	33.0	33.0	13.1	43.35	37.65	10	77.0	68 2	1.271E 06
21	26.0	26.0	10.1	44.85	36.10	10	55.5	68 1	1.271E 06
22	26.0	26.0	10.1	44.85	36.10	10	56.0	68 2	1.271E 06
23	65.0	65.0	14.1	33.85	47.10	10	44.0	68 1	1.247E 06
24	65.0	65.0	14.1	33.85	47.10	10	46.0	68 2	1.247E 06
25	55.0	55.0	14.9	36.90	43.95	10	57.0	68 2	1.247E 06
26	55.0	55.0	14.9	36.90	43.95	10	60.5	68 1	1.247E 06
27	56.0	56.0	13.9	36.65	44.25	10	49.5	68 2	1.147E 06
28	56.0	56.0	13.9	36.65	44.25	10	50.0	68 1	1.147E 06
29	70.0	70.0	17.0	32.10	49.00	10	55.0	68 1	1.147E 06
30	70.0	70.0	17.0	32.10	49.00	10	56.0	68 2	1.147E 06

OBSERVED DATA FOR ROD SPACING = .063 INCHES

RUN	RA	RB	RT	HT	LO	SEN	FLO	T	CHT	COT
1	71.0	71.0	15.9	33.95	47.15	10	69.5	69	1	1.336E 06
2	71.0	71.0	15.9	33.95	47.15	10	71.0	69	2	1.336E 06
3	60.0	60.0	12.7	37.15	43.95	10	56.0	69	2	1.336E 06
4	60.0	60.0	12.7	37.15	43.95	10	54.5	69	1	1.336E 06
5	51.0	51.0	15.3	39.65	41.45	10	83.5	69	2	1.336E 06
6	51.0	51.0	15.3	39.65	41.45	10	85.0	69	1	1.336E 06
7	45.0	45.0	18.1	41.15	40.00	3	43.5	69	2	1.336E 06
8	45.0	45.0	18.1	41.15	40.00	3	44.0	69	1	1.336E 06
9	37.0	37.0	17.7	43.05	38.20	3	51.0	68	1	1.336E 06
10	37.0	37.0	17.7	43.05	38.20	3	53.0	68	2	1.336E 06
11	29.0	29.0	18.4	44.60	36.60	3	69.5	68	2	1.336E 06
12	29.0	29.0	18.4	44.60	36.60	3	70.0	68	1	1.336E 06
13	64.0	64.0	15.0	36.40	44.80	10	72.5	68	1	1.336E 06
14	64.0	64.0	15.0	36.40	44.80	10	75.5	68	2	1.336E 06
15	69.0	69.0	17.0	34.50	46.75	10	80.5	68	2	1.336E 06
16	69.0	69.0	17.0	34.50	46.75	10	80.0	68	1	1.336E 06
17	55.0	55.0	14.9	38.60	42.50	10	78.0	68	2	1.336E 06
18	55.0	55.0	14.9	38.60	42.50	10	79.0	68	1	1.336E 06
19	40.0	40.0	18.1	42.45	38.75	3	53.5	68	2	1.336E 06
20	40.0	40.0	18.1	42.45	38.75	3	54.5	68	1	1.336E 06
21	34.0	34.0	17.9	43.65	37.60	3	62.0	68	1	1.336E 06
22	34.0	34.0	17.9	43.65	37.60	3	61.0	68	2	1.336E 06
23	30.0	30.0	15.1	44.55	36.55	3	51.5	67	2	1.342E 06
24	30.0	30.0	15.1	44.55	36.55	3	52.0	67	1	1.342E 06
25	20.0	20.0	16.9	46.20	35.00	1	33.0	67	2	1.342E 06
26	20.0	20.0	15.9	46.20	35.00	1	32.0	67	1	1.342E 06
27	48.0	48.0	18.1	40.45	40.60	3	45.0	67	1	1.342E 06
28	48.0	48.0	18.1	40.45	40.60	3	46.0	67	2	1.342E 06
29	35.0	35.0	16.1	43.50	37.60	3	50.5	67	2	1.342E 06
30	35.0	35.0	16.1	43.50	37.60	3	52.5	67	1	1.342E 06

OBSERVED DATA FOR ROD SPACING = .127 INCHES

RUN	RA	RB	RT	HT	LC	SEN	FLO	T	CHT	COT
1	28.0	28.0	13.1	45.90	34.90	3	54.0	68	1	1.174E 06
2	28.0	28.0	13.1	45.90	34.90	3	56.0	68	2	1.174E 06
3	33.0	33.0	15.3	45.30	35.50	3	56.5	68	2	1.174E 06
4	33.0	33.0	15.3	45.30	35.50	3	57.5	68	1	1.174E 06
5	38.0	38.0	14.5	44.55	36.30	3	49.0	68	1	1.174E 06
6	38.0	38.0	14.5	44.55	36.30	3	48.0	68	2	1.174E 06
7	43.0	43.0	16.1	43.85	37.00	3	51.0	68	2	1.174E 06
8	43.0	43.0	16.1	43.85	37.00	3	52.0	68	1	1.174E 06
9	48.0	48.0	17.1	43.20	37.65	3	50.0	68	1	1.174E 06
10	48.0	48.0	17.1	43.20	37.35	3	50.0	68	2	1.147E 06
11	58.0	58.0	17.1	41.15	39.90	3	45.0	68	2	1.147E 06
12	58.0	58.0	17.1	41.15	39.90	3	43.5	68	1	1.147E 06
13	53.0	53.0	16.5	42.10	38.85	3	44.0	68	1	1.174E 06
14	53.0	53.0	16.5	42.10	38.85	3	44.0	68	2	1.174E 06
15	67.0	67.0	12.9	39.35	41.65	10	72.0	68	1	1.315E 06
16	67.0	67.0	12.9	39.35	41.65	10	69.0	68	2	1.315E 06
17	58.0	58.0	16.1	41.10	40.00	3	45.5	68	2	1.315E 06
18	58.0	58.0	16.1	41.10	40.00	3	43.5	68	1	1.315E 06
19	63.0	63.0	13.9	40.20	40.85	3	35.5	68	1	1.315E 06
20	63.0	63.0	13.9	40.20	40.85	3	33.5	68	2	1.315E 06
21	48.0	48.0	15.1	43.00	38.05	3	45.0	68	2	1.315E 06
22	48.0	48.0	15.1	43.00	38.05	3	46.0	68	1	1.315E 06
23	17.8	17.8	14.1	47.15	33.90	1	34.0	68	2	1.296E 06
24	17.8	17.8	14.1	47.15	33.90	1	34.5	68	1	1.296E 06
25	22.0	22.0	12.1	46.75	34.35	3	64.5	68	1	1.296E 06
26	22.0	22.0	12.1	46.75	34.35	3	66.0	68	2	1.296E 06
27	27.0	27.0	15.1	46.25	34.85	3	77.0	68	2	1.296E 06
28	27.0	27.0	15.1	46.25	34.85	3	75.0	68	1	1.296E 06

OBSERVED DATA FOR ROD SPACING = .228 INCHES

RUN	RA	RB	PT	HT	LO	SEN	FLO	T	CHT	CCT
1	31.0	31.0	14.2	46.90	34.95	1	32.0	68	1	1.406E 06
2	31.0	31.0	14.2	46.95	34.95	1	31.0	68	2	1.406E 06
3	37.0	37.0	14.1	46.40	35.50	1	26.0	68	2	1.406E 06
4	37.0	37.0	14.1	46.40	35.50	1	26.0	68	1	1.406E 06
5	43.0	43.0	13.1	45.90	35.95	3	55.0	68	1	1.406E 06
6	43.0	43.0	13.1	45.90	35.95	3	55.5	68	2	1.406E 06
7	50.0	50.0	13.1	45.20	36.70	3	48.5	68	2	1.406E 06
8	50.0	50.0	13.1	45.20	36.70	3	50.5	68	1	1.406E 06
9	55.0	55.0	14.1	44.50	37.35	3	49.5	68	1	1.406E 06
10	55.0	55.0	14.1	44.50	37.35	3	50.5	68	2	1.406E 06
11	62.0	62.0	15.1	43.70	38.20	3	51.0	68	2	1.406E 06
12	62.0	62.0	15.1	43.70	38.20	3	50.0	68	1	1.406E 06
13	69.0	69.0	11.1	42.75	39.15	10	69.0	68	1	1.406E 06
14	69.0	69.0	11.1	42.75	39.15	10	70.0	68	2	1.406E 06
15	25.0	25.0	17.1	47.45	34.45	1	47.0	68	1	1.406E 06
16	25.0	25.0	17.1	47.45	34.45	1	48.5	68	2	1.406E 06
17	20.0	20.0	17.1	47.75	34.15	1	58.5	68	2	1.406E 06
18	20.0	20.0	17.1	47.75	34.15	1	57.5	68	1	1.406E 06

OBSERVED PRESSURE UNBALANCED MIXING DATA

OBSERVED DATA FOR ROD SPACING = .011 INCHES

RUN	RA	RB	RT	SEN	FLO	T	CHT	CCT
53	44.0	44.0	17.1	10	40.0	68	2	1.286E 06
54	51.0	51.0	14.1	10	29.0	68	2	1.286E 06
57	58.0	58.0	10.1	30	51.0	68	2	1.286E 06
58	39.0	39.0	15.1	10	55.0	68	2	1.286E 06
60	39.0	39.0	19.5	10	83.0	68	2	1.286E 06
61	34.0	34.0	17.1	10	88.0	68	2	1.286E 06
64	26.0	26.0	12.1	3	61.0	68	2	1.286E 06
65	38.0	38.0	12.1	10	58.0	68	2	1.286E 06

OBSERVED DATA FOR ROD SPACING = .127 INCHES

RUN	RA	RB	RT	SEN	FLO	T	CHT	CCT
101	44.0	44.0	12.1	1	57.5	68	1	1.323E 06
202	44.0	44.0	12.1	1	39.5	68	1	1.323E 06
301	44.0	44.0	12.1	3	54.5	68	1	1.323E 06
303	55.0	55.0	11.1	10	84.0	68	1	1.323E 06
204	55.0	55.0	11.1	3	60.0	68	1	1.323E 06
103	55.0	55.0	11.1	3	85.5	68	1	1.323E 06
106	47.0	47.0	13.1	1	54.0	68	1	1.323E 06
205	47.0	47.0	13.1	1	38.0	68	1	1.323E 06
306	47.0	47.0	13.1	3	56.0	68	1	1.323E 06
307	39.0	39.0	12.1	3	66.0	68	1	1.348E 06
208	39.0	39.0	12.1	1	52.0	68	1	1.348E 06
107	39.0	39.0	12.1	1	70.0	68	1	1.348E 06
110	32.0	32.0	11.1	1	94.0	68	1	1.348E 06
209	32.0	32.0	11.1	1	65.0	68	1	1.348E 06
310	32.0	32.0	11.1	3	72.0	68	1	1.348E 06

APPENDIX F

CALCULATED RESULTS

NOMENCLATURE FOR TWO-CHANNEL AND EIGHT-CHANNEL MIXING MODELS

Symbol	Definition	Dimension
RUN	experimental run number	
CO/CF	initial tracer concentration in traced channel divided by exit tracer concentration for initially untraced channel	dimensionless
WT	turbulent cross-flow	lb_m/hr-ft
SUB-RE	subchannel 7 Reynolds number	dimensionless
WT/M	turbulent cross-flow divided by the total mass flow rate in subchannels 7 and 8	ft^{-1}
E/V	turbulent cross-flow divided by the dynamic viscosity	dimensionless
CT	channel traced	
MF	mass flux for subchannel 7	lb_m/hr-ft^2
U	average velocity for subchannel 7	ft/sec

PRESSURE BALANCED RESULTS

TWO-CHANNEL; ROD SPACING = 0.011 INCHES

RUN	GG/CF	WT	SUB-DF	WT/M	F/V	CT	MF	U
28	841.2	1.57	1.098E 04	4.488E-04	.65	1	7.831E 05	3.49
29	836.8	1.41	1.092E 04	4.029E-04	.58	2	7.786E 05	3.47
30	351.0	5.66	1.645E 04	1.077E-03	2.32	1	1.173E 06	5.23
31	318.0	6.23	1.639E 04	1.189E-03	2.55	2	1.169E 06	5.21
32	313.7	6.31	1.639E 04	1.206E-03	2.59	2	1.169E 06	5.21
33	346.6	5.74	1.645E 04	1.091E-03	2.35	1	1.173E 06	5.23
34	216.3	11.07	1.979E 04	1.752E-03	4.54	1	1.411E 06	6.29
36	216.7	11.01	1.972E 04	1.748E-03	4.52	2	1.406E 06	6.27
35	208.6	11.45	1.972E 04	1.817E-03	4.69	2	1.406E 06	6.27
37	207.8	11.53	1.979E 04	1.824E-03	4.73	1	1.411E 06	6.29
38	171.2	15.67	2.214E 04	2.215E-03	6.43	2	1.579E 06	7.04
39	175.3	15.35	2.221E 04	2.163E-03	6.29	1	1.584E 06	7.06
40	270.7	7.77	1.740E 04	1.398E-03	3.19	2	1.241E 06	5.54
41	281.2	7.51	1.747E 04	1.346E-03	3.08	1	1.246E 06	5.56
42	279.0	7.57	1.747E 04	1.357E-03	3.10	1	1.246E 06	5.56
43	501.5	3.26	1.354E 04	7.534E-04	1.34	1	9.652E 05	4.30
44	438.4	3.71	1.347E 04	8.621E-04	1.52	2	9.607E 05	4.28
45	460.7	3.55	1.354E 04	8.202E-04	1.45	1	9.652E 05	4.30
46	246.1	9.08	1.848E 04	1.539E-03	3.72	1	1.318E 06	5.88
47	241.4	9.23	1.841E 04	1.568E-03	3.78	2	1.313E 06	5.86
48	239.4	9.30	1.841E 04	1.581E-03	3.81	2	1.313E 06	5.86
50	439.2	4.56	1.639E 04	8.605E-04	1.85	2	1.169E 06	5.21
51	426.2	4.66	1.645E 04	8.868E-04	1.91	1	1.173E 06	5.23
67	303.2	7.37	1.848E 04	1.248E-03	3.02	1	1.318E 06	5.88
68	296.2	7.52	1.841E 04	1.277E-03	3.08	2	1.313E 06	5.86
70	177.6	14.88	2.181E 04	2.135E-03	6.10	1	1.556E 06	6.94
71	193.2	13.63	2.175E 04	1.962E-03	5.59	2	1.551E 06	6.92
72	202.2	12.03	2.009E 04	1.874E-03	4.93	2	1.433E 06	6.39
73	196.2	12.44	2.015E 04	1.932E-03	5.10	1	1.437E 06	6.41
74	362.6	5.59	1.679E 04	1.043E-03	2.29	1	1.197E 06	5.34
75	352.3	5.74	1.673E 04	1.073E-03	2.35	2	1.193E 06	5.32
76	659.8	2.62	1.433E 04	5.724E-04	1.07	2	1.022E 06	4.56
77	633.2	2.79	1.440E 04	6.060E-04	1.14	1	1.027E 06	4.58
78	613.7	2.82	1.433E 04	6.154E-04	1.16	2	1.022E 06	4.56
79	550.4	3.16	1.440E 04	6.864E-04	1.29	1	1.027E 06	4.58

TWO-CHANNEL; ROD SPACING = 0.028 INCHES

RUN	CQ/CF	JT	SUB-DF	WT/M	F/V	CT	MF	U
1	51.7	33.17	1.395E 04	7.445E-03	13.60	1	9.398E 05	4.19
2	53.2	32.03	1.388E 04	7.225E-03	13.13	2	9.353E 05	4.17
3	45.2	53.40	1.959E 04	8.535E-03	21.90	1	1.320E 06	5.89
4	46.8	51.34	1.952E 04	8.235E-03	21.05	2	1.315E 06	5.87
5	59.2	18.99	9.181E 03	6.476E-03	7.78	1	6.186E 05	2.76
6	59.1	18.89	9.115E 03	6.491E-03	7.75	2	6.141E 05	2.74
7	46.4	42.68	1.609E 04	8.306E-03	17.50	1	1.084E 06	4.83
8	47.1	40.04	1.602E 04	7.833E-03	16.43	2	1.079E 06	4.81
9	47.4	49.83	1.918E 04	8.137E-03	20.43	2	1.292E 06	5.76
10	46.9	50.36	1.918E 04	8.223E-03	20.65	2	1.292E 06	5.76
11	47.2	52.02	1.987E 04	8.197E-03	21.33	2	1.339E 06	5.97
12	45.4	54.04	1.994E 04	8.487E-03	22.14	1	1.343E 06	5.99
15	50.6	43.19	1.778E 04	7.600E-03	17.70	2	1.198E 06	5.34
16	49.3	44.51	1.785E 04	7.807E-03	18.25	1	1.203E 06	5.36
17	50.3	38.47	1.573E 04	7.657E-03	15.77	1	1.060E 06	4.73
18	50.9	37.76	1.567E 04	7.550E-03	15.49	2	1.056E 06	4.71
19	52.8	30.76	1.323E 04	7.287E-03	12.62	1	8.912E 05	3.97
20	51.3	31.51	1.316E 04	7.497E-03	12.92	2	8.869E 05	3.95
21	55.6	23.55	1.067E 04	6.910E-03	9.66	1	7.189E 05	3.21
22	55.5	23.46	1.061E 04	6.926E-03	9.62	2	7.145E 05	3.19
23	50.6	59.19	2.439E 04	7.599E-03	24.27	1	1.643E 06	7.33
24	48.5	61.51	2.432E 04	7.933E-03	25.26	2	1.639E 06	7.31
25	50.3	51.04	2.091E 04	7.644E-03	20.93	2	1.409E 06	6.28
26	47.2	54.66	2.097E 04	8.160E-03	22.41	1	1.413E 06	6.30
27	47.1	55.62	2.125E 04	8.195E-03	22.80	2	1.432E 06	6.39
28	46.4	56.58	2.132E 04	8.311E-03	23.20	1	1.436E 06	6.41
29	45.8	70.10	2.608E 04	8.418E-03	28.74	1	1.757E 06	7.84
30	45.1	71.02	2.601E 04	8.551E-03	29.12	2	1.752E 06	7.82

TWO-CHANNEL; ROD SPACING = 0.063 INCHES

RUN	CO/CF	WT	SUB-RE	WT/M	E/V	CT	MF	U
1	37.6	97.74	3.013E 04	1.030E-02	40.66	1	1.797E 06	8.02
2	36.9	99.39	3.005E 04	1.050E-02	41.34	2	1.793E 06	8.00
3	38.8	81.36	2.591E 04	9.970E-03	33.84	2	1.545E 06	6.89
4	39.8	79.59	2.598E 04	9.726E-03	33.11	1	1.550E 06	6.91
5	41.2	66.38	2.245E 04	9.388E-03	27.61	2	1.339E 06	5.97
6	40.3	68.11	2.253E 04	9.599E-03	28.33	1	1.344E 06	5.99
7	47.0	51.95	2.011E 04	8.203E-03	21.61	2	1.199E 06	5.35
8	46.2	53.05	2.018E 04	8.346E-03	22.07	1	1.204E 06	5.37
9	46.3	44.69	1.678E 04	8.334E-03	18.32	1	1.016E 06	4.53
10	44.6	46.21	1.671E 04	8.655E-03	18.95	2	1.011E 06	4.51
11	44.9	37.00	1.348E 04	8.591E-03	15.17	2	8.157E 05	3.64
12	44.3	37.73	1.355E 04	8.713E-03	15.47	1	8.202E 05	3.66
13	40.4	83.16	2.715E 04	9.584E-03	34.10	1	1.643E 06	7.33
14	38.9	86.21	2.708E 04	9.964E-03	35.35	2	1.639E 06	7.31
15	36.9	97.06	2.893E 04	1.050E-02	39.80	2	1.751E 06	7.81
16	37.0	96.98	2.901E 04	1.046E-02	39.77	1	1.756E 06	7.83
17	39.3	74.62	2.369E 04	9.856E-03	30.60	2	1.434E 06	6.39
18	38.6	76.13	2.377E 04	1.002E-02	31.21	1	1.438E 06	6.41
19	42.1	52.44	1.790E 04	9.171E-03	21.50	2	1.083E 06	4.83
20	41.1	54.01	1.797E 04	9.406E-03	22.15	1	1.088E 06	4.85
21	41.4	46.49	1.558E 04	9.337E-03	19.06	1	9.430E 05	4.21
22	42.3	45.20	1.551E 04	9.121E-03	18.53	2	9.385E 05	4.19
23	45.1	38.04	1.372E 04	8.558E-03	15.38	2	8.419E 05	3.75
24	44.3	38.90	1.379E 04	8.704E-03	15.72	1	8.464E 05	3.77
25	41.9	28.67	9.593E 03	9.222E-03	11.59	2	5.889E 05	2.63
26	43.1	28.09	9.667E 03	8.965E-03	11.36	1	5.934E 05	2.65
27	42.4	61.44	2.083E 04	9.101E-03	24.84	1	1.278E 06	5.70
28	41.6	62.50	2.075E 04	9.292E-03	25.27	2	1.274E 06	5.68
29	43.5	45.22	1.571E 04	8.880E-03	18.28	2	9.644E 05	4.30
30	41.5	47.70	1.578E 04	9.323E-03	19.28	1	9.689E 05	4.32

TWO-CHANNEL; ROD SPACING = 0.127 INCHES

RUN	CO/CF	WT	SUB-RE	WT/M	F/V	CT	MF	U
1	31.8	48.96	1.251E 04	1.226E-02	20.07	1	6.397E 05	2.85
2	30.7	50.36	1.244E 04	1.269E-02	20.65	2	6.359E 05	2.84
3	33.1	54.39	1.450E 04	1.176E-02	22.30	2	7.411E 05	3.31
4	32.3	56.07	1.457E 04	1.206E-02	22.99	1	7.450E 05	3.32
5	30.7	67.29	1.661E 04	1.270E-02	27.59	1	8.491E 05	3.79
6	31.6	65.11	1.653E 04	1.234E-02	26.70	2	8.452E 05	3.77
7	30.6	75.37	1.855E 04	1.274E-02	30.90	2	9.484E 05	4.23
8	29.8	77.70	1.862E 04	1.308E-02	31.86	1	9.523E 05	4.25
9	30.5	84.17	2.063E 04	1.279E-02	34.51	1	1.055E 06	4.70
10	29.9	85.55	2.055E 04	1.305E-02	35.08	2	1.051E 06	4.69
11	27.8	110.14	2.451E 04	1.408E-02	45.16	2	1.253E 06	5.59
12	28.7	106.65	2.459E 04	1.359E-02	43.73	1	1.257E 06	5.61
13	30.2	93.28	2.261E 04	1.293E-02	38.25	1	1.156E 06	5.16
14	30.3	92.61	2.254E 04	1.288E-02	37.97	2	1.152E 06	5.14
15	27.2	129.31	2.811E 04	1.442E-02	53.02	1	1.437E 06	6.41
16	28.4	122.93	2.804E 04	1.374E-02	50.40	2	1.433E 06	6.39
17	28.8	106.08	2.451E 04	1.356E-02	43.50	2	1.253E 06	5.59
18	30.2	101.44	2.459E 04	1.293E-02	41.59	1	1.257E 06	5.61
19	27.8	119.23	2.655E 04	1.407E-02	48.89	1	1.358E 06	6.05
20	29.8	110.64	2.647E 04	1.310E-02	45.37	2	1.354E 06	6.04
21	32.0	79.81	2.055E 04	1.217E-02	32.72	2	1.051E 06	4.69
22	31.1	82.48	2.063E 04	1.253E-02	33.82	1	1.055E 06	4.70
23	33.3	30.35	8.154E 03	1.167E-02	12.44	2	4.169E 05	1.86
24	32.4	31.49	8.228E 03	1.199E-02	12.91	1	4.207E 05	1.88
25	32.1	38.73	1.001E 04	1.213E-02	15.88	1	5.117E 05	2.28
26	31.4	39.11	9.934E 03	1.234E-02	16.04	2	5.079E 05	2.27
27	31.4	47.57	1.202E 04	1.240E-02	19.50	2	6.147E 05	2.74
28	32.1	46.82	1.210E 04	1.213E-02	19.20	1	6.185E 05	2.76

TWO-CHANNEL; ROD SPACING = 0.228 INCHES

RUN	CP/CF	WT	SUB-RE	WT/M	E/V	CT	MF	U
1	22.4	91.33	1.620E 04	1.763E-02	37.45	1	6.642E 05	2.96
2	23.4	86.80	1.612E 04	1.684E-02	35.59	2	6.607E 05	2.95
3	24.0	99.24	1.892E 04	1.641E-02	40.69	2	7.755E 05	3.46
4	23.9	100.22	1.900E 04	1.649E-02	41.09	1	7.790E 05	3.47
5	24.3	112.59	2.176E 04	1.618E-02	46.16	1	8.920E 05	3.98
6	24.2	112.78	2.168E 04	1.627E-02	46.24	2	8.885E 05	3.96
7	24.1	129.84	2.485E 04	1.634E-02	53.24	2	1.018E 06	4.54
8	23.9	137.00	2.493E 04	1.719E-02	56.17	1	1.022E 06	4.56
9	24.1	142.15	2.717E 04	1.636E-02	58.28	1	1.114E 06	4.97
10	23.6	144.43	2.709E 04	1.668E-02	59.22	2	1.110E 06	4.95
11	23.1	164.94	3.019E 04	1.709E-02	67.63	2	1.237E 06	5.52
12	23.5	162.27	3.028E 04	1.676E-02	66.54	1	1.241E 06	5.53
13	22.5	187.09	3.334E 04	1.755E-02	76.71	1	1.367E 06	6.10
14	22.2	188.87	3.326E 04	1.776E-02	77.44	2	1.363E 06	6.08
15	23.6	71.14	1.335E 04	1.666E-02	29.17	1	5.473E 05	2.44
16	23.9	72.78	1.327E 04	1.716E-02	29.84	2	5.438E 05	2.43
17	23.4	58.43	1.084E 04	1.686E-02	23.96	2	4.442E 05	1.98
18	23.6	58.28	1.092E 04	1.669E-02	23.90	1	4.478E 05	2.00

EIGHT-CHANNEL; ROD SPACING = 0.011 INCHES

RUN	CO/CF	WT	SUB-RF	WT/M	F/V	CT	MF	U
28	841.2	1.83	1.098E 04	5.229F-04	.75	1	7.831E 05	3.49
29	936.8	1.64	1.092E 04	4.691F-04	.67	2	7.786E 05	3.47
30	351.0	6.85	1.645E 04	1.304F-03	2.81	1	1.173E 06	5.23
31	318.0	7.54	1.639E 04	1.440F-03	3.09	2	1.169E 06	5.21
32	313.7	7.65	1.639E 04	1.461F-03	3.14	2	1.169E 06	5.21
33	346.6	6.94	1.645E 04	1.321F-03	2.85	1	1.173E 06	5.23
34	216.3	13.68	1.979E 04	2.165F-03	5.61	1	1.411E 06	6.29
36	216.7	13.60	1.972E 04	2.159F-03	5.58	2	1.406E 06	6.27
35	208.6	14.15	1.972E 04	2.246F-03	5.80	2	1.406E 06	6.27
37	207.8	14.25	1.979E 04	2.255F-03	5.84	1	1.411E 06	6.29
38	171.2	19.63	2.214E 04	2.774F-03	8.05	2	1.579E 06	7.04
39	175.3	19.22	2.221E 04	2.708F-03	7.88	1	1.584E 06	7.06
40	270.7	9.48	1.740E 04	1.704F-03	3.89	2	1.241E 06	5.54
41	281.2	9.15	1.747E 04	1.640F-03	3.75	1	1.246E 06	5.56
42	279.0	9.23	1.747E 04	1.654F-03	3.78	1	1.246E 06	5.56
43	501.5	3.87	1.354E 04	8.950F-04	1.59	1	9.652E 05	4.30
44	438.4	4.41	1.347E 04	1.025F-03	1.81	2	9.607E 05	4.28
45	460.7	4.22	1.354E 04	9.750F-04	1.73	1	9.652E 05	4.30
46	246.1	11.14	1.848E 04	1.887F-03	4.57	1	1.318E 06	5.88
47	241.4	11.32	1.841E 04	1.924F-03	4.64	2	1.313E 06	5.86
48	239.4	11.41	1.841E 04	1.940F-03	4.68	2	1.313E 06	5.86
50	439.2	5.44	1.639E 04	1.039F-03	2.23	2	1.169E 06	5.21
51	426.2	5.63	1.645E 04	1.071F-03	2.31	1	1.173E 06	5.23
67	303.2	9.01	1.848E 04	1.527F-03	3.70	1	1.318E 06	5.88
68	296.2	9.19	1.841E 04	1.563F-03	3.77	2	1.313E 06	5.86
70	177.6	18.59	2.181E 04	2.668F-03	7.62	1	1.556E 06	6.94
71	193.2	17.01	2.175E 04	2.447F-03	6.97	2	1.551E 06	6.92
72	202.2	14.90	2.009E 04	2.322F-03	6.11	2	1.433E 06	6.39
73	196.2	15.42	2.015E 04	2.395F-03	6.32	1	1.437E 06	6.41
74	362.6	6.78	1.679E 04	1.264F-03	2.78	1	1.197E 06	5.34
75	352.3	6.95	1.673E 04	1.301F-03	2.85	2	1.193E 06	5.32
76	659.8	3.12	1.433E 04	6.820F-04	1.28	2	1.022E 06	4.56
77	623.2	3.32	1.440E 04	7.226F-04	1.36	1	1.027E 06	4.58
78	613.7	3.36	1.433E 04	7.336F-04	1.38	2	1.022E 06	4.56
79	550.4	3.77	1.440E 04	8.190F-04	1.54	1	1.027E 06	4.58

EIGHT-CHANNEL; ROD SPACING = 0.028 INCHES

RUN	CO/CF	WT	SUB-RF	WT/M	F/V	CT	MF	U
1	51.7	40.07	1.395E 04	8.995E-03	16.43	1	9.398E 05	4.19
2	53.2	38.60	1.388E 04	8.707E-03	15.83	2	9.353E 05	4.17
3	45.2	67.33	1.959E 04	1.076E-02	27.61	1	1.320E 06	5.89
4	46.8	64.53	1.952E 04	1.035E-02	26.46	2	1.315E 06	5.87
5	59.2	21.85	9.181E 03	7.452E-03	8.96	1	6.186E 05	2.76
6	59.1	21.73	9.115E 03	7.465E-03	8.91	2	6.141E 05	2.74
7	46.4	52.68	1.609E 04	1.025E-02	21.60	1	1.084E 06	4.83
8	49.1	49.24	1.602E 04	9.623E-03	20.19	2	1.079E 06	4.81
9	47.4	62.46	1.918E 04	1.020E-02	25.61	2	1.292E 06	5.76
10	46.9	63.18	1.918E 04	1.032E-02	25.90	2	1.292E 06	5.76
11	47.0	65.46	1.987E 04	1.032E-02	26.84	2	1.339E 06	5.97
12	45.4	68.22	1.994E 04	1.071E-02	27.97	1	1.343E 06	5.99
15	50.6	53.44	1.778E 04	9.411E-03	21.91	2	1.198E 06	5.34
16	49.3	55.23	1.785E 04	9.690E-03	22.65	1	1.203E 06	5.36
17	50.3	47.11	1.573E 04	9.375E-03	19.32	1	1.060E 06	4.73
18	50.9	46.20	1.567E 04	9.233E-03	18.94	2	1.056E 06	4.71
19	52.8	36.95	1.323E 04	8.746E-03	15.15	1	8.912E 05	3.97
20	51.3	37.87	1.316E 04	9.010E-03	15.53	2	8.868E 05	3.95
21	55.6	27.59	1.067E 04	8.098E-03	11.31	1	7.189E 05	3.21
22	55.5	27.47	1.061E 04	8.112E-03	11.26	2	7.145E 05	3.19
23	50.6	75.53	2.439E 04	9.697E-03	30.97	1	1.643E 06	7.33
24	48.5	78.86	2.432E 04	1.015E-02	32.33	2	1.639E 06	7.31
25	50.3	64.21	2.091E 04	9.618E-03	26.33	2	1.409E 06	6.28
26	47.2	69.12	2.097E 04	1.032E-02	28.34	1	1.413E 06	6.30
27	47.0	70.45	2.125E 04	1.038E-02	28.89	2	1.432E 06	6.39
28	46.4	71.77	2.132E 04	1.054E-02	29.43	1	1.436E 06	6.41
29	45.8	90.75	2.608E 04	1.090E-02	37.21	1	1.757E 06	7.84
30	45.1	92.03	2.601E 04	1.108E-02	37.74	2	1.752E 06	7.82

EIGHT-CHANNEL; ROD SPACING = 0.063 INCHES

RUN	CO/CF	WT	SUB-RE	WT/M	E/V	CT	MF	U
1	37.6	113.62	3.013E 04	1.197E-02	47.26	1	1.797E 06	8.02
2	36.9	115.68	3.005E 04	1.222E-02	48.12	2	1.793E 06	8.00
3	38.8	92.46	2.591E 04	1.133E-02	38.46	2	1.545E 06	6.89
4	39.8	90.31	2.598E 04	1.103E-02	37.57	1	1.550E 06	6.91
5	41.2	73.69	2.245E 04	1.042E-02	30.65	2	1.339E 06	5.97
6	40.3	75.76	2.253E 04	1.068E-02	31.52	1	1.344E 06	5.99
7	47.0	56.33	2.011E 04	8.895E-03	23.43	2	1.199E 06	5.35
8	46.2	57.61	2.018E 04	9.063E-03	23.97	1	1.204E 06	5.37
9	46.3	47.38	1.678E 04	8.836E-03	19.43	1	1.016E 06	4.53
10	44.6	49.07	1.671E 04	9.192E-03	20.12	2	1.011E 06	4.51
11	44.9	38.19	1.348E 04	8.867E-03	15.66	2	8.157E 05	3.64
12	44.3	39.01	1.355E 04	9.008E-03	15.99	1	8.202E 05	3.66
13	40.4	94.79	2.715E 04	1.093E-02	38.87	1	1.643E 06	7.33
14	38.9	98.54	2.708E 04	1.139E-02	40.40	2	1.639E 06	7.31
15	36.9	112.41	2.893E 04	1.216E-02	46.09	2	1.751E 06	7.81
16	37.0	112.32	2.901E 04	1.212E-02	46.05	1	1.756E 06	7.83
17	39.3	83.73	2.369E 04	1.106E-02	34.33	2	1.434E 06	6.39
18	38.6	85.57	2.377E 04	1.127E-02	35.09	1	1.438E 06	6.41
19	42.1	56.41	1.790E 04	9.865E-03	23.13	2	1.083E 06	4.83
20	41.1	58.24	1.797E 04	1.014E-02	23.88	1	1.088E 06	4.85
21	41.4	49.17	1.558E 04	9.875E-03	20.16	1	9.430E 05	4.21
22	42.3	47.70	1.551E 04	9.626E-03	19.56	2	9.385E 05	4.19
23	45.1	39.35	1.372E 04	8.851E-03	15.91	2	8.419E 05	3.75
24	44.3	40.30	1.379E 04	9.018E-03	16.29	1	8.464E 05	3.77
25	41.9	28.42	9.593E 03	9.142E-03	11.49	2	5.889E 05	2.63
26	43.1	27.82	9.667E 03	8.881E-03	11.25	1	5.934E 05	2.65
27	42.4	67.38	2.083E 04	9.982E-03	27.24	1	1.278E 06	5.70
28	41.6	68.62	2.075E 04	1.020E-02	27.74	2	1.274E 06	5.68
29	43.5	47.72	1.571E 04	9.370E-03	19.29	2	9.644E 05	4.30
30	41.5	50.53	1.578E 04	9.876E-03	20.42	1	9.689E 05	4.32

EIGHT-CHANNEL; ROD SPACING = 0.127 INCHES

RUN	CO/CF	WT	SUB-RE	WT/M	F/V	CT	MF	U
1	31.8	55.24	1.251E 04	1.384E-02	22.65	1	6.397E 05	2.85
2	30.7	56.98	1.244E 04	1.436E-02	23.36	2	6.359E 05	2.84
3	33.1	61.76	1.450E 04	1.335E-02	25.32	2	7.411E 05	3.31
4	32.3	63.84	1.457E 04	1.373E-02	26.18	1	7.450E 05	3.32
5	30.7	77.70	1.661E 04	1.466E-02	31.86	1	8.491E 05	3.79
6	31.6	74.94	1.653E 04	1.421E-02	30.73	2	8.452E 05	3.77
7	30.6	87.71	1.855E 04	1.482E-02	35.96	2	9.484E 05	4.23
8	29.8	90.70	1.862E 04	1.526E-02	37.19	1	9.523E 05	4.25
9	30.5	98.72	2.063E 04	1.500E-02	40.48	1	1.055E 06	4.70
10	29.9	100.52	2.055E 04	1.533E-02	41.22	2	1.051E 06	4.69
11	27.8	132.12	2.451E 04	1.689E-02	54.17	2	1.253E 06	5.59
12	28.7	127.44	2.459E 04	1.624E-02	52.25	1	1.257E 06	5.61
13	30.2	110.22	2.261E 04	1.528E-02	45.19	1	1.156E 06	5.16
14	30.3	109.36	2.254E 04	1.521E-02	44.84	2	1.152E 06	5.14
15	27.2	157.02	2.811E 04	1.751E-02	64.38	1	1.437E 06	6.41
16	28.4	148.40	2.804E 04	1.659E-02	60.85	2	1.433E 06	6.39
17	28.8	126.70	2.451E 04	1.620E-02	51.95	2	1.253E 06	5.59
18	30.2	120.55	2.459E 04	1.537E-02	49.43	1	1.257E 06	5.61
19	27.8	143.80	2.655E 04	1.698E-02	58.96	1	1.358E 06	6.05
20	29.8	132.34	2.647E 04	1.567E-02	54.24	2	1.354E 06	6.04
21	32.0	93.12	2.055E 04	1.420E-02	38.18	2	1.051E 06	4.69
22	31.1	96.53	2.063E 04	1.467E-02	39.58	1	1.055E 06	4.70
23	33.3	33.09	8.154E 03	1.272E-02	13.57	2	4.169E 05	1.86
24	32.4	34.43	8.228E 03	1.312E-02	14.12	1	4.207E 05	1.88
25	32.1	42.98	1.001E 04	1.346E-02	17.62	1	5.117E 05	2.28
26	31.6	43.45	9.934E 03	1.371E-02	17.81	2	5.079E 05	2.27
27	31.4	53.58	1.202E 04	1.397E-02	21.97	2	6.147E 05	2.74
28	32.1	52.66	1.210E 04	1.364E-02	21.59	1	6.185E 05	2.76

EIGHT-CHANNEL; ROD SPACING = 0.228 INCHES

RUN	CO/CF	WT	SUB-RE	WT/M	E/V	CT	MF	U
1	22.4	89.45	1.620E 04	1.727E-02	36.68	1	6.642E 05	2.96
2	23.4	84.58	1.612E 04	1.641E-02	34.69	2	6.607E 05	2.95
3	24.0	98.15	1.892E 04	1.623E-02	40.24	2	7.755E 05	3.46
4	23.9	99.21	1.900E 04	1.633E-02	40.68	1	7.790E 05	3.47
5	24.3	112.88	2.176E 04	1.622E-02	46.28	1	8.920E 05	3.98
6	24.2	113.09	2.168E 04	1.632E-02	46.37	2	8.885E 05	3.96
7	24.1	132.18	2.485E 04	1.664E-02	54.20	2	1.018E 06	4.54
8	23.0	140.25	2.493E 04	1.759E-02	57.51	1	1.022E 06	4.56
9	24.1	146.13	2.717E 04	1.682E-02	59.92	1	1.114E 06	4.97
10	23.6	148.71	2.709E 04	1.717E-02	60.98	2	1.110E 06	4.95
11	23.1	172.29	3.019E 04	1.785E-02	70.64	2	1.237E 06	5.52
12	23.5	169.20	3.028E 04	1.748E-02	69.38	1	1.241E 06	5.53
13	22.5	198.12	3.334E 04	1.858E-02	81.23	1	1.367E 06	6.10
14	22.2	200.23	3.326E 04	1.883E-02	82.10	2	1.363E 06	6.08
15	23.6	67.84	1.335E 04	1.589E-02	27.82	1	5.473E 05	2.44
16	23.0	69.55	1.327E 04	1.640E-02	28.52	2	5.438E 05	2.43
17	23.4	54.54	1.084E 04	1.574E-02	22.36	2	4.442E 05	1.98
18	23.6	54.39	1.092E 04	1.557E-02	22.30	1	4.478E 05	2.00

PRESSURE BALANCE RESULTS FOR TWO-CHANNEL ANALYSIS FOR TEST SECTION AS A TWO-CHANNEL SYSTEM; CHANNEL I AND CHANNEL II

The same nomenclature form of the subchannel system applies with the following exceptions:

Symbol	Definition	Dimension
SUB-RE	channel I Reynolds number	
F	Fanning friction factor for channel I	
MF	mass flux for channel I	lb_m/ft^2-hr
U	average velocity for channel I	ft/sec

ROD SPACING - 0.011 INCHES

RUN	CC/CE	WT	SUB-RE	WT/M	F/V	CT	F	MF	U
28	841.2	2.64	5.231E 03	4.488E-04	1.08	1	5.996E-03	5.670E 05	2.53
29	936.8	2.35	5.198E 03	4.029E-04	.96	2	6.073E-03	5.634E 05	2.51
30	351.0	9.86	8.148E 03	1.077E-03	4.04	1	5.147E-03	8.832E 05	3.94
31	318.0	10.84	8.113E 03	1.189E-03	4.44	2	5.191E-03	8.794E 05	3.92
32	313.7	10.99	8.113E 03	1.206E-03	4.51	2	5.191E-03	8.794E 05	3.92
33	346.6	9.99	8.148E 03	1.091E-03	4.09	1	5.147E-03	8.832E 05	3.94
34	216.3	19.63	9.976E 03	1.752E-03	8.05	1	4.799E-03	1.081E 06	4.82
36	216.7	19.51	9.940E 03	1.748E-03	8.00	2	4.834E-03	1.077E 06	4.81
35	208.6	20.28	9.940E 03	1.817E-03	8.32	2	4.834E-03	1.077E 06	4.81
37	207.8	20.43	9.976E 03	1.824E-03	8.38	1	4.799E-03	1.081E 06	4.82
38	171.2	28.08	1.129E 04	2.215E-03	11.51	2	4.577E-03	1.223E 06	5.46
39	175.3	27.51	1.132E 04	2.163E-03	11.28	1	4.548E-03	1.227E 06	5.47
40	270.7	13.61	8.667E 03	1.398E-03	5.58	2	5.120E-03	9.394E 05	4.19
41	291.2	13.15	8.702E 03	1.346E-03	5.39	1	5.078E-03	9.432E 05	4.21
42	279.0	13.25	8.702E 03	1.357E-03	5.44	1	5.078E-03	9.432E 05	4.21
43	501.5	5.57	6.579E 03	7.534E-04	2.28	1	5.650E-03	7.131E 05	3.18
44	438.4	6.34	6.545E 03	8.621E-04	2.60	2	5.709E-03	7.094E 05	3.16
45	460.7	6.05	6.579E 03	8.202E-04	2.48	1	5.650E-03	7.131E 05	3.18
46	246.1	15.00	9.256E 03	1.539E-03	6.56	1	4.965E-03	1.003E 06	4.47
47	241.4	16.24	9.220E 03	1.568E-03	6.66	2	5.003E-03	9.994E 05	4.46
48	239.4	16.38	9.220E 03	1.581E-03	6.72	2	5.003E-03	9.994E 05	4.46
50	439.2	7.84	8.113E 03	8.605E-04	3.21	2	5.223E-03	8.794E 05	3.92
51	426.2	8.12	8.148E 03	8.868E-04	3.33	1	5.178E-03	8.832E 05	3.94
67	303.2	12.97	9.256E 03	1.248E-03	5.32	1	4.867E-03	1.003E 06	4.47
68	296.2	13.23	9.220E 03	1.277E-03	5.42	2	4.905E-03	9.994E 05	4.46
70	177.6	26.62	1.110E 04	2.135E-03	10.91	1	4.587E-03	1.203E 06	5.37
71	193.2	24.38	1.107E 04	1.962E-03	10.00	2	4.617E-03	1.199E 06	5.35
72	202.2	21.35	1.014E 04	1.874E-03	8.74	2	4.794E-03	1.099E 06	4.90
73	196.2	22.08	1.018E 04	1.932E-03	9.04	1	4.761E-03	1.103E 06	4.92
74	362.6	9.76	8.333E 03	1.043E-03	4.00	1	5.132E-03	9.032E 05	4.03
75	352.3	10.09	8.298E 03	1.073E-03	4.10	2	5.176E-03	8.994E 05	4.01
76	659.8	4.50	7.006E 03	5.724E-04	1.85	2	5.599E-03	7.594E 05	3.39
77	623.2	4.79	7.040E 03	6.060E-04	1.96	1	5.545E-03	7.631E 05	3.40
78	613.7	4.84	7.006E 03	6.154E-04	1.99	2	5.599E-03	7.594E 05	3.39
79	550.4	5.43	7.040E 03	6.864E-04	2.23	1	5.545E-03	7.631E 05	3.40

ROD SPACING = 0.028 INCHES

RUN	CC/CF	WT	SUB-DF	WT/M	F/V	CT	F	MF	U
1	51.7	54.24	6.462E 03	7.445E-03	22.24	1	5.558E-03	6.764E 05	3.02
2	53.2	52.36	6.428E 03	7.225E-03	21.47	2	5.616E-03	6.729E 05	3.00
3	45.2	90.51	9.405E 03	8.535E-03	37.11	1		9.845E 05	4.39
4	46.3	86.93	9.370E 03	8.235E-03	35.64	2		9.809E 05	4.37
5	59.2	29.72	4.071E 03	6.476E-03	12.19	1	7.352E-03	4.261E 05	1.90
6	59.1	29.55	4.039E 03	6.491E-03	12.13	2	7.470E-03	4.227E 05	1.89
7	46.4	70.85	7.566E 03	8.306E-03	29.05	1	5.474E-03	7.920E 05	3.53
8	49.1	66.58	7.531E 03	7.833E-03	27.27	2	5.524E-03	7.883E 05	3.52
9	47.4	84.26	9.186E 03	8.137E-03	34.56	2	5.047E-03	9.615E 05	4.29
10	46.9	85.15	9.186E 03	8.223E-03	34.91	2	5.047E-03	9.615E 05	4.29
11	47.0	88.28	9.554E 03	8.197E-03	36.20	2	5.048E-03	1.000E 06	4.46
12	45.4	91.75	9.589E 03	8.487E-03	37.62	1	5.010E-03	1.004E 06	4.48
15	50.6	72.43	8.451E 03	7.600E-03	29.69	2	5.411E-03	8.846E 05	3.94
16	49.3	74.65	8.485E 03	7.807E-03	30.62	1	5.367E-03	8.882E 05	3.96
17	50.3	63.72	7.382E 03	7.657E-03	26.13	1	5.622E-03	7.727E 05	3.45
18	50.9	62.54	7.348E 03	7.550E-03	25.64	2	5.675E-03	7.691E 05	3.43
19	52.8	50.07	6.044E 03	7.287E-03	20.53	1	5.968E-03	6.370E 05	2.85
20	51.3	51.22	6.061E 03	7.497E-03	21.00	2	6.034E-03	6.344E 05	2.83
21	55.6	37.45	4.807E 03	6.910E-03	15.35	1	6.529E-03	5.032E 05	2.24
22	55.5	37.27	4.774E 03	6.926E-03	15.28	2	6.619E-03	4.997E 05	2.23
23	50.6	102.63	1.198E 04	7.599E-03	42.08	1	4.609E-03	1.254E 06	5.59
24	48.5	106.81	1.194E 04	7.933E-03	43.79	2	4.637E-03	1.250E 06	5.58
25	50.3	87.08	1.011E 04	7.644E-03	35.71	2	5.069E-03	1.058E 06	4.72
26	47.2	93.39	1.014E 04	8.160E-03	38.25	1	5.033E-03	1.061E 06	4.73
27	47.0	95.06	1.029E 04	8.195E-03	38.98	2	5.010E-03	1.077E 06	4.80
28	46.4	96.74	1.033E 04	8.311E-03	39.67	1	4.975E-03	1.081E 06	4.82
29	45.3	122.42	1.290E 04	8.418E-03	50.19	1	4.484E-03	1.350E 06	6.02
30	45.1	123.99	1.286E 04	8.551E-03	50.84	2	4.510E-03	1.346E 06	6.00

ROD SPACING = 0.063 INCHES

RUN	CO/CF	JT	SUB-RE	WT/M	F/V	CT	F	MF	U
1	37.6	151.94	1.323E 04	1.030E-02	63.20	1	4.736E-03	1.278E 06	5.70
2	36.9	154.45	1.319E 04	1.050E-02	64.25	2	4.764E-03	1.274E 06	5.68
3	38.8	123.91	1.115E 04	9.970E-03	51.54	2	5.171E-03	1.076E 06	4.80
4	39.8	121.27	1.119E 04	9.726E-03	50.44	1	5.137E-03	1.080E 06	4.82
5	41.2	99.16	9.476E 03	9.388E-03	41.25	2	5.535E-03	9.149E 05	4.08
6	40.3	101.74	9.512E 03	9.599E-03	42.34	1	5.493E-03	9.183E 05	4.10
7	47.3	76.45	8.360E 03	8.203E-03	31.80	2	5.880E-03	8.072E 05	3.60
8	46.2	78.11	8.396E 03	8.346E-03	32.49	1	5.831E-03	8.104E 05	3.62
9	46.3	64.17	6.809E 03	8.334E-03	26.31	1	6.355E-03	6.660E 05	2.97
10	44.6	66.31	6.775E 03	8.655E-03	27.19	2	6.419E-03	6.636E 05	2.96
11	44.9	51.57	5.309E 03	8.591E-03	21.15	2	7.287E-03	5.200E 05	2.32
12	44.3	52.64	5.342E 03	8.713E-03	21.58	1	7.197E-03	5.232E 05	2.33
13	40.4	127.46	1.176E 04	9.584E-03	52.26	1	4.845E-03	1.152E 06	5.14
14	38.9	132.09	1.172E 04	9.954E-03	54.16	2	4.875E-03	1.148E 06	5.12
15	36.9	150.04	1.264E 04	1.050E-02	61.53	2	4.877E-03	1.238E 06	5.52
16	37.6	149.93	1.258E 04	1.046E-02	61.50	1	4.848E-03	1.242E 06	5.54
17	39.3	112.28	1.007E 04	9.856E-03	46.04	2	5.346E-03	9.866E 05	4.40
18	38.6	114.59	1.011E 04	1.002E-02	46.99	1	5.308E-03	9.902E 05	4.42
19	42.1	75.96	7.324E 03	9.171E-03	31.15	2	6.098E-03	7.174E 05	3.20
20	41.1	78.28	7.359E 03	9.406E-03	32.19	1	6.042E-03	7.208E 05	3.21
21	41.4	66.09	6.259E 03	9.337E-03	27.19	1	6.653E-03	6.130E 05	2.73
22	42.3	64.21	6.225E 03	9.121E-03	26.33	2	6.725E-03	6.097E 05	2.72
23	45.1	53.15	5.415E 03	8.558E-03	21.49	2	6.810E-03	5.379E 05	2.40
24	44.3	54.34	5.447E 03	8.704E-03	21.99	1	6.729E-03	5.412E 05	2.41
25	41.9	38.17	3.608E 03	9.222E-03	15.43	2	8.569E-03	3.584E 05	1.60
26	43.1	37.43	3.640E 03	8.965E-03	15.13	1	8.420E-03	3.616E 05	1.61
27	42.4	90.84	8.791E 03	9.101E-03	36.72	1	5.602E-03	8.644E 05	3.85
28	41.6	92.38	8.667E 03	9.292E-03	37.34	2	5.647E-03	8.610E 05	3.84
29	43.5	64.35	6.318E 03	8.880E-03	26.01	2	6.451E-03	6.277E 05	2.80
30	41.5	67.92	6.351E 03	9.323E-03	27.46	1	6.384E-03	6.310E 05	2.81

ROD SPACING = 0.127 INCHES

RUN	CC/CF	WT	SUB-DF	WT/M	F/V	CT	F	VF	U
1	31.8	71.55	5.129E 03	1.226E-02	29.34	1	6.369E-03	4.500E 05	2.01
2	30.7	73.55	5.096E 03	1.269E-02	30.14	2	6.451E-03	4.471E 05	1.99
3	33.1	80.36	6.007E 03	1.176E-02	32.95	2	5.954E-03	5.270E 05	2.35
4	32.3	82.88	6.040E 03	1.206E-02	33.93	1	5.888E-03	5.290E 05	2.36
5	30.7	100.43	6.952E 03	1.270E-02	41.13	1	5.710E-03	6.090E 05	2.72
6	31.6	97.14	6.918E 03	1.234E-02	39.83	2	5.766E-03	6.060E 05	2.71
7	30.6	113.41	7.829E 03	1.274E-02	46.50	2	5.402E-03	6.858E 05	3.06
8	29.8	116.96	7.863E 03	1.308E-02	47.96	1	5.355E-03	6.899E 05	3.08
9	30.5	127.66	8.775E 03	1.279E-02	52.34	1	5.068E-03	7.698E 05	3.43
10	29.9	129.71	8.740E 03	1.305E-02	53.18	2	5.109E-03	7.668E 05	3.42
11	27.3	169.20	1.056E 04	1.408E-02	69.32	2	4.947E-03	9.266E 05	4.13
12	28.7	163.88	1.060E 04	1.359E-02	67.19	1	4.914E-03	9.298E 05	4.15
13	30.2	142.44	9.687E 03	1.293E-02	58.40	1	5.042E-03	8.498E 05	3.79
14	30.3	141.36	9.651E 03	1.288E-02	57.97	2	5.079E-03	8.467E 05	3.78
15	27.2	200.69	1.224E 04	1.442E-02	82.28	1	4.619E-03	1.074E 06	4.79
16	28.4	190.73	1.220E 04	1.374E-02	78.21	2	4.647E-03	1.070E 06	4.77
17	28.8	162.96	1.056E 04	1.356E-02	66.83	2	5.000E-03	9.266E 05	4.13
18	30.2	155.87	1.050E 04	1.393E-02	63.91	1	4.966E-03	9.298E 05	4.15
19	27.3	184.26	1.151E 04	1.407E-02	75.55	1	4.732E-03	1.010E 06	4.50
20	29.8	179.35	1.147E 04	1.310E-02	70.09	2	4.762E-03	1.007E 06	4.49
21	32.0	121.01	8.740E 03	1.217E-02	49.62	2	5.315E-03	7.668E 05	3.42
22	31.1	125.09	8.775E 03	1.253E-02	51.29	1	5.273E-03	7.698E 05	3.43
23	33.3	42.98	3.238E 03	1.167E-02	17.62	2	7.522E-03	2.840E 05	1.27
24	32.4	44.60	3.260E 03	1.199E-02	18.29	1	7.376E-03	2.868E 05	1.28
25	32.1	55.67	4.035E 03	1.213E-02	22.83	1	6.901E-03	3.540E 05	1.58
26	31.6	56.18	4.003E 03	1.234E-02	23.03	2	7.012E-03	3.512E 05	1.57
27	31.4	69.31	4.914E 03	1.240E-02	28.42	2	6.286E-03	4.311E 05	1.92
28	32.1	68.26	4.947E 03	1.213E-02	27.99	1	6.203E-03	4.340E 05	1.94

ROD SPACING = 0.228 INCHES

RUN	CO/CF	WT	SUR-DF	WT/M	F/V	CT	F	VF	U
1	22.4	113.81	5.622E 03	1.763E-02	46.66	1	6.455E-03	4.245E 05	1.89
2	23.4	108.1[illegible]	5.590E 03	1.684E-02	44.3[illegible]	2	6.531E-03	4.221E 05	1.88
3	24.[illegible]	125.71	6.673E 03	1.641E-02	51.54	2	6.041E-03	5.038E 05	2.25
4	23.[illegible]	127.00	6.706E 03	1.649E-02	52.07	1	5.981E-03	5.063E 05	2.26
5	24.3	144.73	7.790E 03	1.618E-02	59.34	1	5.401E-03	5.882E 05	2.62
6	24.2	144.[illegible]	7.755E 03	1.627E-02	59.42	2	5.448E-03	5.856E 05	2.61
7	24.1	169.2[illegible]	9.019E 03	1.634E-02	69.40	2	5.131E-03	6.810E 05	3.04
8	23.[illegible]	178.66	9.[illegible]54E 03	1.719E-02	73.2[illegible]	1	5.092E-03	6.836E 05	3.05
9	24.1	187.0[illegible]	9.957E 03	1.636E-02	76.7[illegible]	1	5.052E-03	7.518E 05	3.35
10	23.[illegible]	189.9[illegible]	9.921E 03	1.668E-02	77.9[illegible]	2	5.088E-03	7.491E 05	3.34
11	23.1	219.4[illegible]	1.118E 04	1.709E-02	89.99	2	4.819E-03	8.445E 05	3.77
12	23.[illegible]	215.9[illegible]	1.122E 04	1.676E-02	88.56	1	4.788E-03	8.472E 05	3.78
13	22.[illegible]	251.57	1.248E 04	1.755E-02	103.15	1	4.621E-03	9.427E 05	4.20
14	22.2	253.9[illegible]	1.245E 04	1.774E-02	104.11	2	4.649E-03	9.399E 05	4.19
15	23.[illegible]	86.85	4.539E 03	1.666E-02	35.61	1	6.753E-03	3.427E 05	1.53
16	23.[illegible]	88.7[illegible]	4.507E 03	1.716E-02	36.41	2	6.850E-03	3.403E 05	1.52
17	23.4	69.79	3.604E 03	1.686E-02	28.62	2	7.854E-03	2.721E 05	1.21
18	23.[illegible]	69.66	3.636E 03	1.669E-02	28.56	1	7.717E-03	2.745E 05	1.22

PRESSURE UNBALANCED RESULTS

ROD GAP SPACING = .011 INCHES

RUN	CO/CF	WT	SUB-DF	WT/M	E/V	CT	MF	U
53	114.2	17.43	1.639E 04	3.330E-03	7.15	2	1.169E 06	5.21
54	102.2	22.32	1.875E 04	3.726E-03	9.15	2	1.337E 06	5.96
57	103.6	24.76	2.109E 04	3.675E-03	10.15	2	1.504E 06	6.71
58	77.5	23.12	1.468E 04	4.930E-03	9.48	2	1.047E 06	4.67
60	74.0	24.23	1.468E 04	5.166E-03	9.93	2	1.047E 06	4.67
61	66.5	23.81	1.295E 04	5.755E-03	9.76	2	9.236E 05	4.12
64	28.8	43.89	1.014E 04	1.355E-02	18.00	2	7.229E 05	3.22
65	52.4	33.62	1.433E 04	7.342E-03	13.79	2	1.022E 06	4.56

ROD GAP SPACING = .127 INCHES

RUN	CO/CF	WT	SUB-DF	WT/M	E/V	CT	MF	U
101	5.9	478.62	1.903E 04	7.885E-02	196.25	1	9.728E 05	4.34
202	8.9	291.18	1.903E 04	4.797E-02	119.39	1	9.728E 05	4.34
301	19.7	122.52	1.903E 04	2.018E-02	50.23	1	9.728E 05	4.34
303	21.9	135.70	2.341E 04	1.817E-02	55.64	1	1.197E 06	5.34
204	12.1	253.59	2.341E 04	3.396E-02	103.98	1	1.197E 06	5.34
103	8.3	386.72	2.341E 04	5.179E-02	158.56	1	1.197E 06	5.34
106	6.7	429.07	2.023E 04	6.648E-02	175.93	1	1.034E 06	4.61
205	10.0	271.77	2.023E 04	4.211E-02	111.43	1	1.034E 06	4.61
306	20.5	124.68	2.023E 04	1.932E-02	51.12	1	1.034E 06	4.61
307	18.4	117.59	1.701E 04	2.166E-02	48.21	1	8.698E 05	3.88
208	7.5	316.84	1.701E 04	5.838E-02	129.91	1	8.698E 05	3.88
107	5.4	469.91	1.701E 04	8.658E-02	192.67	1	8.698E 05	3.88
110	4.1	565.17	1.416E 04	1.251E-01	231.73	1	7.240E 05	3.23
209	6.1	337.28	1.416E 04	7.465E-02	138.29	1	7.240E 05	3.23
310	17.5	103.64	1.416E 04	2.294E-02	42.50	1	7.240E 05	3.23